NASA/CR-2000-209353

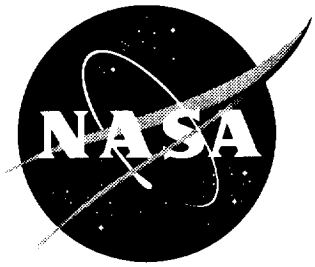

Rotorcraft Noise Abatement Flight Path Modeling

Hema Murty and Charles R. Berezin
Sikorsky Aircraft Corporation, Stratford, Connecticut

February 2000

The NASA STI Program Office ... in Profile

Since its founding, NASA has been dedicated to the advancement of aeronautics and space science. The NASA Scientific and Technical Information (STI) Program Office plays a key part in helping NASA maintain this important role.

The NASA STI Program Office is operated by Langley Research Center, the lead center for NASA's scientific and technical information. The NASA STI Program Office provides access to the NASA STI Database, the largest collection of aeronautical and space science STI in the world. The Program Office is also NASA's institutional mechanism for disseminating the results of its research and development activities. These results are published by NASA in the NASA STI Report Series, which includes the following report types:

- TECHNICAL PUBLICATION. Reports of completed research or a major significant phase of research that present the results of NASA programs and include extensive data or theoretical analysis. Includes compilations of significant scientific and technical data and information deemed to be of continuing reference value. NASA counterpart of peer-reviewed formal professional papers, but having less stringent limitations on manuscript length and extent of graphic presentations.

- TECHNICAL MEMORANDUM. Scientific and technical findings that are preliminary or of specialized interest, e.g., quick release reports, working papers, and bibliographies that contain minimal annotation. Does not contain extensive analysis.

- CONTRACTOR REPORT. Scientific and technical findings by NASA-sponsored contractors and grantees.

- CONFERENCE PUBLICATION. Collected papers from scientific and technical conferences, symposia, seminars, or other meetings sponsored or co-sponsored by NASA.

- SPECIAL PUBLICATION. Scientific, technical, or historical information from NASA programs, projects, and missions, often concerned with subjects having substantial public interest.

- TECHNICAL TRANSLATION. English-language translations of foreign scientific and technical material pertinent to NASA's mission.

Specialized services that complement the STI Program Office's diverse offerings include creating custom thesauri, building customized databases, organizing and publishing research results ... even providing videos.

For more information about the NASA STI Program Office, see the following:

- Access the NASA STI Program Home Page at ***http://www.sti.nasa.gov***

- E-mail your question via the Internet to help@sti.nasa.gov

- Fax your question to the NASA STI Help Desk at (301) 621-0134

- Phone the NASA STI Help Desk at (301) 621-0390

- Write to:
  NASA STI Help Desk
  NASA Center for AeroSpace Information
  7121 Standard Drive
  Hanover, MD 21076-1320

NASA/CR-2000-209353

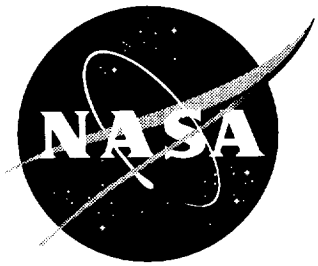

Rotorcraft Noise Abatement Flight Path Modeling

Hema Murty and Charles R. Berezin
Sikorsky Aircraft Corporation, Stratford, Connecticut

National Aeronautics and
Space Administration

Langley Research Center
Hampton, Virginia 23681-2199

Prepared for Langley Research Center
under Contract NAS1-20097

February 2000

The use of trademarks or names of manufacturers in the report is for accurate reporting and does not constitute an official endorsement, either expressed or implied, of such products or manufacturers by the National Aeronautics and Space Administration.

Available from:

NASA Center for AeroSpace Information (CASI)
7121 Standard Drive
Hanover, MD 21076-1320
(301) 621-0390

National Technical Information Service (NTIS)
5285 Port Royal Road
Springfield, VA 22161-2171
(703) 605-6000

SUMMARY

A joint industry-government flight test in 1996 at Crows Landing, CA demonstrated that high deceleration rates can significantly benefit noise abatement approach procedures for the Sikorsky S-76 [1]. Deceleration increases aircraft angle-of-attack, thereby decreasing blade vortex interaction (BVI) noise emissions for the S-76 at descent rates exceeding 600 fpm. It is believed that deceleration effects are likely to play a beneficial role for other rotorcraft. However, testing with large microphone arrays such as at Crows Landing is both impractical and costly. Therefore the capability of predicting noise levels for decelerating approach procedures is needed to support future noise abatement flight procedure development.

The current effort addresses development of a noise modeling capability for decelerating approaches. The resulting technique employs discretization of the descent trajectory as multiple steady state segments for input to CAMRAD.Mod1 to predict rotor states for acoustic analysis. Deceleration is included by modifying the CAMRAD.Mod1 free flight trim options to allow trim to the specified acceleration components.

The Sikorsky effort included the following subtasks:

1. Develop and document a CAMRAD.Mod1 input deck for the S-76B main rotor. Also, develop an aerodynamic coefficient look-up table input file for the S-76B fuselage including control surface contributions.
2. Exercise this input deck for several sample cases that match fixed operating conditions flown during the 1996 Crows Landing flight test. Correlate the predicted rotor trim state for each sample case with the measured rotor data. Assess accuracy of input decks through a combination of wind tunnel mode (rotor only) and free flight (complete aircraft) trim cases.
3. Develop a standalone kinematic trajectory analysis tool that will define the trajectory as a one-parameter function of time or distance. Constant glideslope descents or constant rate-of-descent flight conditions will be included in the analysis. Fixed flight parameters will be input while the free parameters will be calculated. To incorporate unsteady flight effects, the flight path trajectory will then be discretized using the distance or time parameter into a sequence of flight conditions to be run using CAMRAD.Mod1. At each discrete point in the trajectory, the inputs for CAMRAD.Mod1 will be extracted and written to a script file in namelist form. These namelists correspond to the .scr file for CAMRAD.Mod1. From the trajectory analysis will come namelist inputs such as altitude, flight-path angle, vehicle velocity vector, and vehicle acceleration vector. The outputs will be in a form such that CAMRAD.Mod1 will be run with the input variable NCASES equal to the number of discretized points needed to accurately define the trajectory. Therefore, only one CAMRAD.Mod1 job will be submitted for a complete trajectory analysis. This tool can become another component of the TRAC analysis allowing a standalone capability for flight path modeling.

4. Using the results from step 3 above, the CAMRAD.Mod1 code will be used to predict the vehicle trim state and rotor loads for each discretized point along the flight trajectory. The CAMRAD.Mod1 free flight trim options will be modified to allow trim to the specified acceleration components. These components are input from the trajectory analysis code. A 'low frequency' approximation will be used in which the pitch acceleration is assumed zero.
5. The CAMRAD.Mod1 input deck and an informal task report will be submitted to NASA.

The CAMRAD.Mod1 input deck was developed by modifying an input deck provided by NASA Langley. Owing to the fact that a leased S-76B aircraft was used for the Crows Landing flight test, the comprehensive aircraft state data typically available from an experimental aircraft was not available for this effort. In addition, the available aircraft state data evidenced significant fluctuations for the level flight cases initially used to exercise the CAMRAD.Mod1 input deck. Hence additional correlations against other Sikorsky S-76 flight test data and predictions were used to evaluate the CAMRAD.Mod1 input deck. The predicted levels were provided by GEN HEL, a Sikorsky handling qualities model [2].

After showing good correlations between the CAMRAD.Mod1 results and the flight test/GEN HEL data, the standalone kinematic trajectory analysis tool developed in Subtask 3 was implemented with the CAMRAD.Mod1 model to evaluate vehicle trim state and rotor loads along the flight trajectory for decelerating approaches. Two test cases were used to assess the results for a decelerating approach at constant rate-of-descent (ROD) and a decelerating approach at constant glide slope. The resulting comparisons with test data showed good agreement between the predictions and the flight test data, in particular for angle-of-attack.

Comparisons of trim conditions for rotor alone and pitch and sideslip angle comparisons for full aircraft cases are presented in this report. A description of the standalone kinematic trajectory analysis tool and interface to CAMRAD.Mod1 is included. The flowchart for approach trajectory acoustic analysis is included here to illustrate the logic flow of the total acoustic analysis.

Problem Statement

The objective of this task was to develop the analytical tools required to model noise abatement approach flight paths flown by Sikorsky's S-76B helicopter in a joint industry-government flight test at Crow's Landing, CA in 1996. The completed tools will be used by NASA researchers to assess current capability in predicting noise footprints on the ground. Rotor trim state predictions were compared to wind tunnel rotor alone test data. Vehicle trim state predictions were compared to Sikorsky flight test data and Crow's Landing data. Flight trajectory cases consisting of decelerating approaches at constant rate-of-descent and a constant glideslope were used to predict free flight vehicle trim and compared with flight test data from Crow's Landing. For this purpose a standalone

kinematic trajectory analysis tool was developed and implemented to interface with CAMRAD.Mod1. In addition, vehicle acceleration was included in the CAMRAD.Mod1 trim controller for each segment of the quasi-steady analysis.

A look-up table of aerodynamic forces and moments for an S-76B fuselage as functions of angle-of-attack and sideslip was synthesized from one-fifth scale model wind tunnel test data [3].

The following sections describe efforts and results involved in each subtask of this task. Listings of required FORTRAN routines are included. All comparisons with test data are included in this report.

Information on CAMRAD.Mod1 can be obtained from [4].

CAMRAD Input Verification and Look Up Table

CAMRAD.Mod1 input files for the S-76B were obtained from NASA Langley. These files were compared with existing S-76B analytic rotor models at Sikorsky and updated accordingly. Rotor trim states obtained from rotor alone cases were compared with wind tunnel test data [5].

Fuselage aerodynamic loads and moments for fuselage and horizontal and vertical tails were obtained from a one fifth model scale wind tunnel test carried out at the UTRC main tunnel [3]. The data were formulated as a look up table of loads and moments as functions of fuselage angle of attack and sideslip angle. The switch WBTTAB in the namelist NLBODY was turned on in CAMRAD.Mod1 according to the description in Reference 2. This information is referenced to the location specified by the parameters FSWB, BLWB and WLWB in namelist NLBODY. Higher order effects of the rotor on the body angle-of-attack, which is a function of the forward flight speed, were ignored in determining these airloads. In addition, the effect of the rotor on the tail angle-of-attack as a function of forward speed was also ignored. The data specifying the variation of vertical tail sideflow angle with aircraft yaw angle appeared to be unusually high as obtained from the wind tunnel data [3]. Therefore the vertical tail angle-of-attack was made equivalent to the aircraft yaw angle. This assumption didn't seem to adversely affect the predictions obtained from CAMRAD.Mod1. The aerodynamic loads and moments are tabulated for the following variations of fuselage angle-of-attack and sideslip (in degrees):

Fuselage pitch:	-10.0, -7.8, -5.6, -3.3, -1.1, 1.1, 3.3, 5.6, 7.8, and 10.0
Fuselage yaw:	-20.0, -15.0, -10.0, -7.8, -5.6, -3.3, -1.1, 1.1, 3.3, 5.6, 7.8, 10.0, 15.0, 20.0

Current setup for nacelle angles, aileron and rudder deflections are still included and dummy variations are included for these. These make up 4480 data points in the input aerodynamic data file.

RESULTS

Subtask 2 Correlation of Rotor Trim State with Test Data

Test cases with fixed operating conditions were compared for this subtask. Rotor alone case were compared with full scale isolated S-76 rotor 40 ft by 80 ft wind tunnel data from [5]. Sample case for a collective sweep chosen with a forward flight speed of 100 kts, 293 main rotor rpm, and a shaft angle of -4 degrees. This is equivalent to an advance ratio of 0.25. Figure 1 is a comparison of the collective obtained from wind tunnel data and CAMRAD.Mod1 predictions obtained as a function of C_L/σ. Fairly good agreement was obtained. Lateral (θ_{1c}) and longitudinal (θ_{1s}) cyclic variations for zero flapping are shown in Figures 2 and 3, respectively. Comparison of the longitudinal cyclic is better than that of the lateral cyclic although both are within generally expected comparisons for cyclic pitch values.

CAMRAD.Mod1 predictions were compared with Sikorsky flight test data for steady level flight conditions. Crow's Landing data for level flight were found to be highly oscillatory and not deemed satisfactory for comparison with CAMRAD.Mod1 for the level flight comparison only. The results from the comparison with the flight test and GEN HEL [2] data are given in Figures 4 to 8 for level flight speeds from 60 to 150 kts. Owing to the nature of the data, the values of the dependent variables have been removed in the figures. However, it is clear from these results that the relative comparisons between CAMRAD.Mod1, flight test data and GEN HEL simulations are reasonably close. Figure 4 is the fuselage pitch angle and the CAMRAD.Mod1 values are close to the flight test data. Figure 5 shows the fuselage yaw values with forward flight speed. Flight test did not obtain a yaw angle. However the GEN HEL values seem to be close to the CAMRAD.Mod1 values for this case. Very good results were obtained for the main rotor collective as shown in Figure 6. Comparisons with the flight test data and GEN HEL are included in this figure. Lateral and longitudinal main rotor cyclic variation are shown in Figures 7 and 8 respectively. Longitudinal cyclic CAMRAD.Mod1 predictions compare well with flight test data as shown in Figure 8. Lateral cyclic CAMRAD.Mod1 predictions agree well with GEN HEL simulations. Perhaps this indicates that both numerical simulations have the same level of difficulty in predicting lateral cyclic.

Subtask 3 Standalone Kinematic Trajectory Analysis Tool

This subtask has been defined to develop a procedure for the numerical analysis of noise generated by a helicopter during an approach to landing. The unique description of an approach to landing requires a description of the trajectory taken by the helicopter from the start of the approach until landing. This description can come from several possible sources such as flight test or flight simulation software. In this task, the flight path

trajectories are classified by descriptors such as constant glideslope or constant rate-of-descent. Because these descriptors concern only the trajectory itself, and are not vehicle specific, it is possible to use a very simple kinematic analysis to describe the aircraft trajectory. If any descriptors had been aircraft specific, a full blown rotorcraft simulation like GEN HEL would have been necessary.

The procedure will use the CAMRAD.Mod1 code for the prediction of quasi-steady vehicle trim and rotor loads. Quasi-steady here means that CAMRAD.Mod1 will be used to analyze a sequence of trajectory snapshots. Each snapshot can represents a constant time or constant downrange distance increment. At each snapshot, the instantaneous vehicle velocities, attitudes, and accelerations from the trajectory analysis will be converted to a CAMRAD.Mod1 input case and written to a file that will become the CAMRAD.Mod1 script file. The script file will contain the sequence of runs which will completely describe the flight path trajectory. Therefore, only one CAMRAD.Mod1 job need be submitted for each trajectory analysis. The description of the kinematic trajectory analysis now follows.

Analysis Description

The analysis allows several options to describe the trajectory, the end point data, and the trajectory discretization method. These options are as follow:

Trajectory Options:
1) Constant glideslope descent
2) Constant rate-of-descent

End Point Specification Options:
1) Specify initial point location
2) Specify initial point acceleration

Trajectory Discretization Options:
1) Constant time increments
2) Constant downrange distance increments

One assumption used in the determination of the trajectories is that the acceleration is constant throughout the maneuver. Using this assumption and the following relations the trajectory can be uniquely defined.

$$S(t) = \int_0^t V(\tau)d\tau$$

$$V(t) = V_i + at$$

where S is the distance along the flight path from the initiation of the maneuver, V is the

velocity or the individual velocity components, a is the acceleration, and t is the time from start of the maneuver. The figure below shows a simple line drawing of the path for the constant glideslope trajectory.

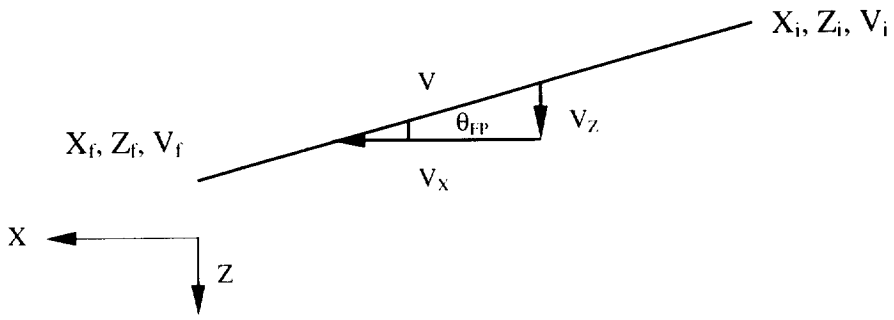

$$\tan\theta_{FP} = \frac{V_z}{V_x} = \frac{z_i - z_f}{x_i}$$

$$\frac{V_z}{V_x} = const$$

$$S_t = \sqrt{x_i^2 + (z_i - z_f)^2}$$

There are several possible combinations of flight path trajectory description and initial condition specification. Appropriate combinations which are available in the current analysis include: 1) constant glide slope, initial point location, 2) constant glide slope, initial point acceleration, 3) constant rate-of-descent, initial point location, and 4) constant rate-of-descent, initial point acceleration. Descriptions of the calculations involved for each combination are now given. In each case, the solution involves identifying the time history of the aircraft position, velocity, and acceleration.

Case 1: Constant Glide Slope, Initial Point Location

In this case, the proper initial and end point conditions which are given include:

x_i, z_i, z_f, v_i, v_f

Now, the total time for the descent maneuver, t_t, can be solved for using the expression for the known total distance for the maneuver. This is written as

$$s_t = \int_0^{t_t} v(\tau)d\tau = \int_0^{t_t} (v_i + a\tau)d\tau = v_i t_t + \tfrac{1}{2} a t_t^2 = v_i t_t + \tfrac{1}{2}(a t_t)t_t$$

but s_t is known from the following expression:

$$s_t = \sqrt{x_i^2 + (z_i - z_f)^2}$$

The acceleration may be solved for using the following equation for velocity:

$$v_f = v_i + at_f$$

$$a = \frac{v_f - v_i}{t_f}$$

$$at_f = v_f - v_i$$

Now, s_f may be equated to solve for the total time t_f:

$$s_f = \tfrac{1}{2}\left(v_f + v_i\right)t_f$$

$$t_f = \frac{2s_f}{v_f + v_i}$$

Using the above with the following relations:

$$\sin\theta_{FP} = \frac{z_f - z_i}{s_f}, \cos\theta_{FP} = -\frac{x_i}{s_f}$$

$$v_{xi} = v_i\cos\theta_{FP}, v_{zi} = v_i\sin\theta_{FP}, v_{xf} = v_f\cos\theta_{FP}, v_{zf} = v_f\sin\theta_{FP}$$

the final expressions for the discretized trajectory may now be written:

$$x(t) = x_i + \int_0^t \left(v_{xi} + a_x\tau\right) = x_i + v_{xi}t + \tfrac{1}{2}a_x t^2$$

$$z(t) = z_i + v_{zi}t + \tfrac{1}{2}a_z t^2$$

$$v_x(t) = v_{xi} + \int_0^t a_x d\tau = v_{xi} + a_x t$$

$$v_z(t) = v_{zi} + a_z t$$

$$a_x = a\cos\theta_{FP}$$

$$a_z = a\sin\theta_{FP}$$

Case 2: Constant Glide Slope, Initial Point Acceleration

A valid set of end point data is:

$$z_f, v_{xi}, v_{zi}, v_{xf}, v_{zf}, a$$

In this case, the initial velocity components are known and the initial starting point must be determined. This requires a simple manipulation of the terms above to determine the total trajectory length after which the start point coordinates may be computed. The expressions below are used in this computation:

$$v_i = \sqrt{v_{xi}^2 + v_{zi}^2}$$

$$v_f = \sqrt{v_{xf}^2 + v_{zf}^2}$$

$$t_t = \frac{v_f - v_i}{a}$$

$$s_t = \frac{t_t\left(v_f + v_i\right)}{2}$$

Now the initial coordinates are computed geometrically:

$$x_i = s_t \cos\theta_{FP} = -s_t \frac{v_{xi}}{v_i}$$

$$z_i = z_f + s_t \sin\theta_{FP} = z_f - s_t \frac{v_{zi}}{v_i}$$

The instantaneous values for the trajectory may now be evaluated using the same final expressions from Case 1 above.

Case 3: Constant Rate-of-Descent, Initial Point Location

A logical set of end point conditions for this case is:

$$x_i, z_i, z_f, v_i, v_z$$

In this situation, the total time for the maneuver can be directly calculated:

$$t_t = \frac{z_f - z_i}{v_z}$$

$$v_{xi} = \sqrt{v_i^2 - v_z^2}$$

We need to compute the x acceleration to determine the final x velocity.

$$x_f = 0 = x_i + \int_0^{t_t} \left(v_{xi} + a_x \tau\right) d\tau$$

$$x_i = -v_{xi} t_t - a_x \frac{t_t^2}{2}$$

which gives for the x acceleration and final x velocity,

$$a_x = \frac{-2(x_i + v_{xi}t_f)}{t_f^2}$$

$$v_{xf} = v_{xi} + a_x t_f$$

Now the time dependent trajectory information may be calculated as follows:

$$x(t) = x_i + v_{xi}t + \tfrac{1}{2}a_x t^2$$

$$z(t) = z_i + v_z t$$

$$v_x(t) = v_{xi} + a_x t$$

$$v_z = const$$

Case 4: Constant Rate-of-Descent, Initial Point Acceleration

The inputs for this case are:

$$z_f, v_{xi}, v_{xf}, v_z, a$$

The starting point coordinates need to be calculated here. Several terms can be directly determined:

$$a_x = a$$

$$t_f = \frac{(v_{xf} - v_{xi})}{a_x}$$

Now the starting point coordinates are computed:

$$x_i = -v_{xi}t_f - \tfrac{1}{2}a_x t_f^2$$

$$z_i = z_f - v_z t_f$$

All the terms required to compute the trajectory as in Case 3 are now available.

Trajectory Discretization

There are two options for discretizing the flight path trajectory as listed above. The constant time increments are easily calculated from:

$$\Delta t = \frac{t_f}{(nt - 1)}$$

where *nt* is the total number of discrete time steps. For the constant distance option, the discrete times at which snapshots of the trajectory are to be taken must be calculated. These times may be computed from the equation for trajectory distance as follows:

$$s(t) = \int_0^t v(\tau)d\tau = \int_0^t (v_i + a\tau)d\tau = v_i t + \tfrac{1}{2}at^2$$

For constant distance, the individual distances are determined from:

$$\Delta s = \frac{s_t}{(nt-1)}$$

Now, t may be calculated for a given distance as:

$$\tfrac{1}{2}at^2 + v_i t - s(t) = 0$$

$$t = \frac{-v_i \pm \sqrt{v_i^2 + 2as(t)}}{a}$$

In this case, to move forward in time, the positive root is chosen.

Figure 9 is a flowchart showing the logic used to obtain the CAMRAD.Mod1 solutions for a specified flight trajectory. These results will be subsequently used in an acoustic analysis that was not the subject of this task effort. Trajectories are classified as constant rate-of-descent or constant glideslope. Constant rate-of-descent trajectories can be described with equal range increments or as equal time increments. Trajectories defined as constant glideslope are described with equal time or range increments. These specifications are illustrated in Figure 10.

Subtask 4 Prediction of Vehicle Trim State and Rotor Loads along Trajectory

In order to accurately predict the external noise for a helicopter during an approach to landing, the time history of the vehicle operating state is needed over the descent trajectory. As part of the current task, a separate trajectory analysis described previously is used to generate CAMRAD.Mod1 input for discrete points along the trajectory. The vehicle operating state is then solved for at each point and the output becomes available for the external acoustic analysis. One important thing to note about the approach trajectories is the fact that the vehicle is undergoing a deceleration. Until now, CAMRAD.Mod1 had been configured to trim to zero net accelerations for the free flight trim options (OPTRIM=1-6). This was modified to allow trim to a specified acceleration in the vertical and/or horizontal directions. The modifications are meaningful only for the free flight trim mode.

The modifications were implemented, from a user standpoint, through the addition of two new inputs in the namelist NLTRIM. These are the accelerations in the inertial reference frame, AXTRIM for the trimmed acceleration in the x-direction and AZTRIM for the z-direction. They are activated by loading values for them into the input file. To return to the original form of CAMRAD.Mod1, set them equal to zero. The units for the accelerations are either ft/s^2 or m/s^2, whichever is appropriate.

The free flight trim equations in CAMRAD.Mod1 are written for a body-fixed frame of reference. The acceleration terms, which are more convenient to specify in the inertial frame from the trajectory analysis, must be transformed to the body reference frame. The transformation is described by the aircraft pitch and roll Euler angles. This transformation is already available in CAMRAD.Mod1 and is continually updated during the trimming procedure. It is stored under the array name RFE and is computed in subroutine BODYC. The sign convention for the inputs are given below noting that the in the CAMRAD.Mod1 inertial frame +x is in the forward direction while +z is down:

AXTRIM = + forward = $+a_x$
AZTRIM = + up = $-a_z$

Now, the accelerations in the body frame of reference may be written:

$$\begin{Bmatrix} a_{xb} \\ a_{yb} \\ a_{zb} \end{Bmatrix} = [RFE] \begin{Bmatrix} AXTRIM \\ 0 \\ AZTRIM \end{Bmatrix}$$

or symbolically,

$$a_{xb} = RFE(1,1) * AXTRIM - RFE(1,3) * AZTRIM$$
$$a_{yb} = RFE(2,1) * AXTRIM - RFE(2,3) * AZTRIM$$
$$a_{zb} = RFE(3,1) * AXTRIM - RFE(3,3) * AZTRIM$$

The trim equations are written in terms of force rather than acceleration, therefore these terms must be converted to forces and then normalized. Converting to forces is accomplished by multiplying the accelerations by the vehicle mass. The conversion to forces and the normalization are both accomplished using the following conversion factor:

$$F_{ax} = ma_x = \left(\frac{GW}{g}\right) a_x$$

$$\frac{CF_{ax}}{\sigma} = \frac{F_{ax}}{\rho \pi R^2 (\Omega R)^2 \sigma} = \left(\frac{GW}{g}\right) \frac{1}{\rho \pi R^2 (\Omega R)^2 \sigma} a_x$$

The normalization parameters are already available in CAMRAD.Mod1 under the symbolic names

HMASS= $\left(\frac{GW}{g}\right)$

DENSE= ρ

FSCALE= Ω

RSCALE= R

SSCALE= σ

The normalization factor in CAMRAD.Mod1 may now be written as:

```
AFAC=HMASS/(DENSE*3.141593*RSCALE**2*(FSCALE*RSCALE)**2*SSCALE)
```

The free flight trim equations in CAMRAD.Mod1 can now be modified using the force terms described above. The original force equations become (x-direction shown as an example):

$$\sum\left(\frac{C_{FX}}{\sigma}\right)=0$$

which is written in modified form as:

$$\sum\left(\frac{C_{FX}}{\sigma}\right)=\left(\frac{C_{FAX}}{\sigma}\right)$$

or

$$\sum\left(\frac{C_{FX}}{\sigma}\right)-\left(\frac{C_{FAX}}{\sigma}\right)=0$$

where $\sum\left(\frac{C_{FX}}{\sigma}\right)$ contains the x-force contributions due to weight, rotor, fuselage, etc. and $\left(\frac{C_{FAX}}{\sigma}\right)$ contains the contributions to the x-force due to the specified inertial accelerations.

Appropriate printout has been added to the CAMRAD.Mod1 output to reflect the new capability. The modifications have been confined to the following subroutines: INITC, INPTN, PRNT, TRIMI, and TRIMP. The two common blocks TMDATA and TRIMCM have also been expanded to accommodate the additional data and these two appear in many subroutines.

CAMRAD.Mod1 was modified to allow free flight trim option based on specified acceleration components. A preprocessor FORTRAN program determined the

acceleration components and these values were subsequently used in the CAMRAD.Mod1 input file. Pitch acceleration was ignored as described by the subtask. Three Crow's Landing data sets were used for comparison with the numerical results. Two cases with 600 ft/min constant rate-of-descent and decelerations of 0.25 kt/sec and 0.75 kt/sec were used.

Case 1 Data Set 12563 600 FPM ROD W/0.25 KT/SEC DECEL FROM 90 TO 40 KIAS

Characteristics of this data set obtained for a 600 ft/min rate-of-descent trajectory with a deceleration of 0.25 kt/sec are plotted in Figures 11 to 25. Figure 11 is a plot of the measured rate-of-descent. This data seems to indicate an average rate-of-descent of 800 ft/min which is higher than the 600 intended. Figure 12 shows the actual trajectory of Z (ft) versus X (ft) and the chosen CAMRAD.Mod1 points that were selected for the comparisons are shown superimposed on this trajectory. This same information is shown as a function of time in Figure 13. The rate-of-descent can be calculated from this distance plot of the aircraft and it varies from 840 to 660 ft/min during the course of the trajectory. Additionally, as a function of airspeed, the descent from 64 kts (at which point the data is given) to 40 kts and lower is shown in Figure 14. The intended flight was supposed to start at 90 kts but this data was not in the data file for this data set. CAMRAD.Mod1 selected data points are superimposed on this graph at speeds distributed throughout the trajectory. Figure 15 shows the airspeed during the trajectory as a function of time. Figure 16 shows the sideward flight of the aircraft during the trajectory. The magnitude is not that large over the course of 10000 ft indicating that the pilot was able to keep the aircraft on the course of the trajectory. The measured values of the angle-of-attack of the aircraft as measured from the aircraft boom is shown in Figure 17 as a function of distance. The average value of 15° angle of attack seems to be too high for this flight. Hence, the angle of attack was not used in this comparison with CAMRAD.Mod1 values. This data was plotted with time in Figure 18 showing the same trend around 15 degrees. Roll was plotted as a function of distance in Figure 19. The value of roll was around 0° which is what the desired value should be as the aircraft trims to a zero roll value in actual flight. Figure 20 is the flight test data value of sideslip as a function of distance. It is very oscillatory in behavior as the pilot responds to the flight conditions encountered. Figure 21 shows the comparison of sideslip with time compared with results from CAMRAD.Mod1. This comparison shows that the general trend of increasing sideslip with decrease in velocity with time is followed. At the larger velocity, the flight test required a higher sideslip value than that predicted. Sideslip is plotted with airspeed in Figure 22. As noted from Figure 21 in the plot with time, the comparison with sideslip at the higher speed was not matched for this flight test, probably owing to the local flight conditions at the time the flight test occurred which necessitated a higher sideslip. In general at the other speeds, the comparison with prediction is good. Figure 23 shows the aircraft angle of pitch with distance and the CAMRAD.Mod1 predictions. Although the aircraft pitch angle oscillates by about a degree in the flight test, the general trend of increasing pitch angle with lower speed as the pilot prepares to land is reflected by both sets of data. The comparison is generally good, considering that the flight test would have to compensate for any sudden gusts during the flight and these

are not simulated in the CAMRAD.Mod1 predictions. Figure 24 shows this same comparison with time and a similar trend is observed in this comparison as well. The oscillatory nature of the pitch amplitude is also present here as the pitch angle oscillates by one or two degrees during the flight trajectory. It is also interesting to look at the variation of pitch angle with airspeed as shown in Figure 25. The scatter in the pitch angle is apparent in this graph with a two degree variation at any speed indicating differing flight conditions during the trajectory as previously indicated. The CAMRAD.Mod1 predictions seem to fall in the general mean of the flight test data as would be expected by the ideal conditions used for the predictions.

Case 2 Data Set 12565 600 FPM ROD W/0.75 KT/SEC DECEL FROM 90 TO 40 KIAS

This case is the same constant rate-of-descent as the previous case 12563, with a larger deceleration rate of 0.75 kt/sec. Figure 26 shows the flight test data rate-of-descent measurement. Again it is around 800 ft/min on average throughout the trajectory with a large amplitude of oscillation of approximately 600 ft/min going to a maximum of 1400 ft/min at some point. Figure 27 shows the trajectory in space with the CAMRAD.Mod1 points selected for this comparison shown on the graph. Figure 28 shows this same information as a function of time. These values indicate a rate-of-descent closer to 600 ft/min than the previous case. The position with airspeed is shown in Figure 29. Actual airspeed during the trajectory is shown in Figure 30. In addition, it is interesting to note the variation in side motion given by the Y coordinate in Figure 31 shown with time. The actual flight trajectory confronts conditions which are not ideal, giving rise to some sideflight motion. Figure 32 shows the measured angle of attack during the trajectory. As in the previous case the average amplitude of the angle of attack of 15 degrees seems too large for this case and is therefore not being used during this comparison. The roll distribution with time is shown in Figure 33. The average value of roll here is a little over 1°, which is expected for a flight test trajectory when a 0 value of roll is difficult to maintain. This same distribution is shown with time in Figure 34. The distribution of roll with airspeed is shown in Figure 35. This distribution indicates a difficulty to maintain zero roll at the large starting velocities. It is possible that flight conditions at that time may have prevented trim to a value of roll close to zero. Sideslip for this trajectory is given in Figure 36 with CAMRAD.Mod1 predictions. For this case also, as in the previous case, there is a large oscillation in the sideslip value during the trajectory. Although the CAMRAD.Mod1 solution seems reasonable, gradually increasing in sideslip as the velocity decreases, the flight test data seems to indicate that the flight conditions were not as ideal as that assumed by CAMRAD.Mod1. The same information is shown with time in Figure 37 and the same CAMRAD.Mod1 trend is seen here. Additionally, the sideslip variation with airspeed is shown in Figure 38 indicating that the agreement with prediction was good at the initial part of the trajectory and not so as the airspeed was decreasing. CAMRAD.Mod1 solutions and flight test comparison of aircraft pitch angle are shown in Figure 39. In this case, generally good agreement was obtained throughout the trajectory. A difference of approximately two degrees in pitch is acceptable for comparison with flight test under conditions which may not be ideal throughout the trajectory. Figure 40 shows this data as a function of time and similarly,

the agreement is fairly good. Pitch variation with airspeed is shown in Figure 41. In general, the comparison with CAMRAD.Mod1 results seems good. It appears that the comparison improves with lower velocity.

Case 3 Data Set 12567 5.5 DEGREE APPROACH W/ 0.25 KT/SEC DECEL FROM 90 TO 40 KIAS

This case is a constant glideslope case of 5.5 degrees. Figure 42 shows the trajectory of height Z with distance X. It is approximately 5.5 degrees over the whole trajectory. Figure 43 shows the same information with time as the independent variable. Height as a function of airspeed is shown in Figure 44 showing the CAMRAD.Mod1 sample points for this trajectory. Figure 45 shows the airspeed variation of the trajectory with time. This trajectory shows some slight variations in the generally constant glideslope flight test. Figure 46 shows the side variation during the flight trajectory with time. During this flight there appears to be a large sideward flight component. This may have been the pilot compensating for flight conditions that are not ideal. Figure 47 shows the angle of attack variation with distance during this flight test and indicates an average of 15 degrees as in the previous two test cases chosen for this study. Again, this value seems too large for these flight conditions and therefore, angle of attack will not be used for this comparison. The roll angle with time is shown in Figure 48. For this case, the average roll is not 0 but approximately 2 degrees. In CAMRAD.Mod1, all computations were carried out with the assumption of trim to 0 degrees of roll as in ideal flight conditions. This difference could contribute to any differences in flight test and computational results. In addition, the roll is seen to be quite oscillatory and attains a maximum value of approximately 6 degrees at an early point in trajectory. Figure 49 shows the variation of roll with airspeed. This graph more clearly shows the high value of roll at the initial large value of velocity in the trajectory. Figure 50 show the sideslip measured by flight test and that predicted by CAMRAD.Mod1 as a variation of distance. In general the trend of the CAMRAD.Mod1 results is correct in that the sideslip generally increases with decreasing velocity as the landing approaches. The flight test data is generally 5 degrees higher than predictions for this case. One can also observe the oscillations in the sideslip flight test data probably corresponding to varying flight conditions. Sideslip variation with time is shown in Figure 51 showing similar information to that just discussed. Figure 52 shows the variation of sideslip with airspeed during the trajectory. The general trend is indicated to be correct between the flight test data and the CAMRAD.Mod1 predictions. Figure 53 shows the aircraft angle of pitch with distance from flight test data and CAMRAD.Mod1 solutions. The agreement here is good interrupted only by the large angle of pitch experienced by the aircraft during mid-trajectory. This is probably owing to flight conditions encountered during the constant glideslope trajectory. As the flight speed decreases toward the landing the pitch angle increases as expected for both sets of data presented. This information is presented as a function of time in Figure 54. The variation with airspeed can be seen in Figure 55. The agreement is good and shows the location of the CAMRAD.Mod1 points throughout the trajectory as a function of speed. Varying flight conditions are probably responsible for the scatter of data from the flight test.

Conclusion

Analytical tools were developed to model noise abatement flight paths flown by Sikorsky's S-76B helicopter. Sikorsky S-76B fuselage airloads data was included in CAMRAD.Mod1. Rotor alone and full aircraft trim cases using CAMRAD.Mod1 were compared with wind tunnel and flight test data respectively and the comparison was satisfactory. A kinematic trajectory analysis tool was developed and interfaced with CAMRAD.Mod1 to be used in decelerating descents with constant glideslope and constant rate-of-descent trajectories. The comparison of the modified CAMRAD.Mod1 aircraft pitch and sideslip conditions generally agree with the Crow's Landing flight test data.

References

1. Jacobs, E. W., Prillwitz, R. D., Chen, R. T. N., Santa Maria, O. L., "The Development and Flight Test Demonstration of Noise Abatement Approach Procedures for the Sikorsky S-76," Procedures of the American Helicopter Society Technical Specialists Meeting for Rotorcraft Acoustics and Aerodynamics, Williamsburg, VA, October 28-30, 1997.

2. Howlett, J.,"UH-60A Black Hawk Engineering Simulation Program: Volume I Mathematical Model," NASA CR 166309, December 1981.

3. Jepson, D., Moffitt, R., Hilzinger, K., Bissell, J., "Analysis and Correlation of Test Data From an Advanced Technology Rotor System," NASA Contractor Report 3714, August 1983.

4. Johnson, W., "A Comprehensive Analytical Model of Rotorcraft Aerodynamics and Dynamics. Part II: User's Manual," NASA TM 81183, July 1980.

5. Balch, David T., "Full-Scale Wind Tunnel Test of a Modern Helicopter Main Rotor Correlation with Model Rotor Test Data and with Theory", AHS 34th Annual National Forum, Washington, D.C., May 1978.

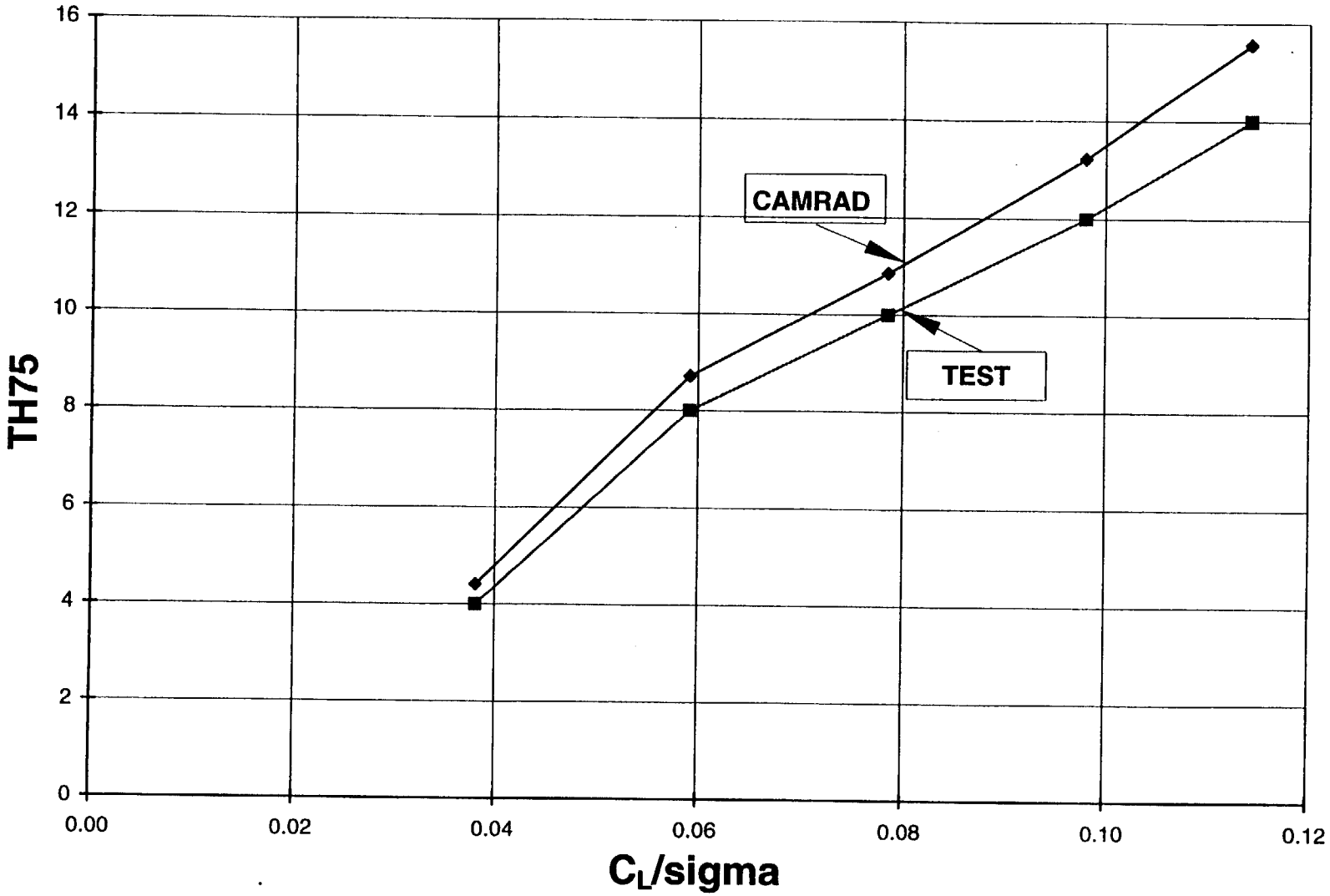

FIGURE 1 ISOLATED ROTOR (SHAFT ANGLE = -4 DEG, ADVANCE RATIO = 0.25, RPM = 293, 100 KTS)

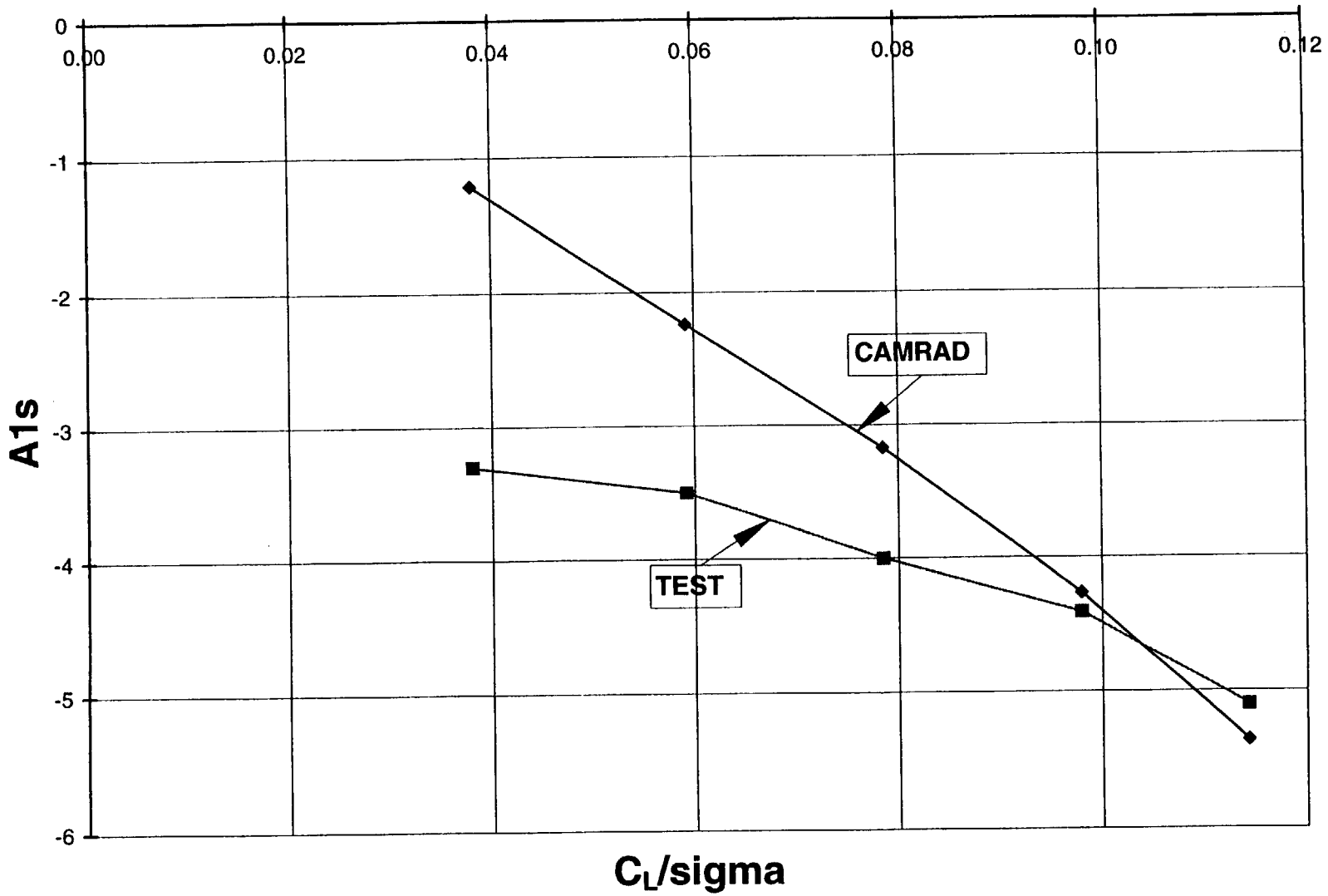

FIGURE 2 ISOLATED ROTOR (SHAFT ANGLE = -4 DEG, ADVANCE RATIO = 0.25, RPM = 293, 100 KTS)

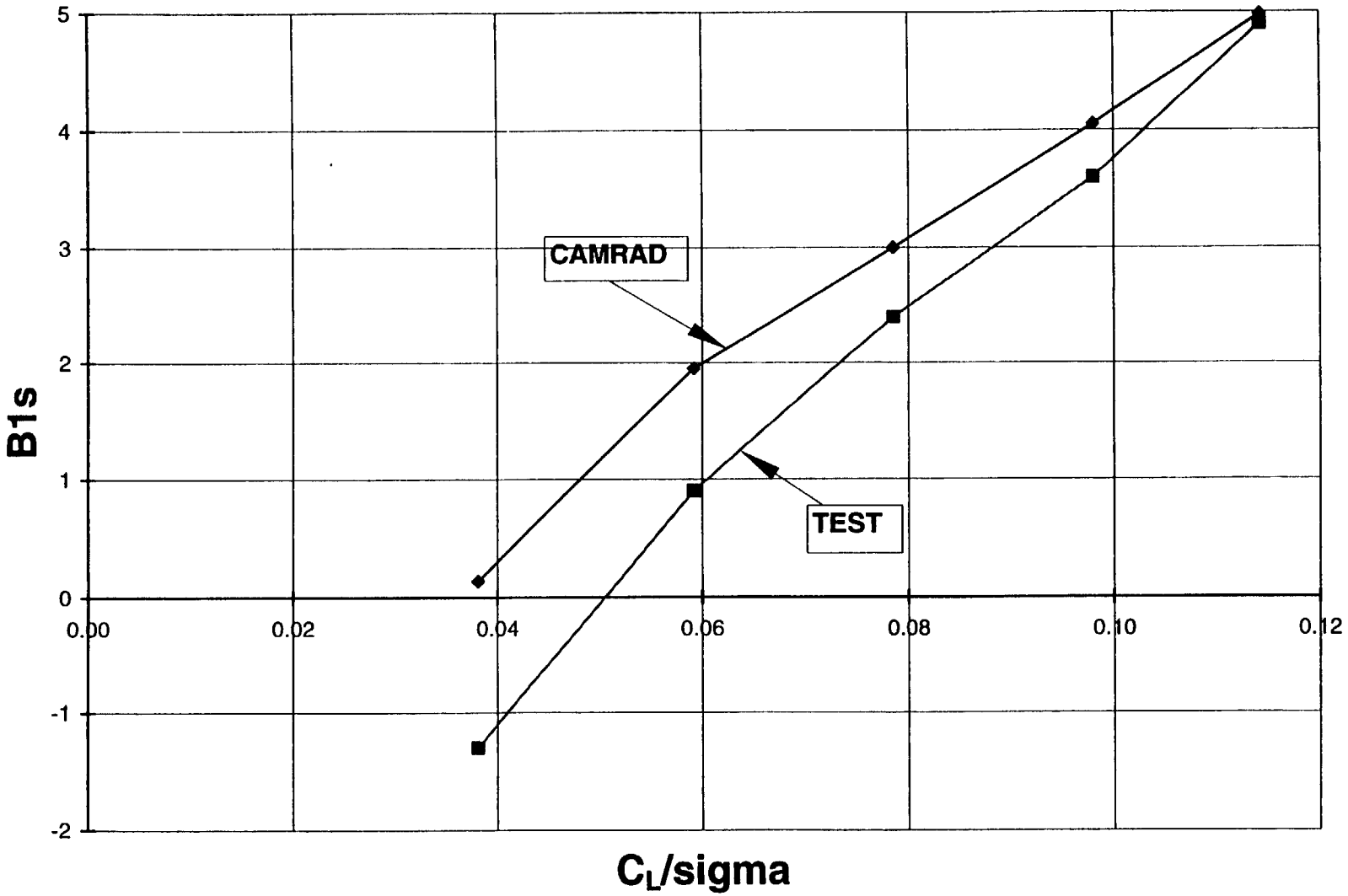

FIGURE 3 ISOLATED ROTOR (SHAFT ANGLE = -4 DEG, ADVANCE RATIO = 0.25, RPM = 293, 100 KTS)

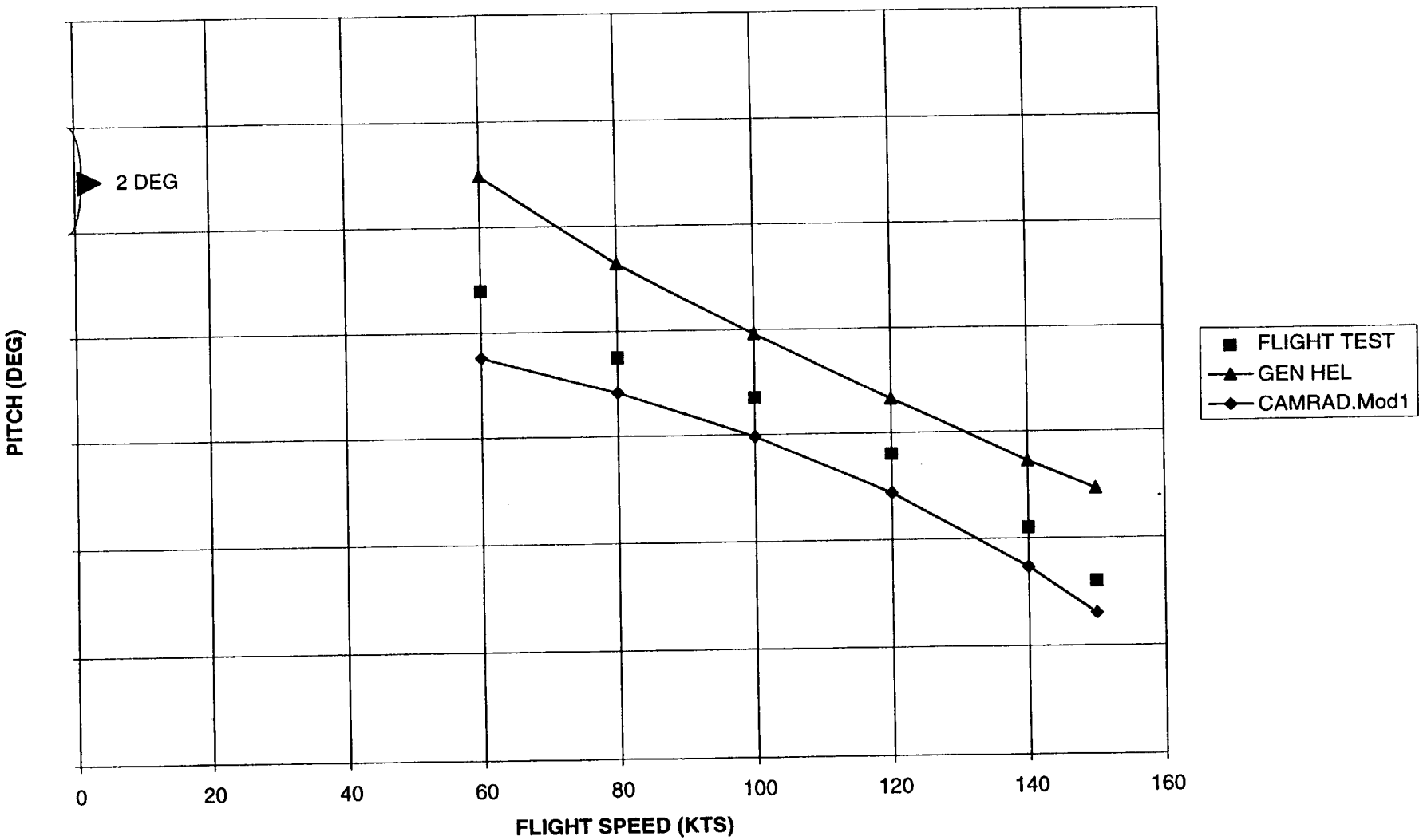

FIGURE 4 AIRCRAFT PITCH ANGLE IN LEVEL FLIGHT

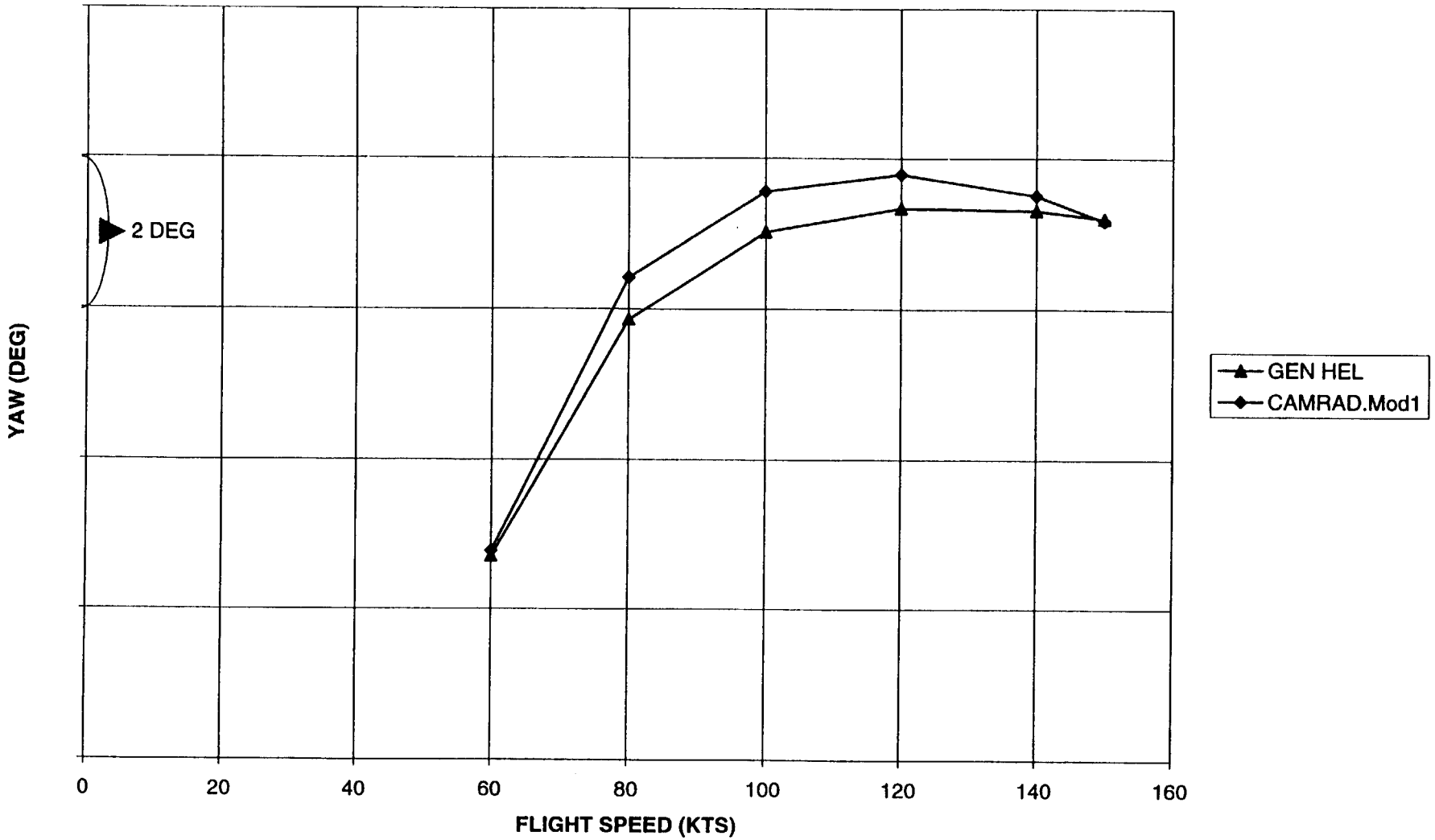

FIGURE 5 AIRCRAFT YAW ANGLE IN LEVEL FLIGHT

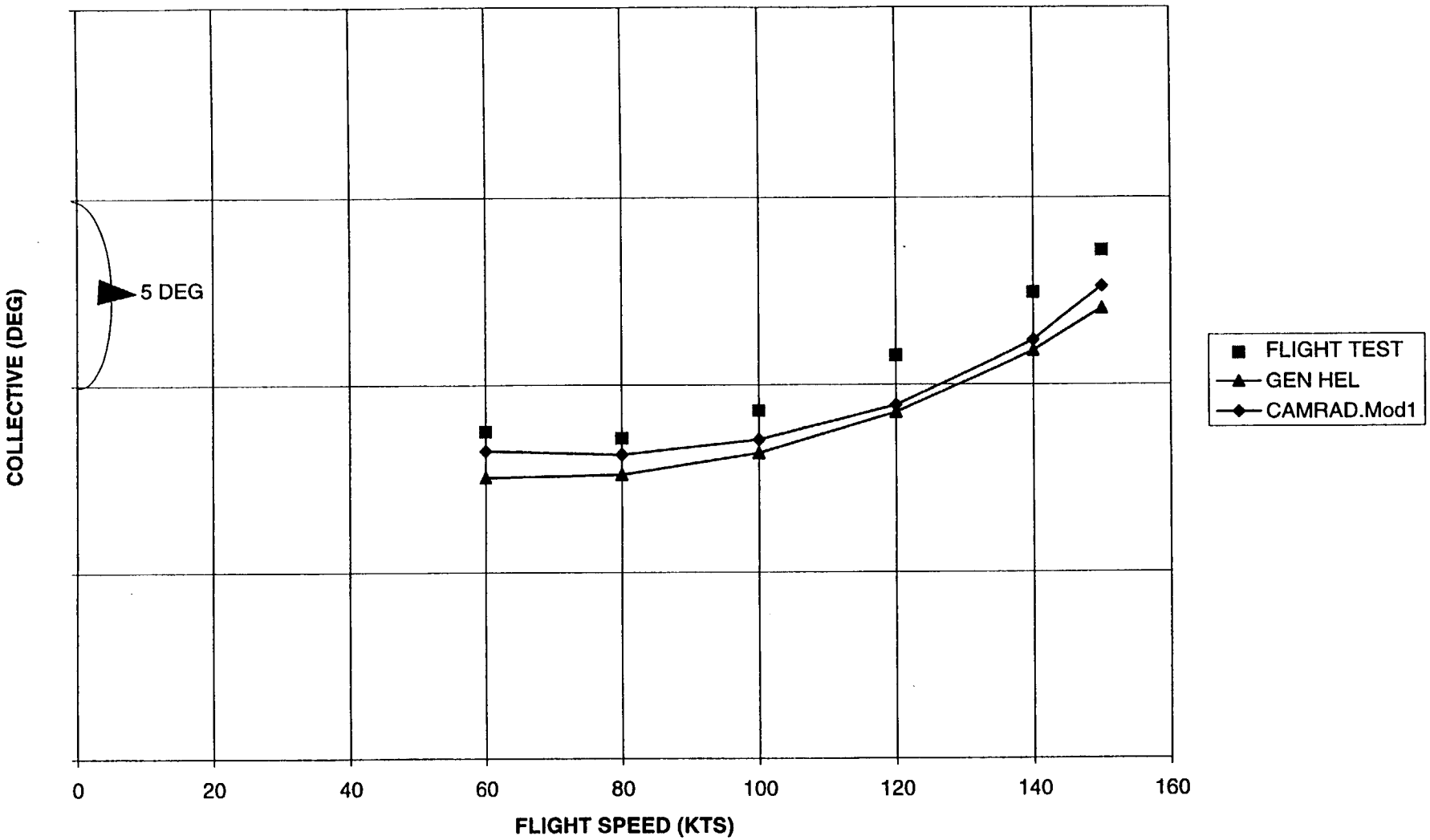

FIGURE 6 MAIN ROTOR COLLECTIVE IN AIRCRAFT LEVEL FLIGHT

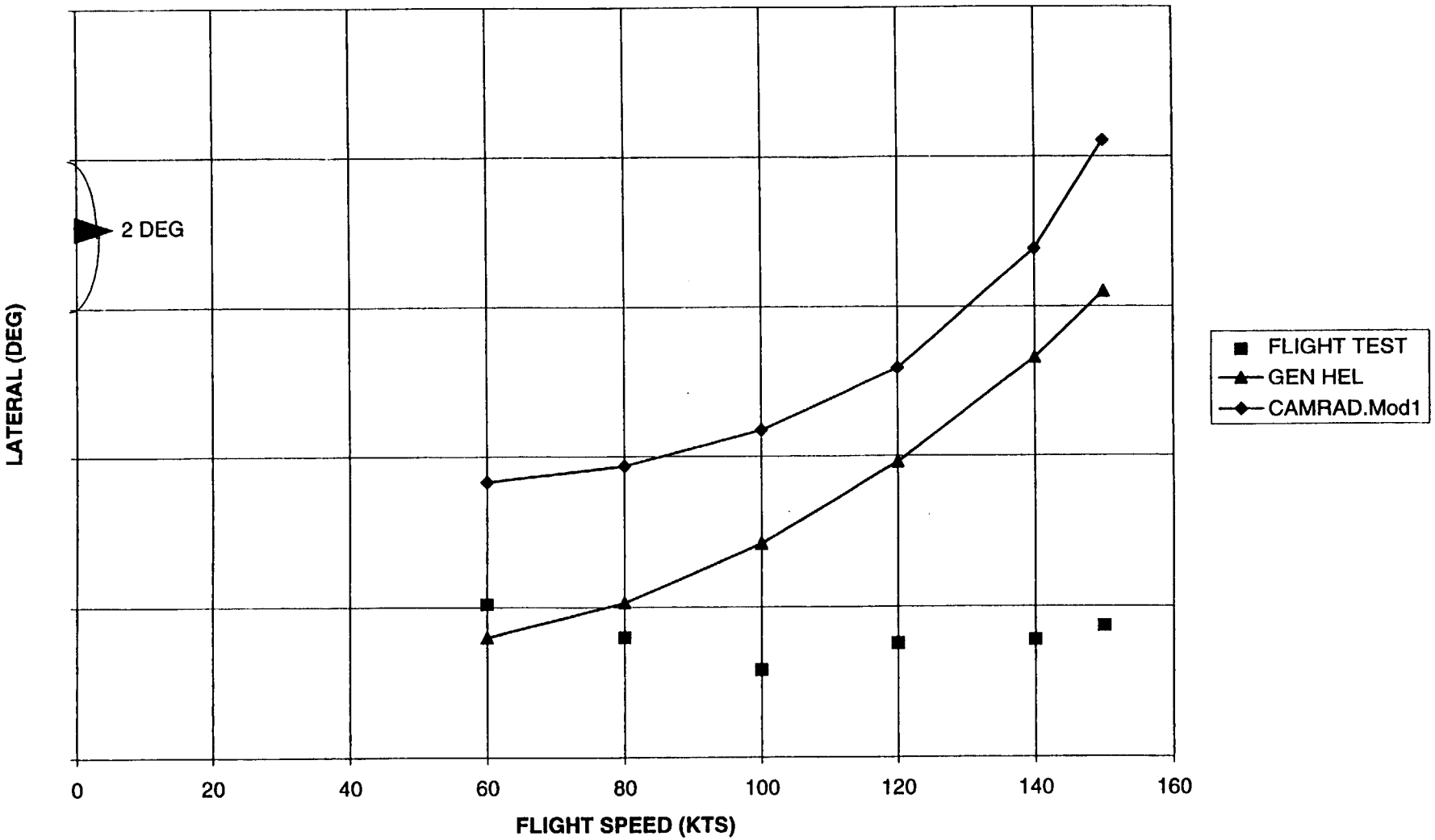

FIGURE 7 MAIN ROTOR LATERAL CYCLIC DURING LEVEL FLIGHT

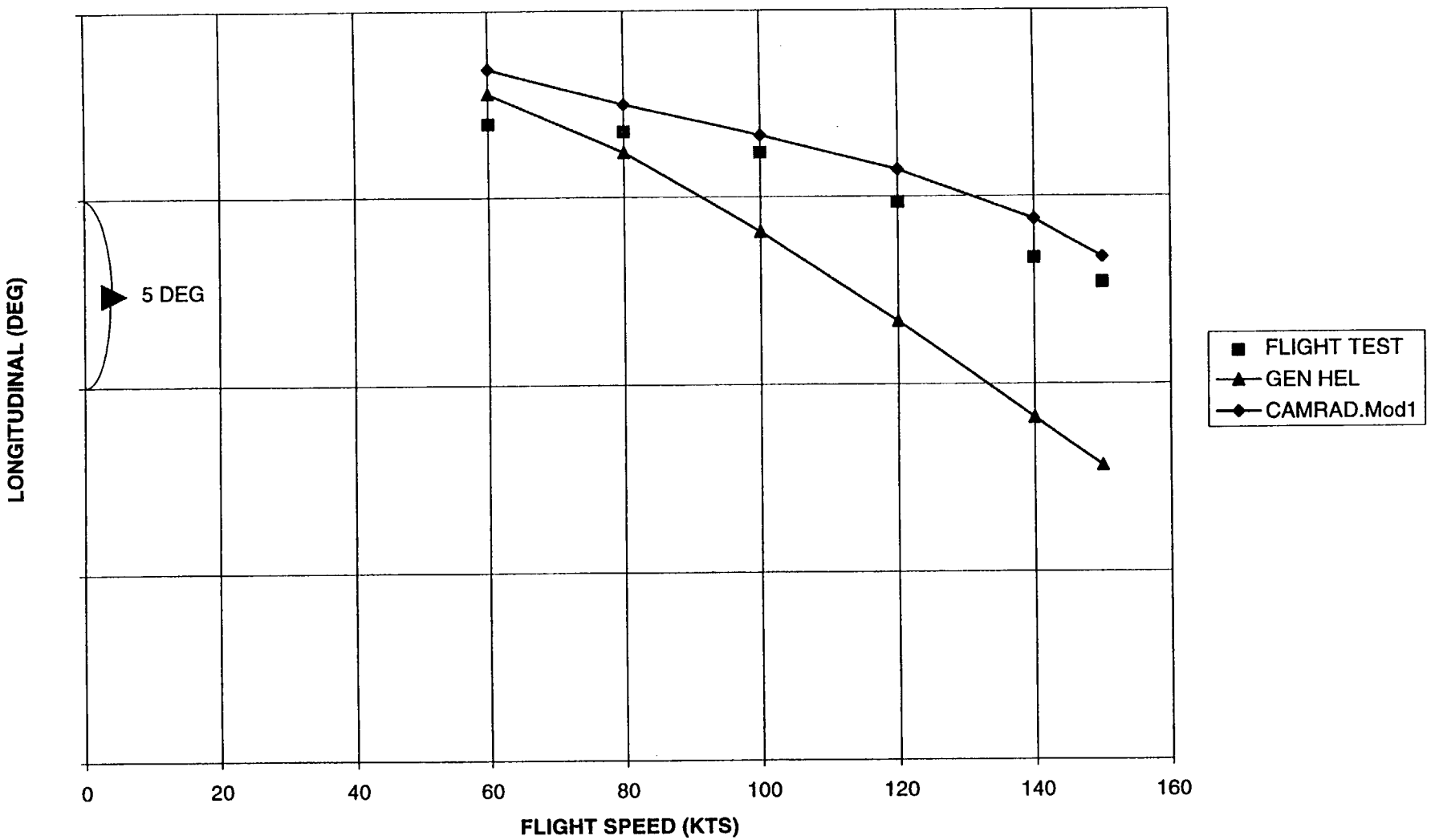

FIGURE 8 MAIN ROTOR LONGITUDINAL CYCLIC DURING LEVEL FLIGHT

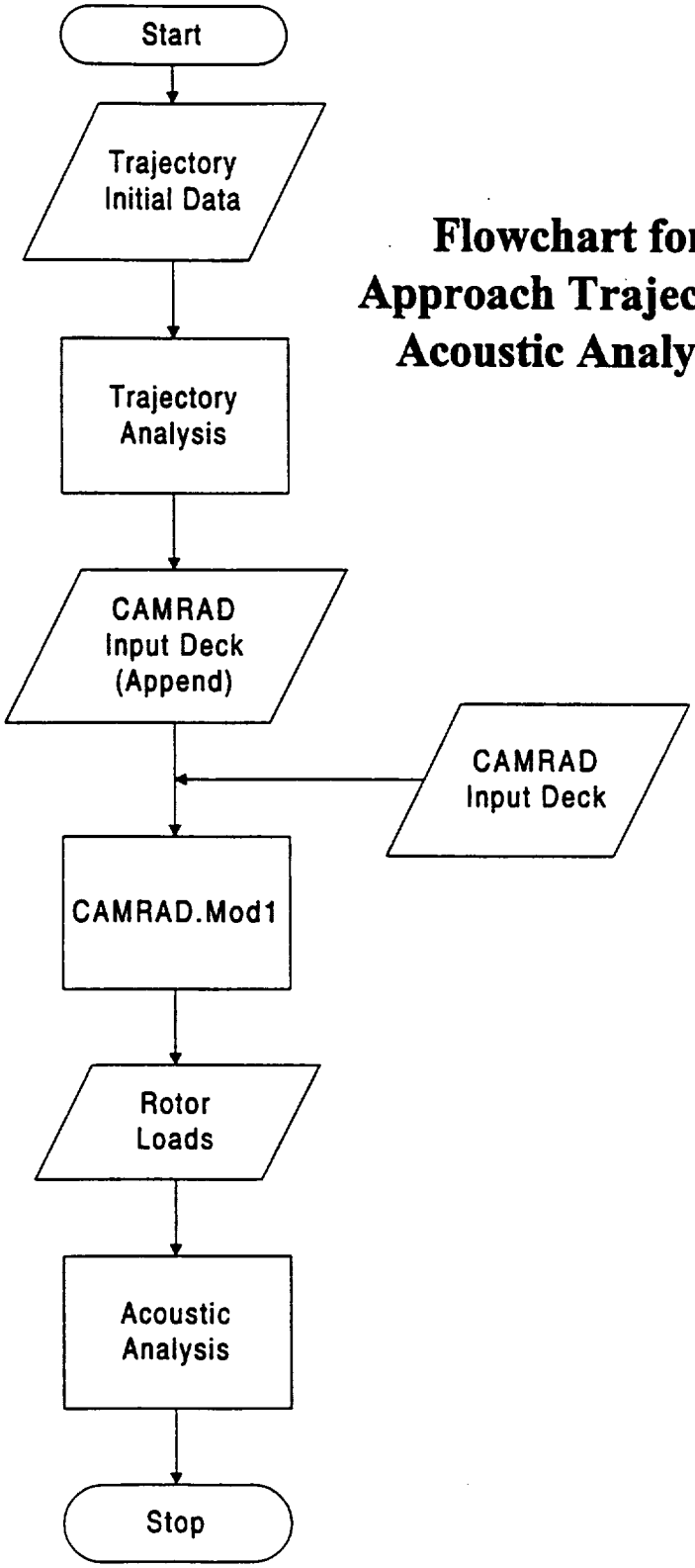

FIGURE 9 FLOWCHART FOR APPROACH TRAJECTORY ACOUSTIC ANALYSIS

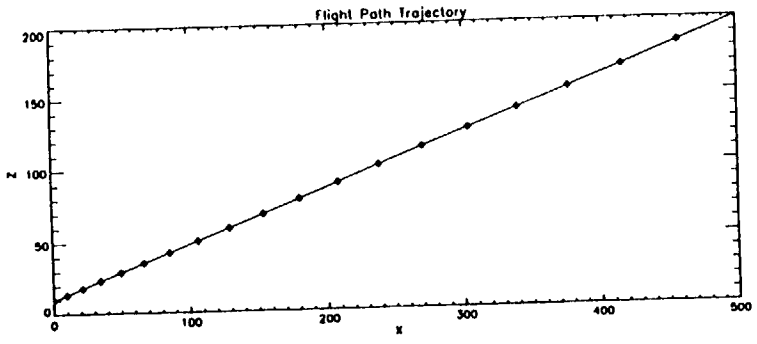

Constant Glideslope
Equal Time Increments

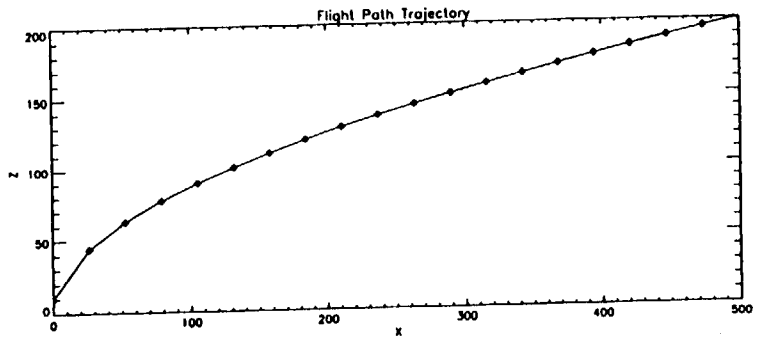

Constant Rate-of-Descent
Equal Range Increments

Constant Rate-of-Descent
Equal Time Increments

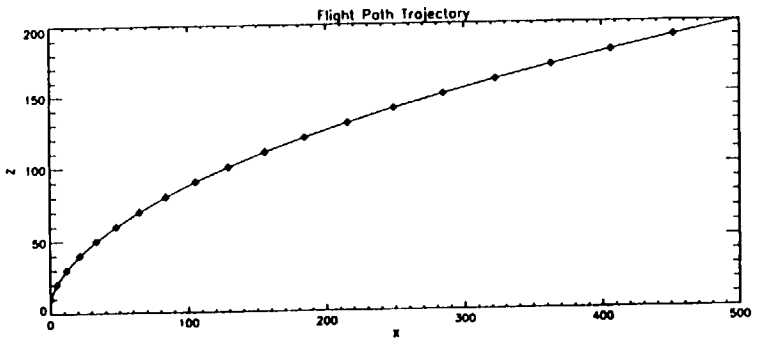

FIGURE 10 CONSTANT GLIDESLOPE SPECIFIED BY EQUAL TIME INCREMENTS, CONSTANT RATE-OF-DESCENT SPECIFIED BY EQUAL RANGE INCREMENTS AND EQUAL TIME INCREMENTS

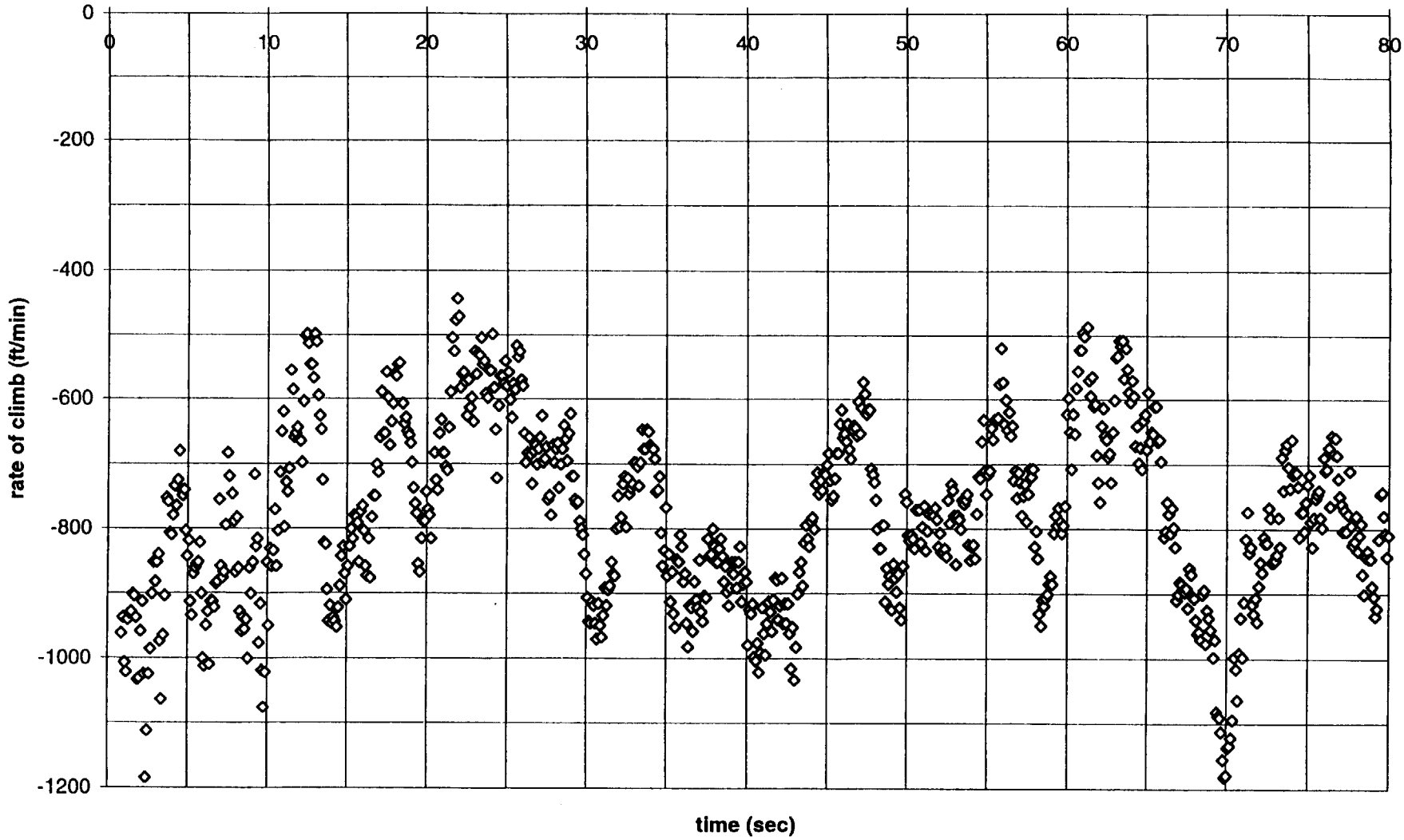

FIGURE 11 RATE-OF-CLIMB FROM TEST DATA FOR TEST NUMBER 12563 (600 FT/MIN ROD)

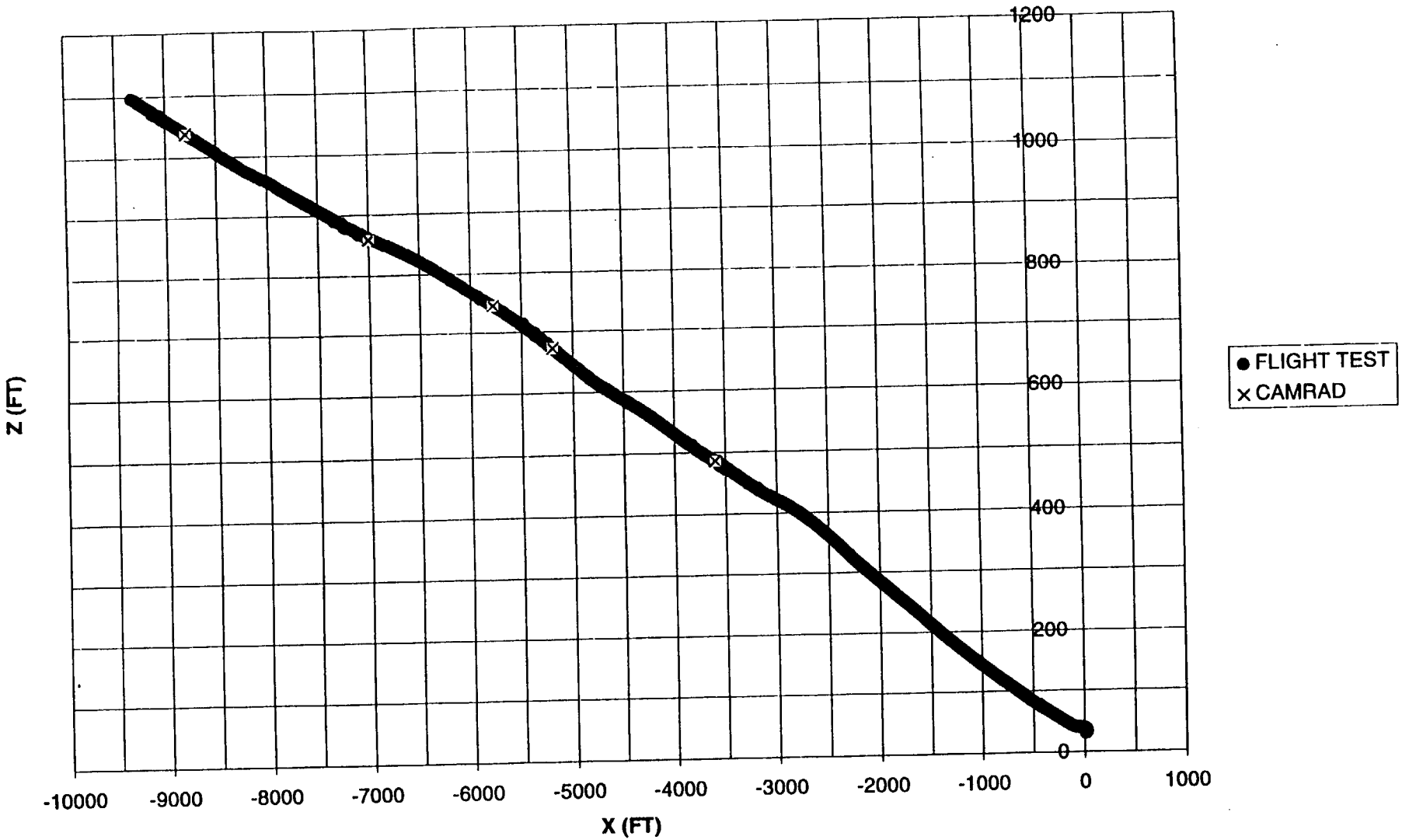

FIGURE 12 TRAJECTORY IN SPACE COORDINATES FOR TEST NUMBER 12563 (600 FT/MIN ROD)

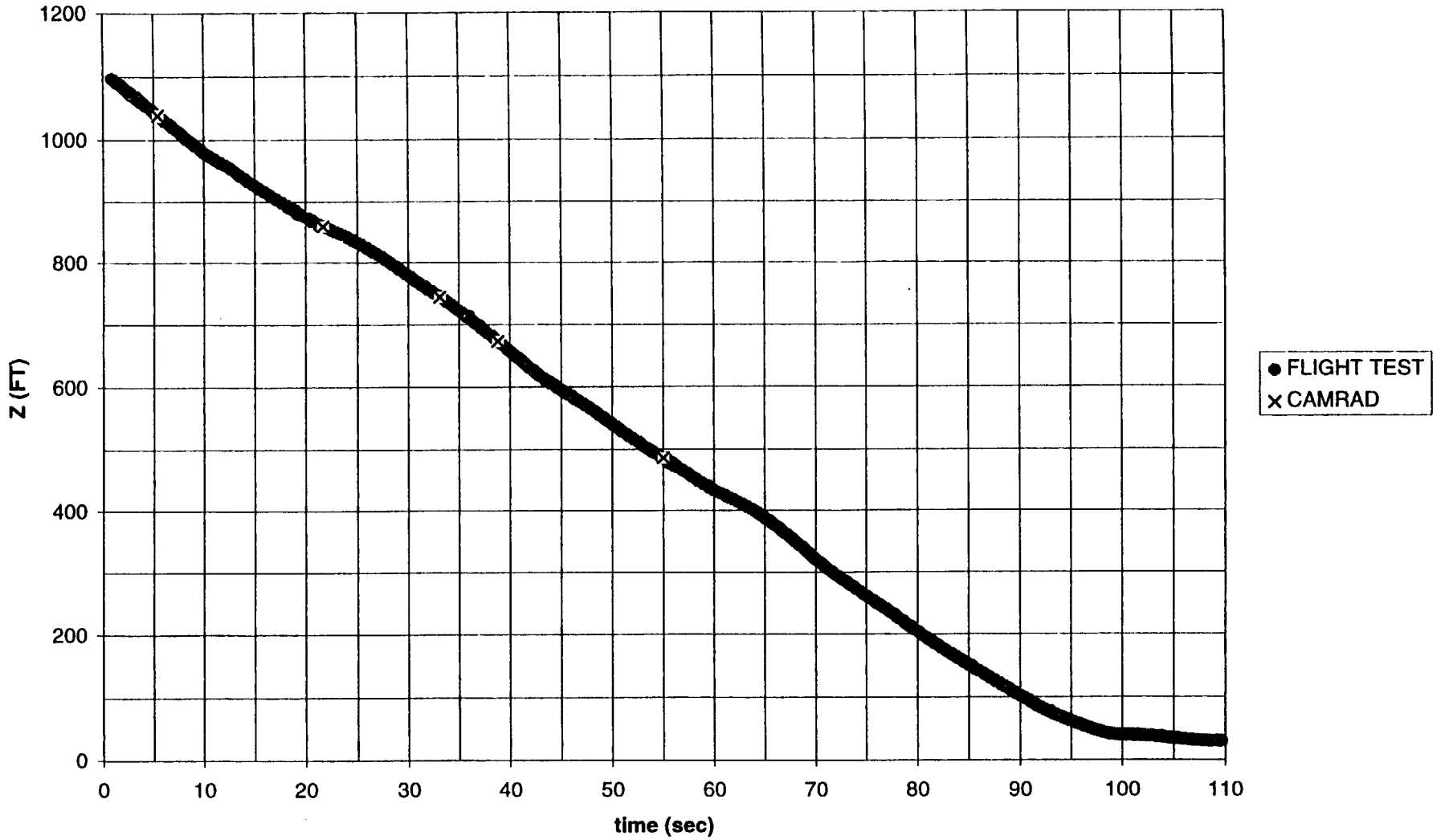

FIGURE 13 TRAJECTORY IN TIME FOR TEST NUMBER 12563 (600 FT/MIN ROD)

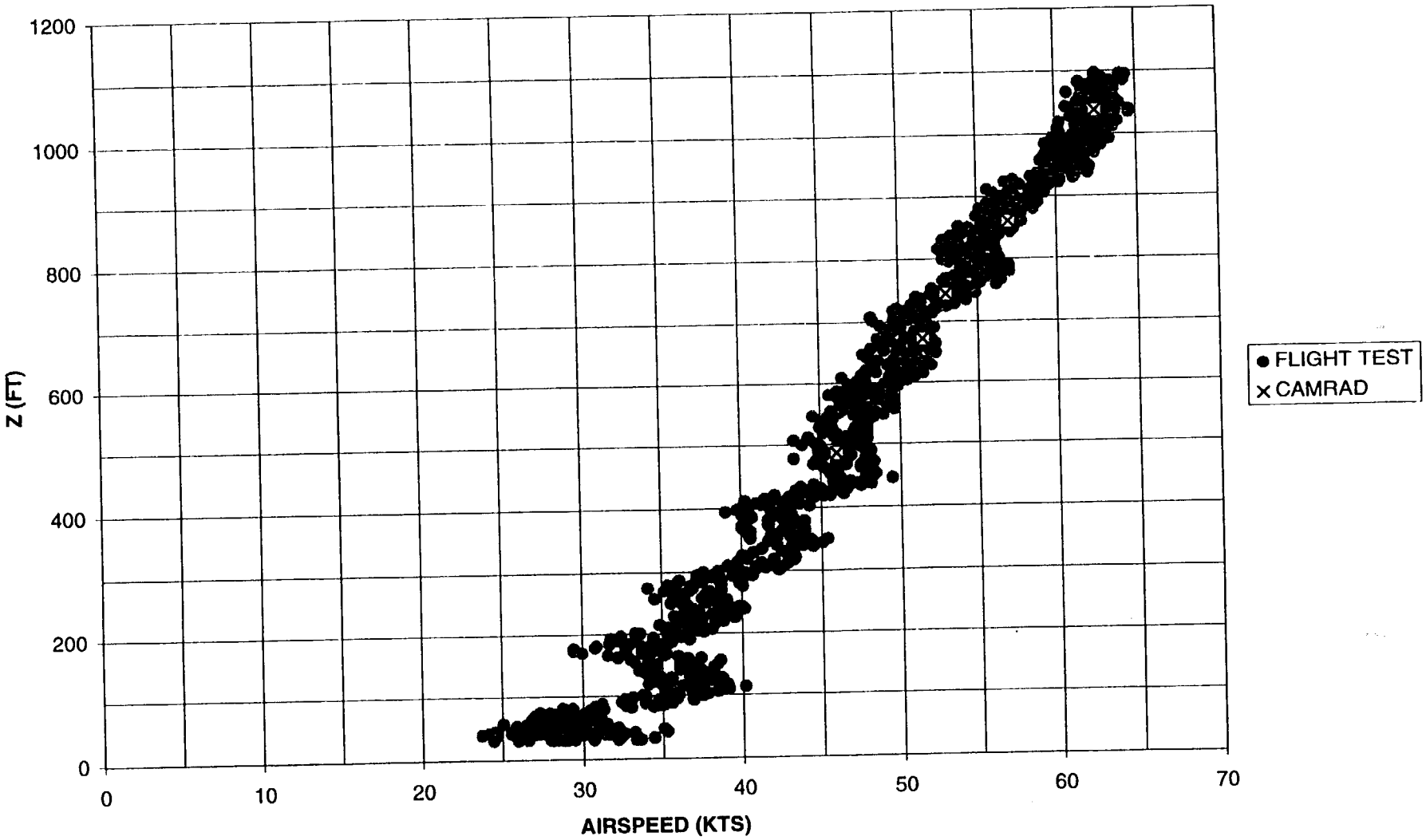

FIGURE 14 TRAJECTORY WITH AIRSPEED FOR TEST NUMBER 12563 (600 FT/MIN ROD)

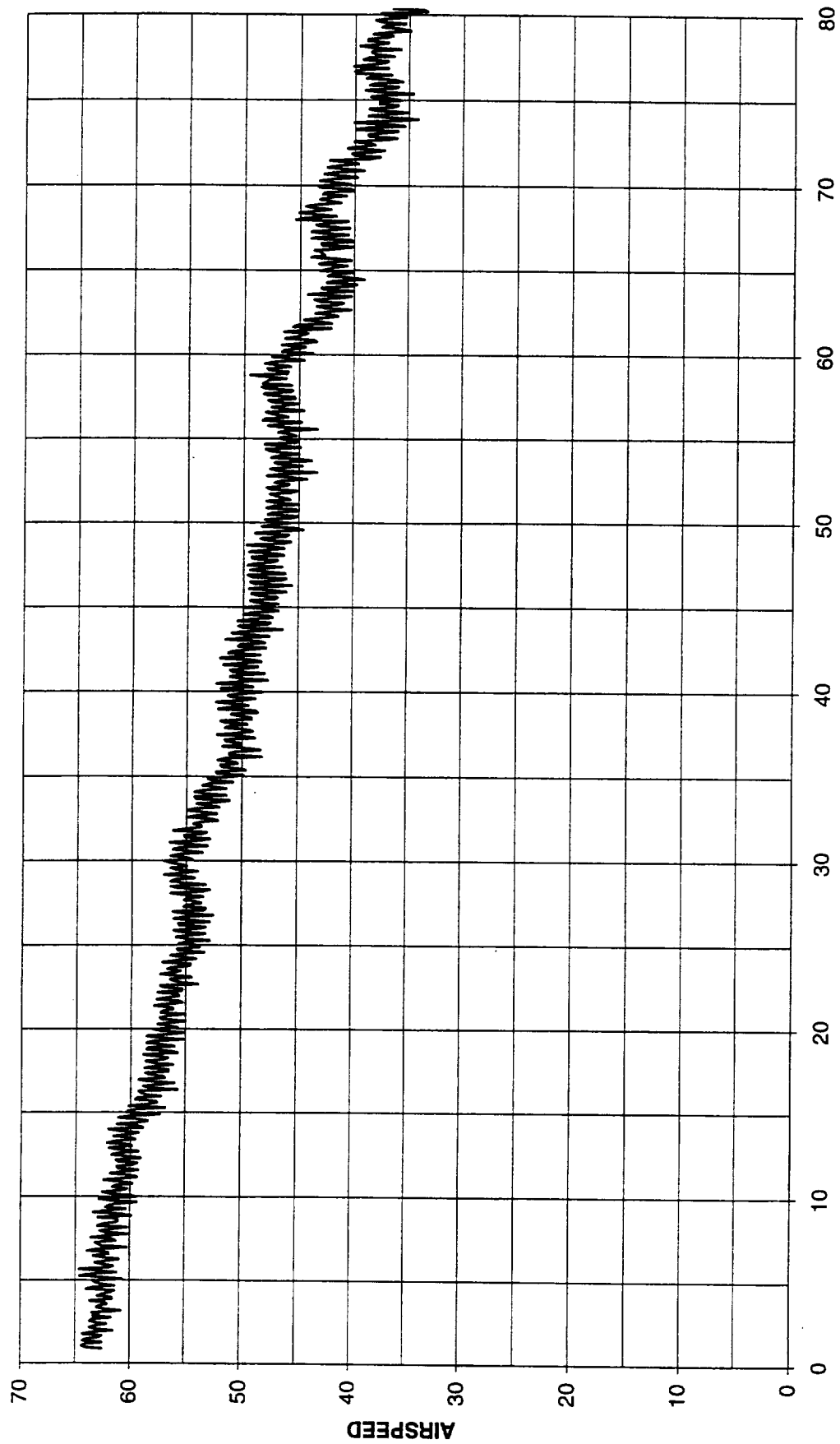

FIGURE 15 AIRSPEED DURING TRAJECTORY FOR TEST NUMBER 12563 (600 FT/MIN ROD)

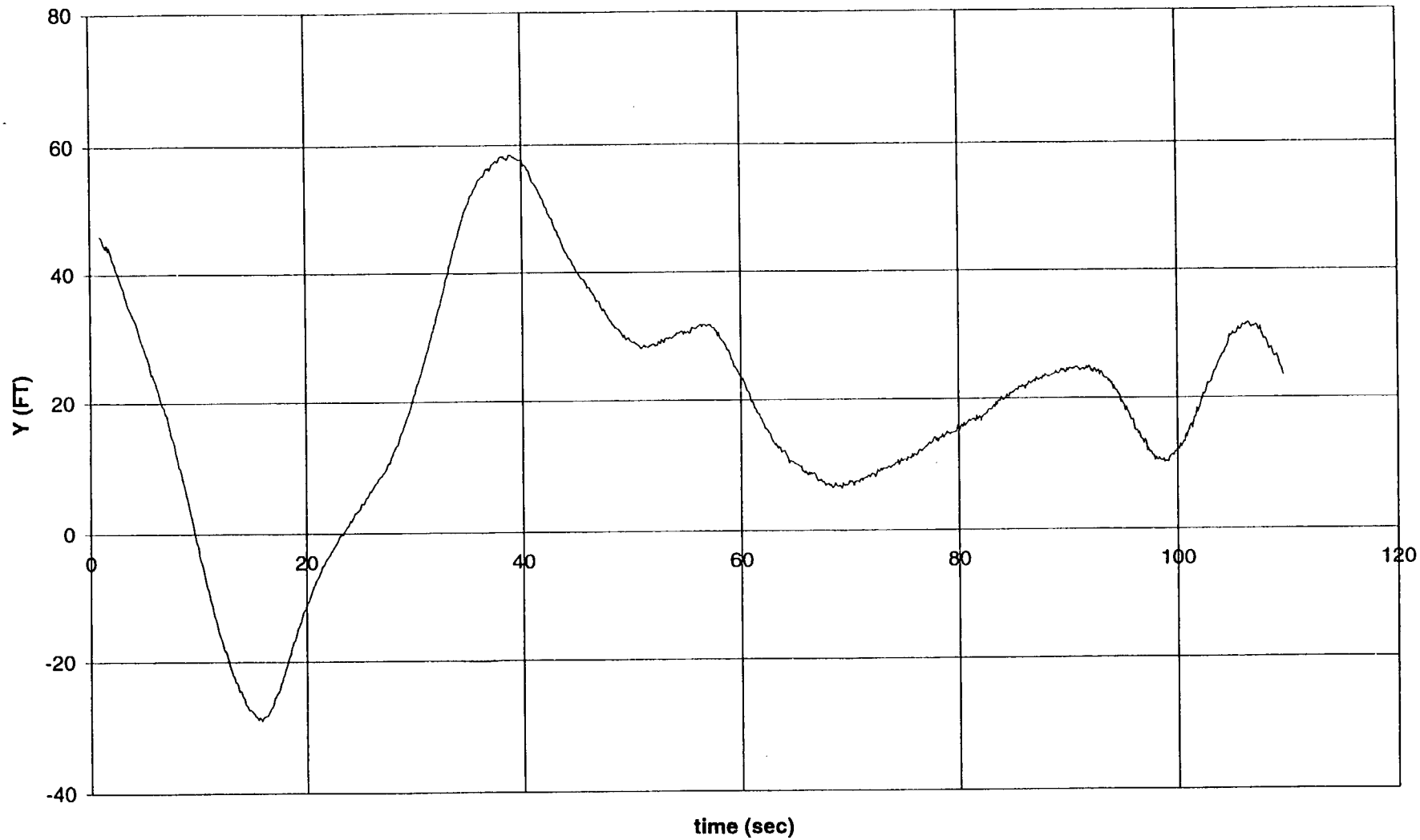

FIGURE 16 SIDEWARD DISTANCE DURING TRAJECTORY FOR TEST NUMBER 12563 (600 FT/MIN ROD)

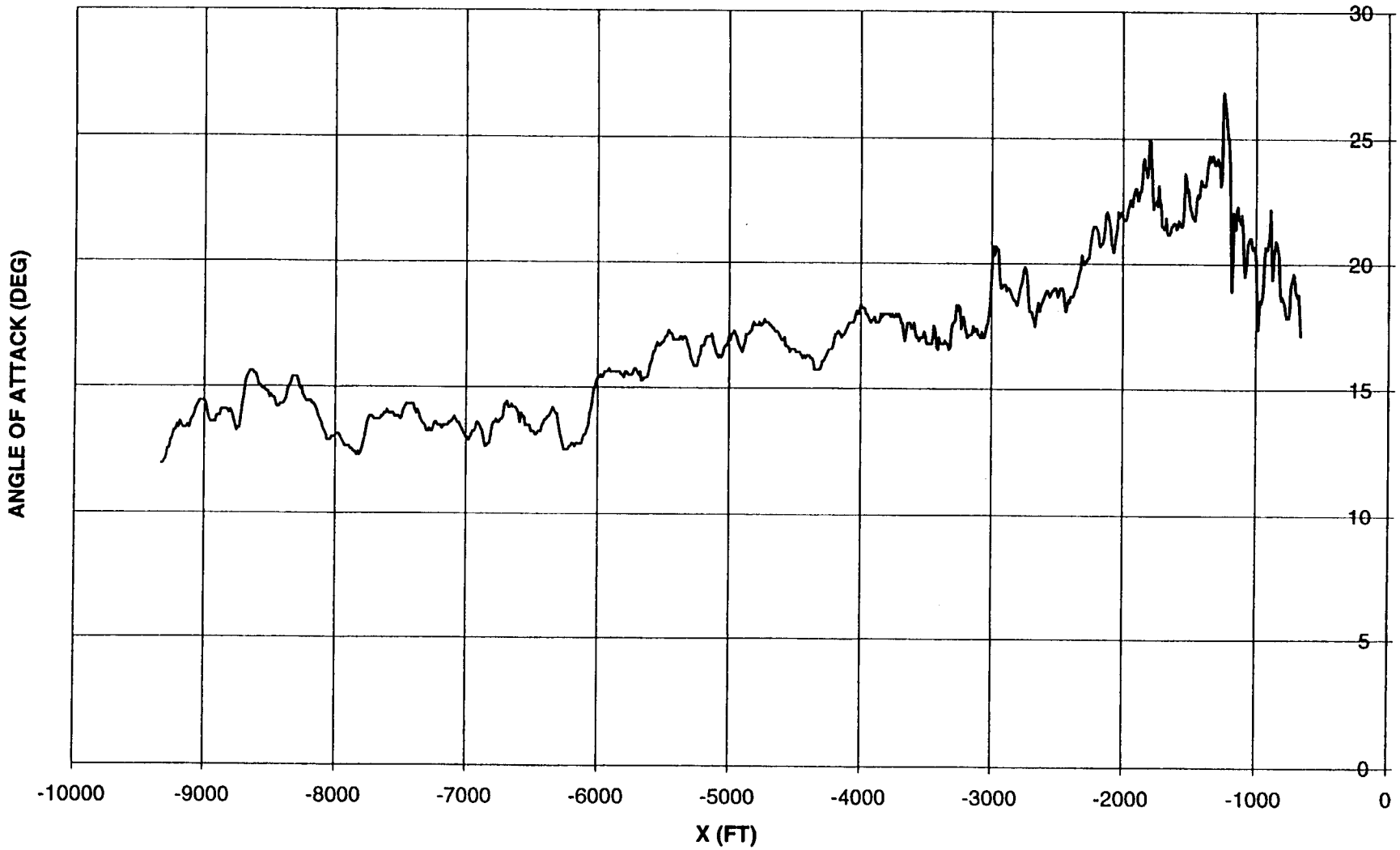

FIGURE 17 ANGLE OF ATTACK DURING TRAJECTORY FOR TEST NUMBER 12563 (600 FT/MIN ROD)

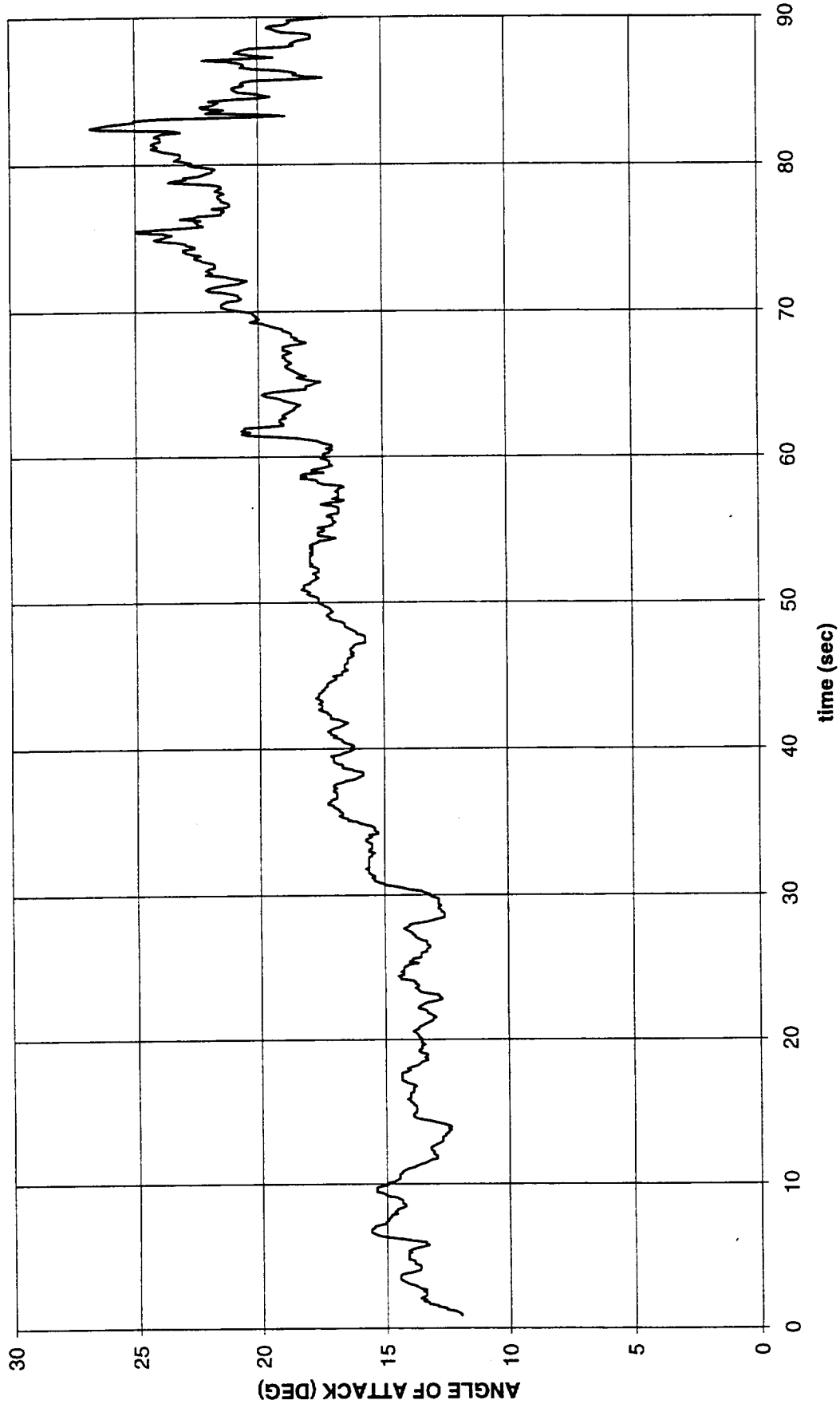

FIGURE 18 ANGLE OF ATTACK(WITH TIME) DURING TRAJECTORY FOR TEST NUMBER 12563 (600 FT/MIN ROD)

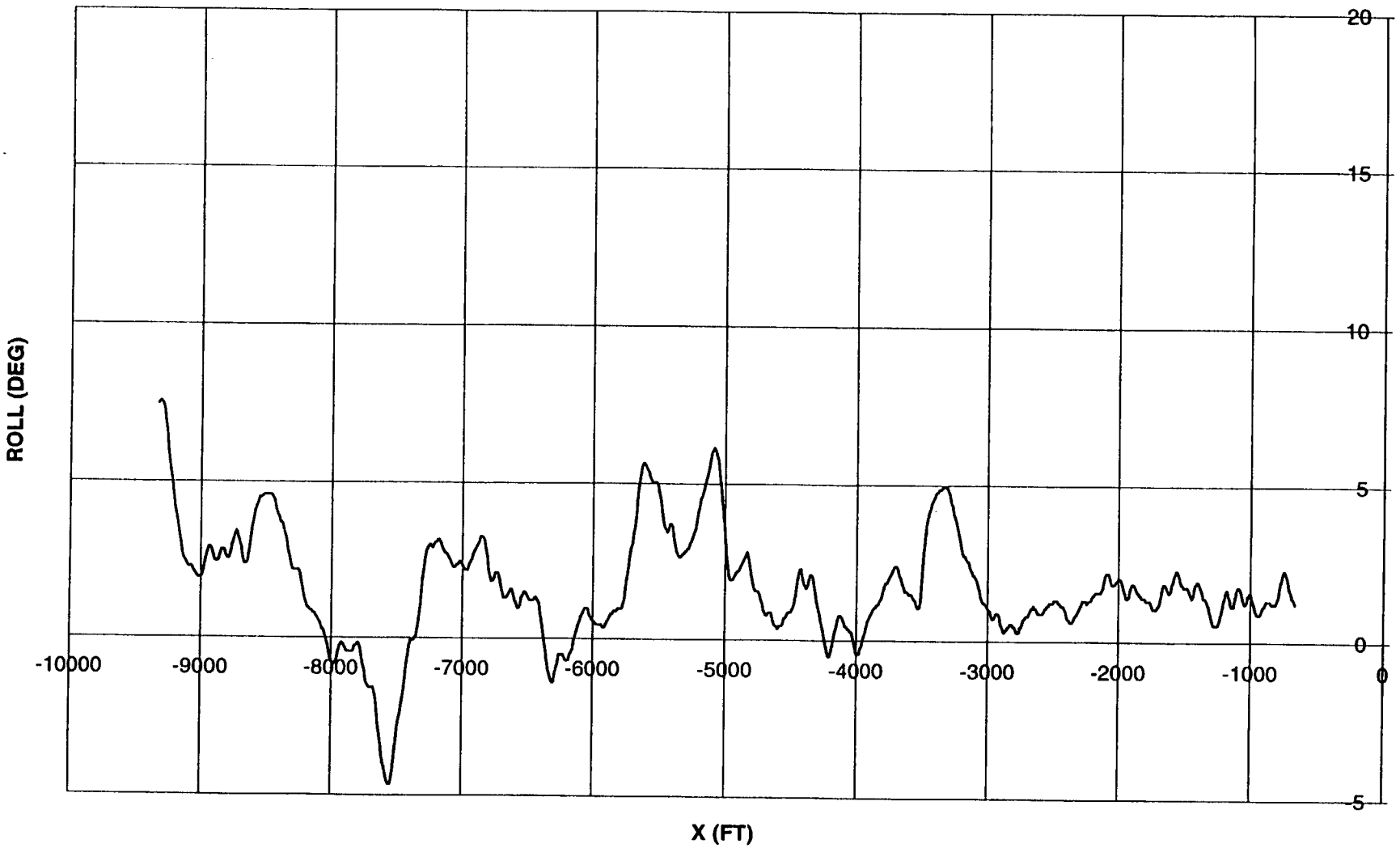

FIGURE 19 ROLL DURING TRAJECTORY (FLIGHT TEST DATA) FOR TEST NUMBER 12563 (600 FT/MIN ROD)

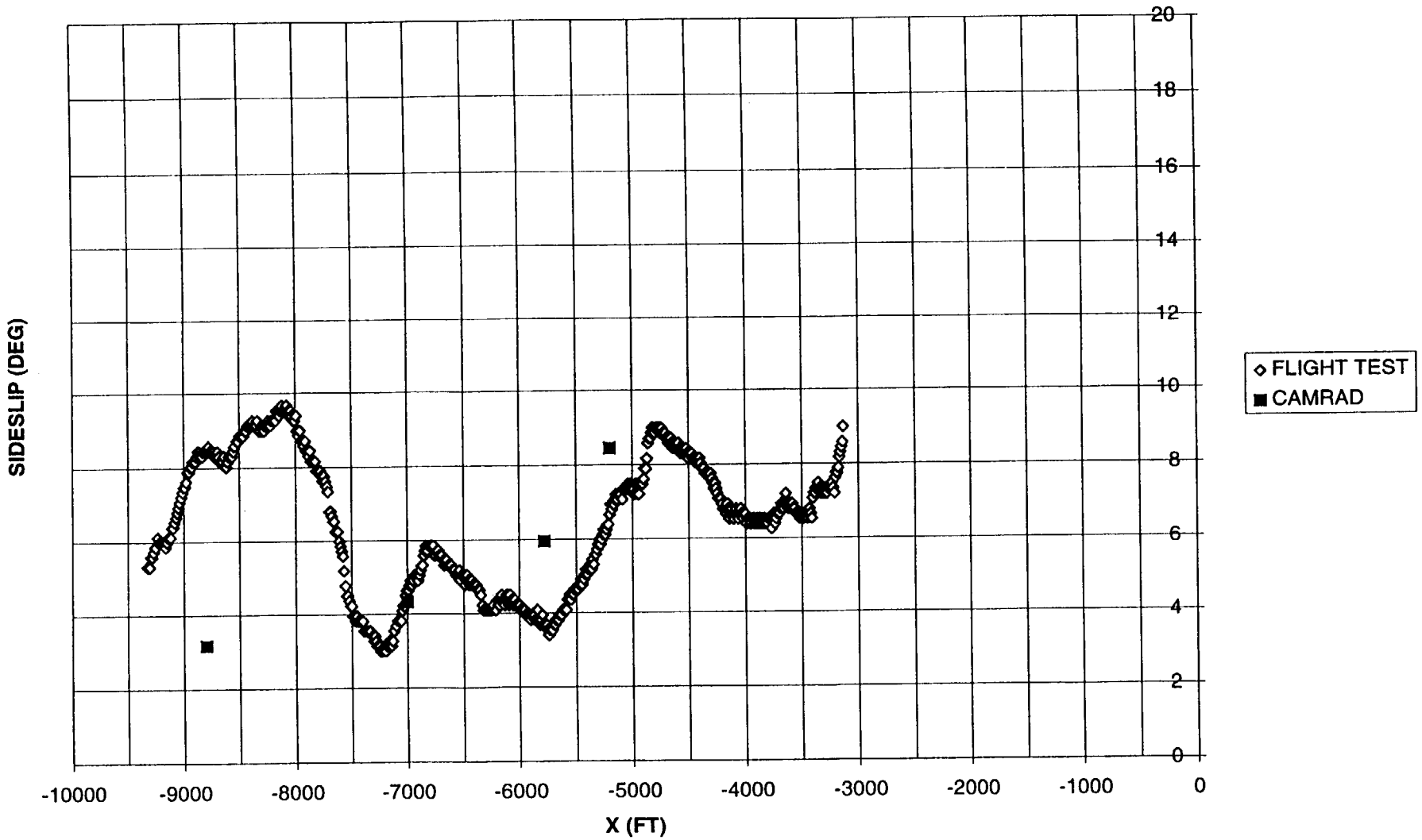

FIGURE 20 SIDESLIP DURING TRAJECTORY FOR TEST NUMBER 12563 (600 FT/MIN ROD)

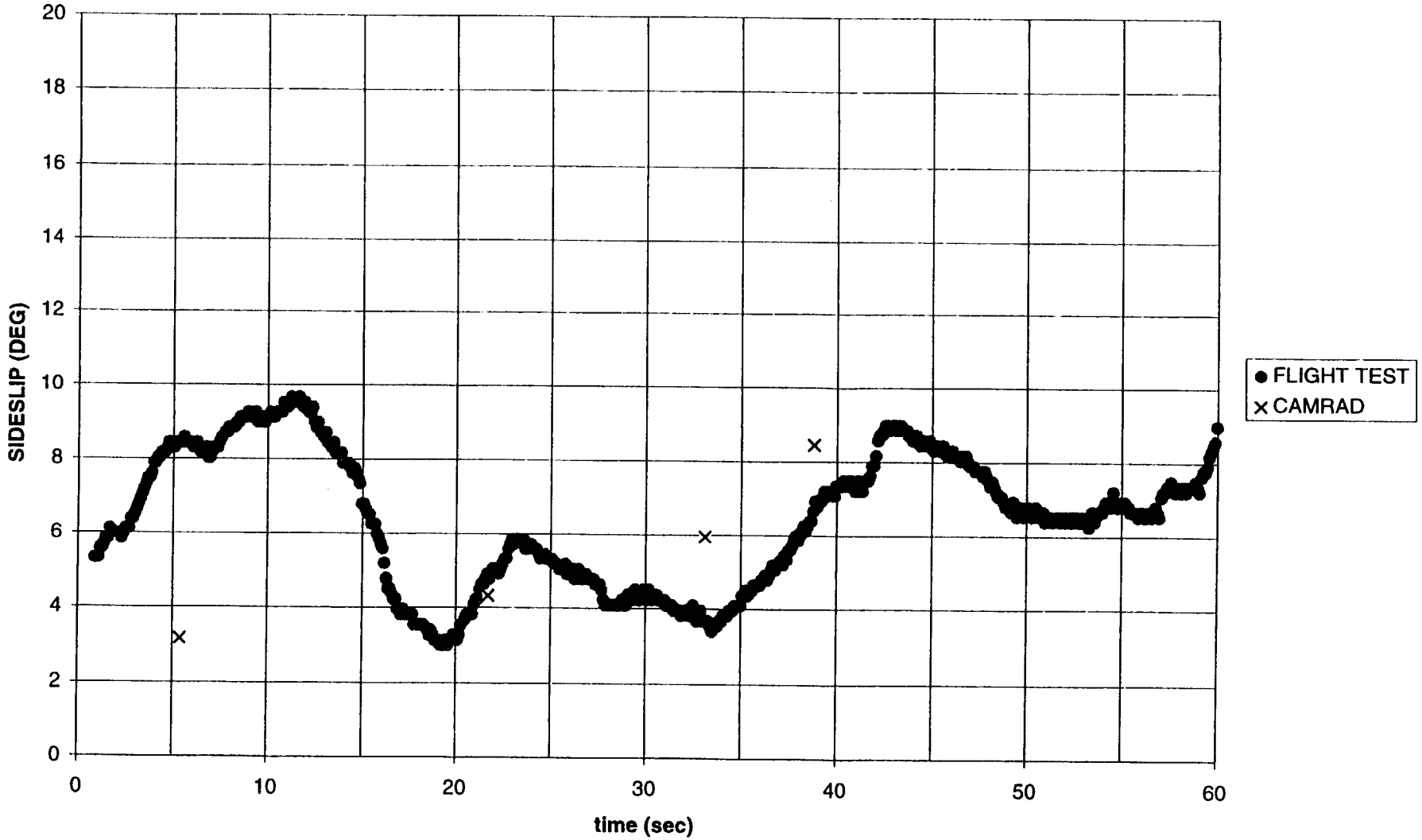

FIGURE 21 SIDESLIP DURING TRAJECTORY FOR TEST NUMBER 12563 (600 FT/MIN ROD)

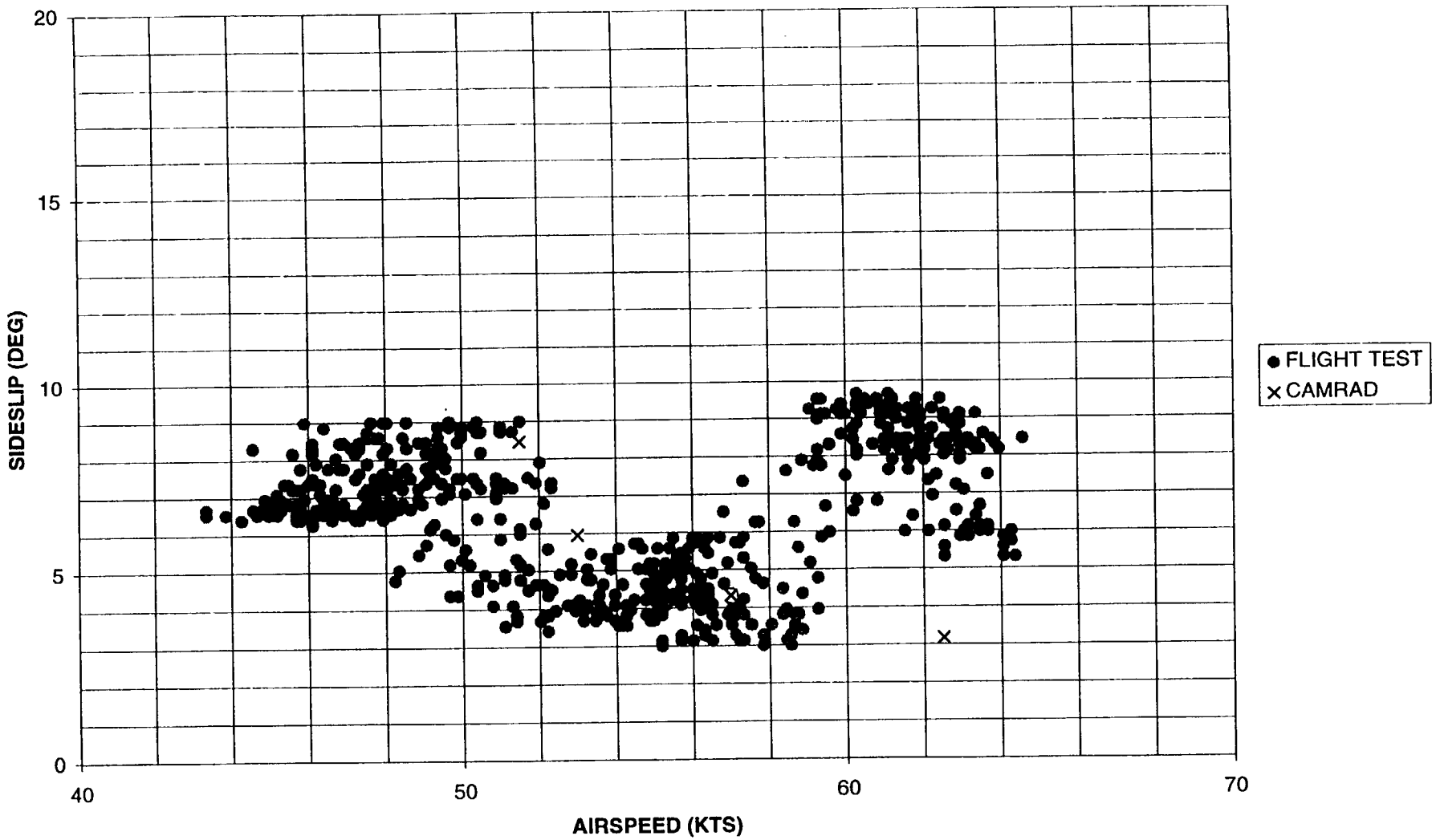

FIGURE 22 SIDESLIP DURING TRAJECTORY FOR TEST NUMBER 12563 (600 FT/MIN ROD)

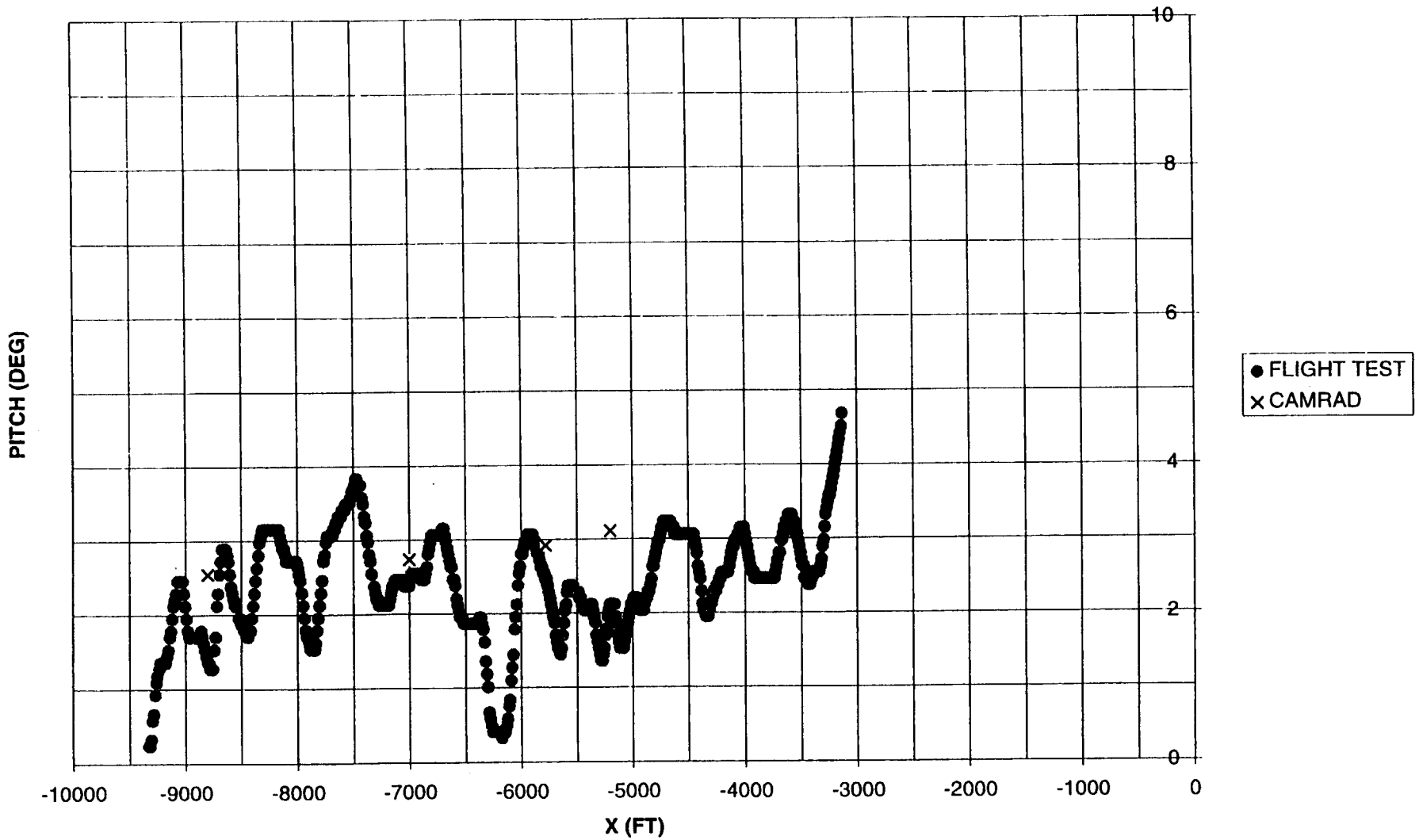

FIGURE 23 AIRCRAFT PITCH ANGLE DURING TRAJECTORY FOR TEST NUMBER 12563 (600 FT/MIN ROD)

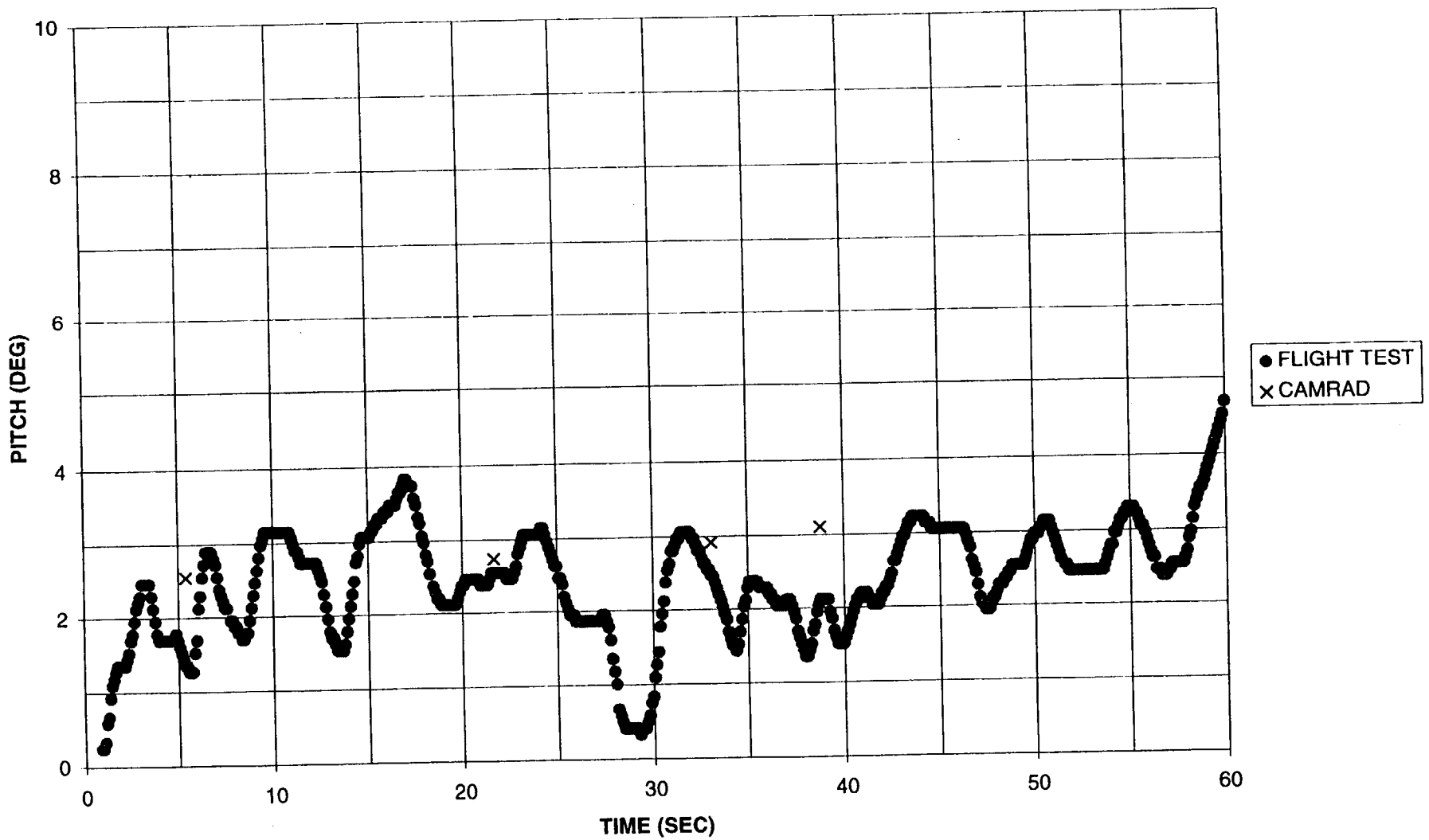

FIGURE 24 AIRCRAFT PITCH ANGLE (WITH TIME) DURING TRAJECTORY FOR TEST NUMBER 12563 (600 FT/MIN ROD)

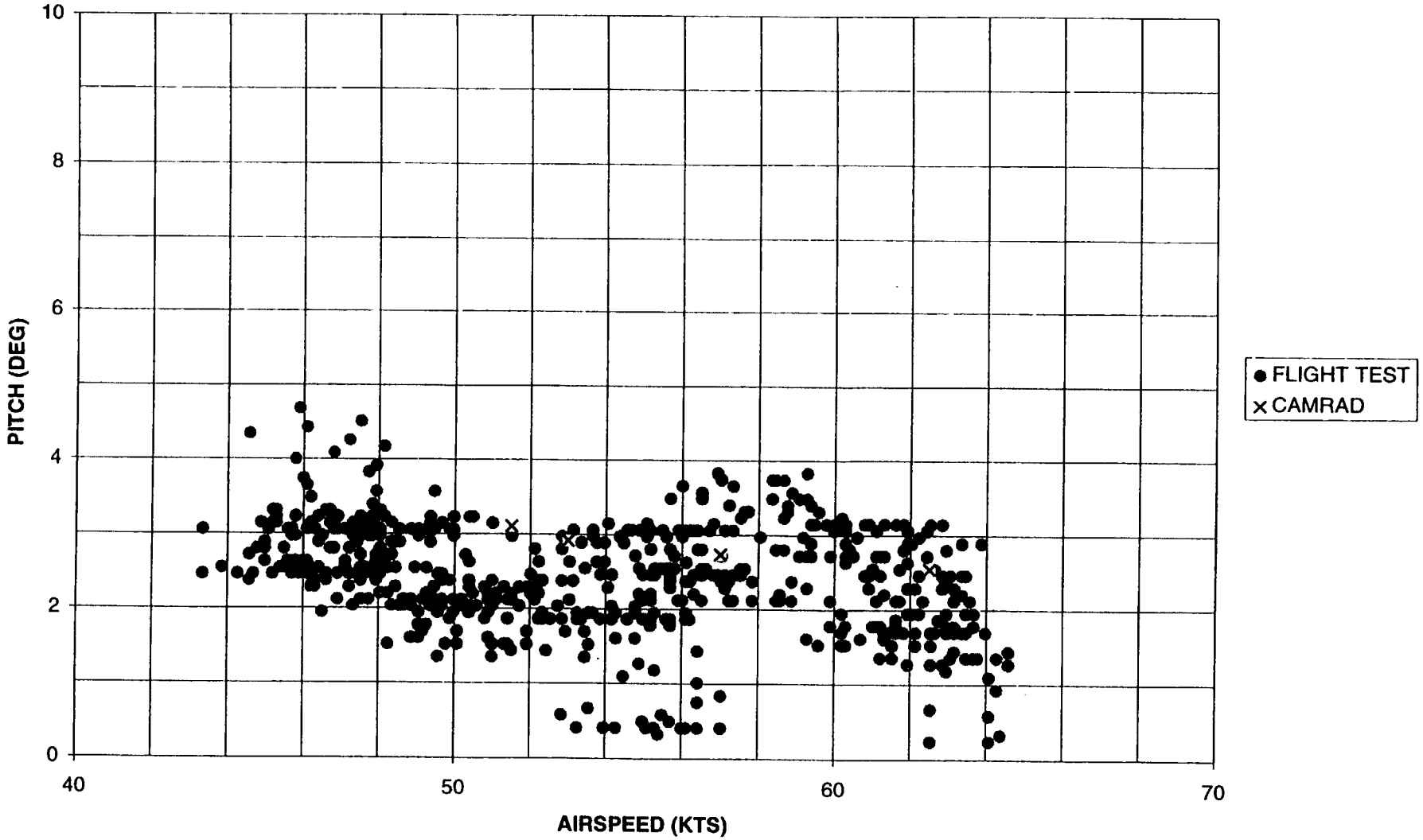

FIGURE 25 AIRCRAFT PITCH ANGLE (WITH AIRSPEED) DURING TRAJECTORY FOR TEST NUMBER 12563 (600 FT/MIN ROD)

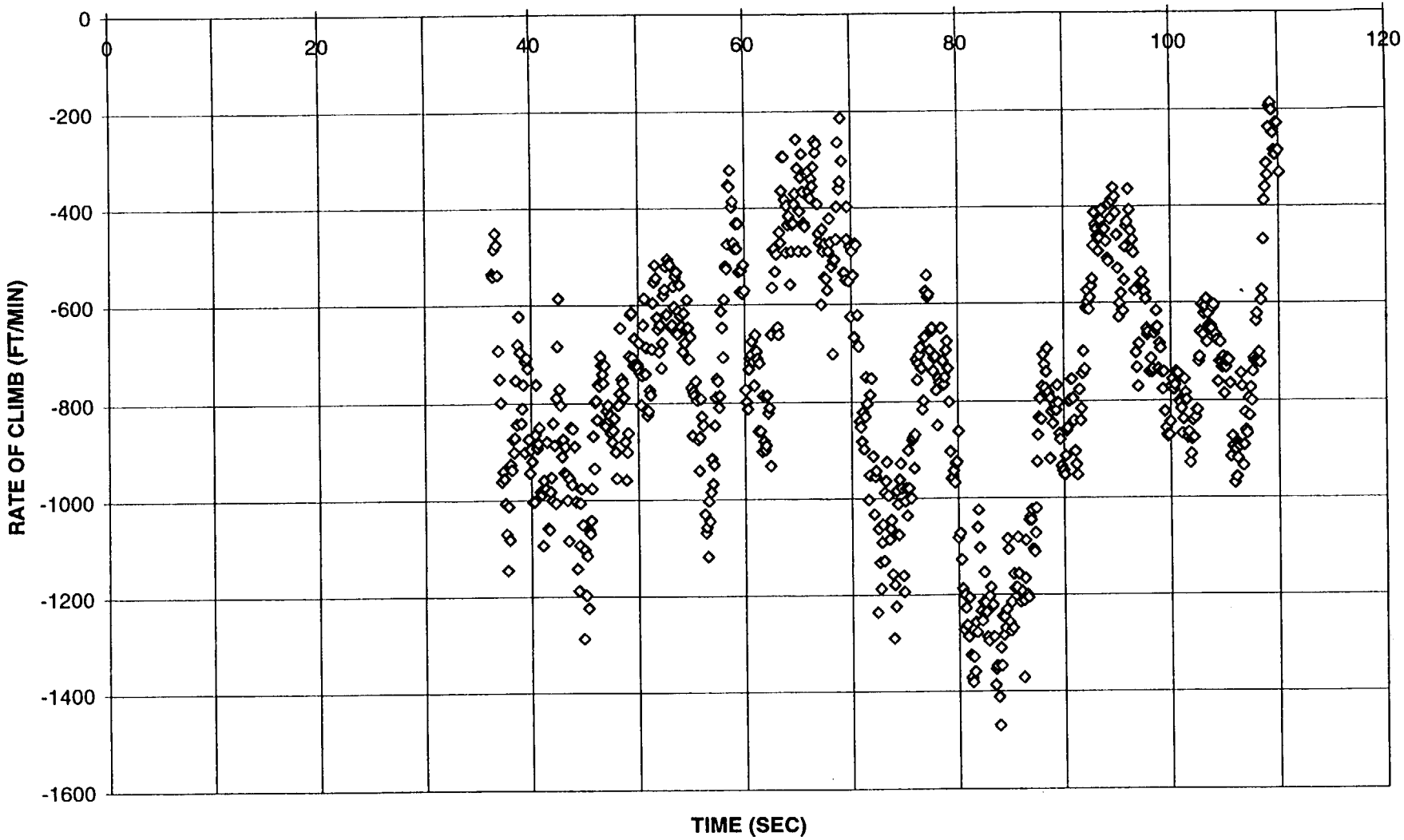

FIGURE 26 AIRCRAFT RATE OF CLIMB(WITH TIME) DURING TRAJECTORY FOR TEST NUMBER 12565 (600 FT/MIN ROD)

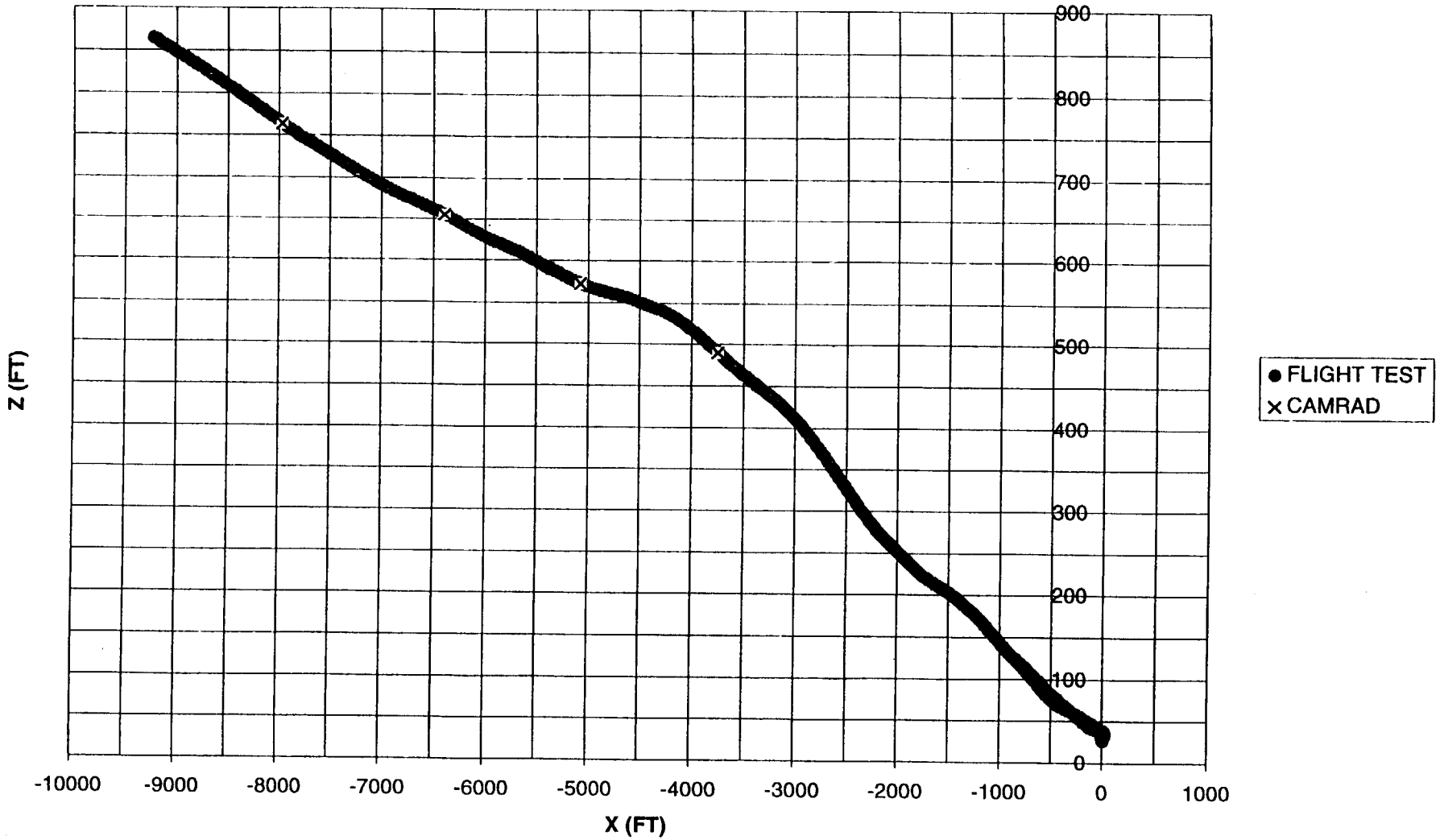

FIGURE 27 TRAJECTORY IN SPACE COORDINATES FOR TEST NUMBER 12565 (600 FT/MIN ROD)

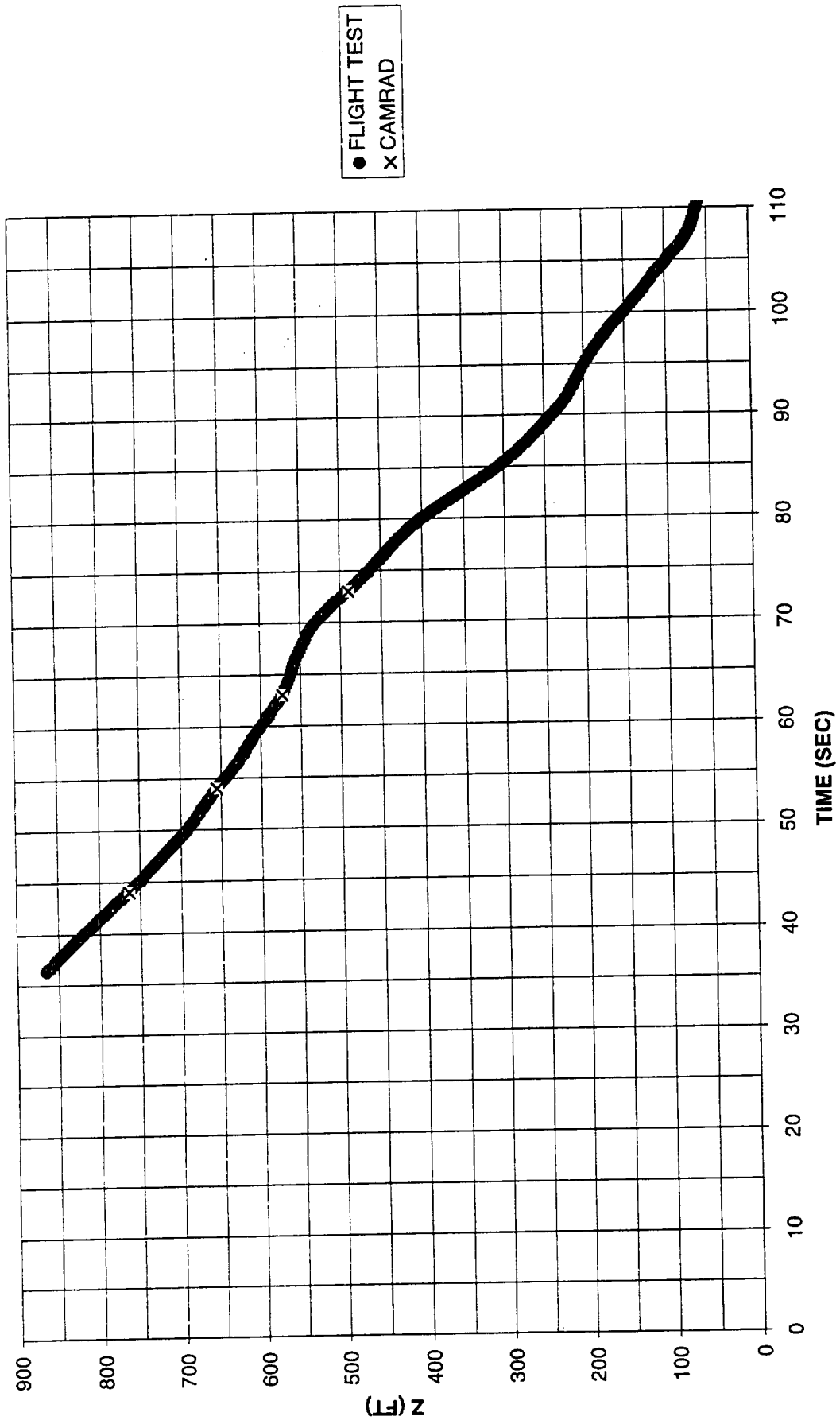

FIGURE 28 TRAJECTORY IN TIME FOR TEST NUMBER 12565 (600 FT/MIN ROD)

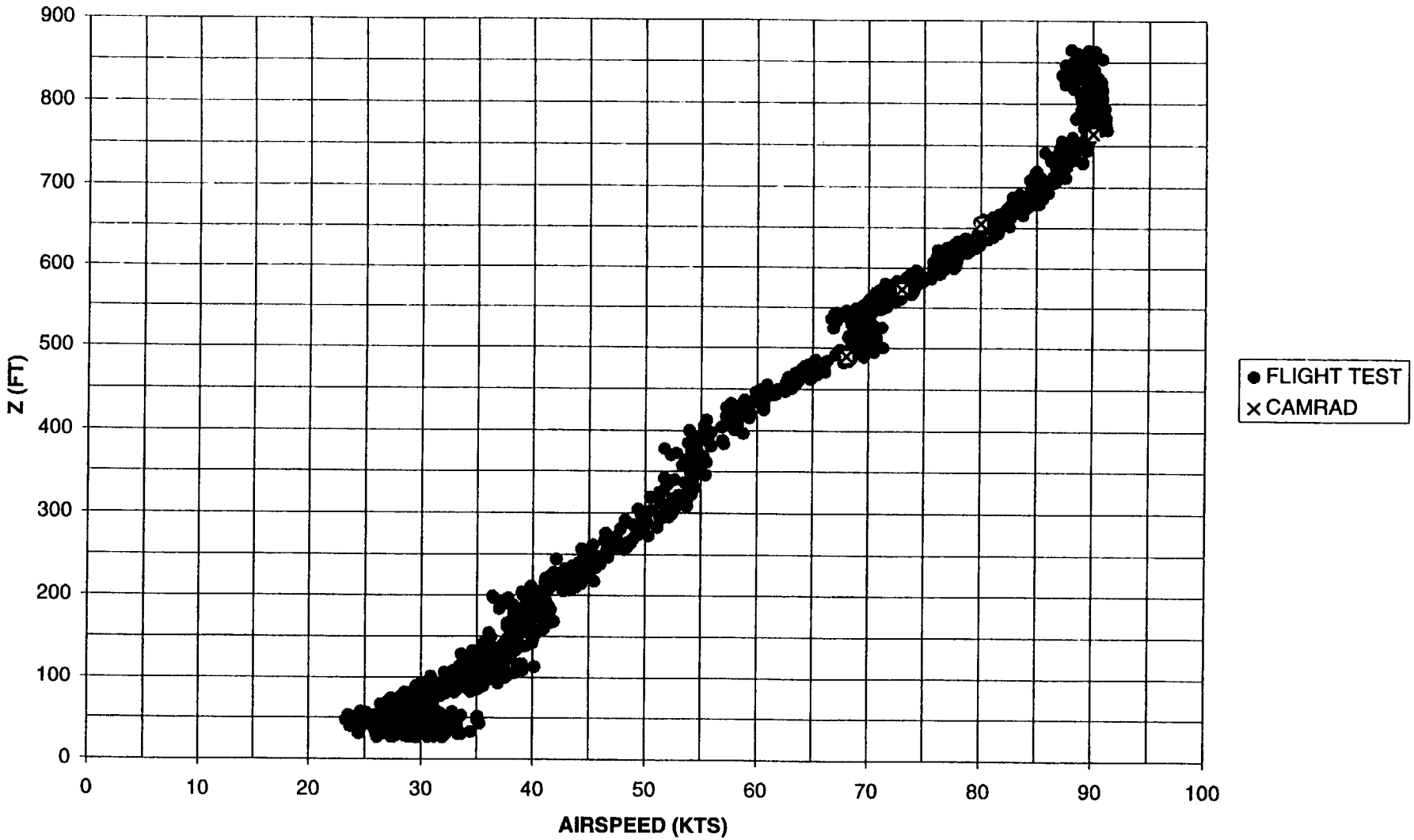

FIGURE 29 TRAJECTORY WITH AIRSPEED FOR TEST NUMBER 12565 (600 FT/MIN ROD)

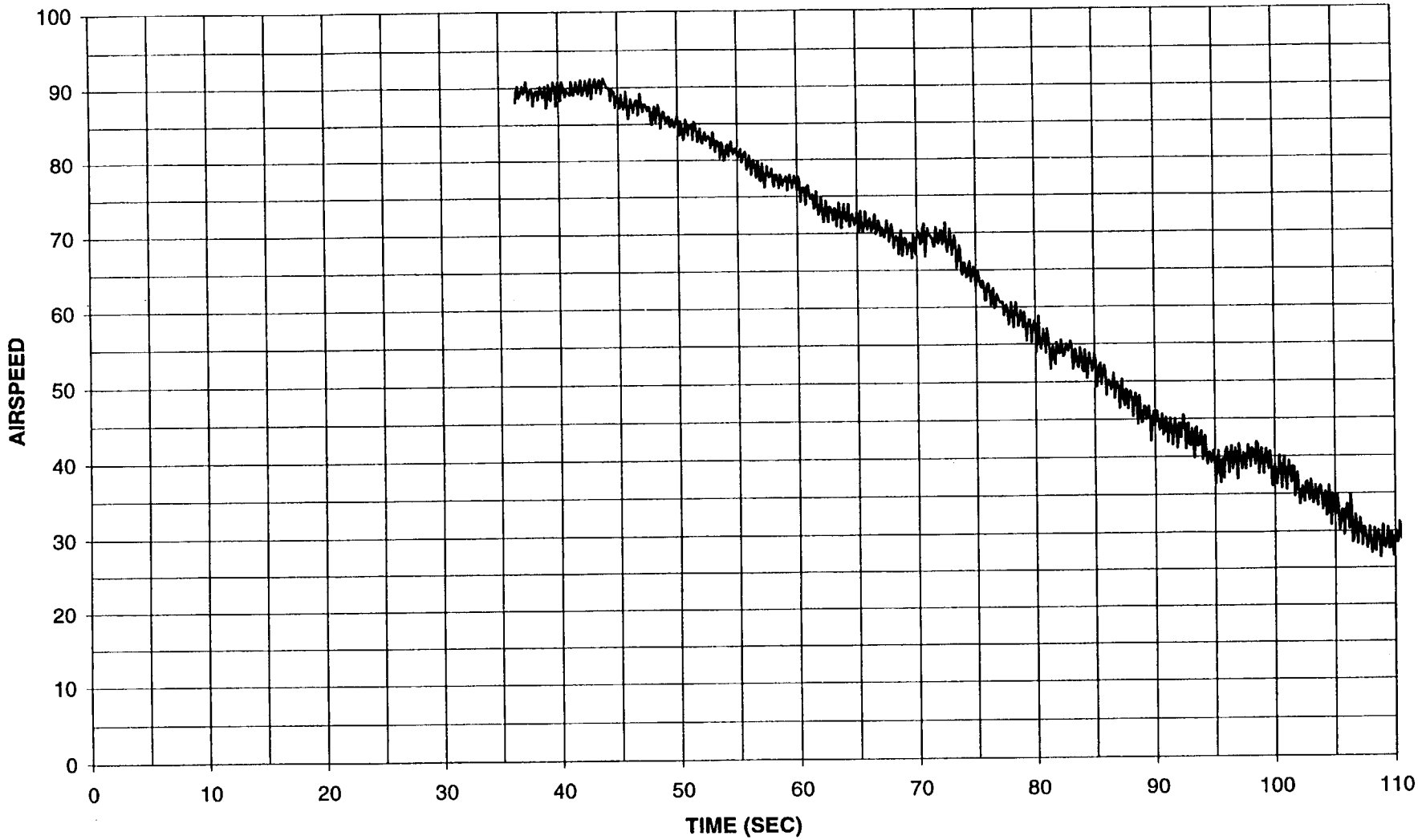

FIGURE 30 AIRSPEED DURING TRAJECTORY FOR TEST NUMBER 12565 (600 FT/MIN ROD)

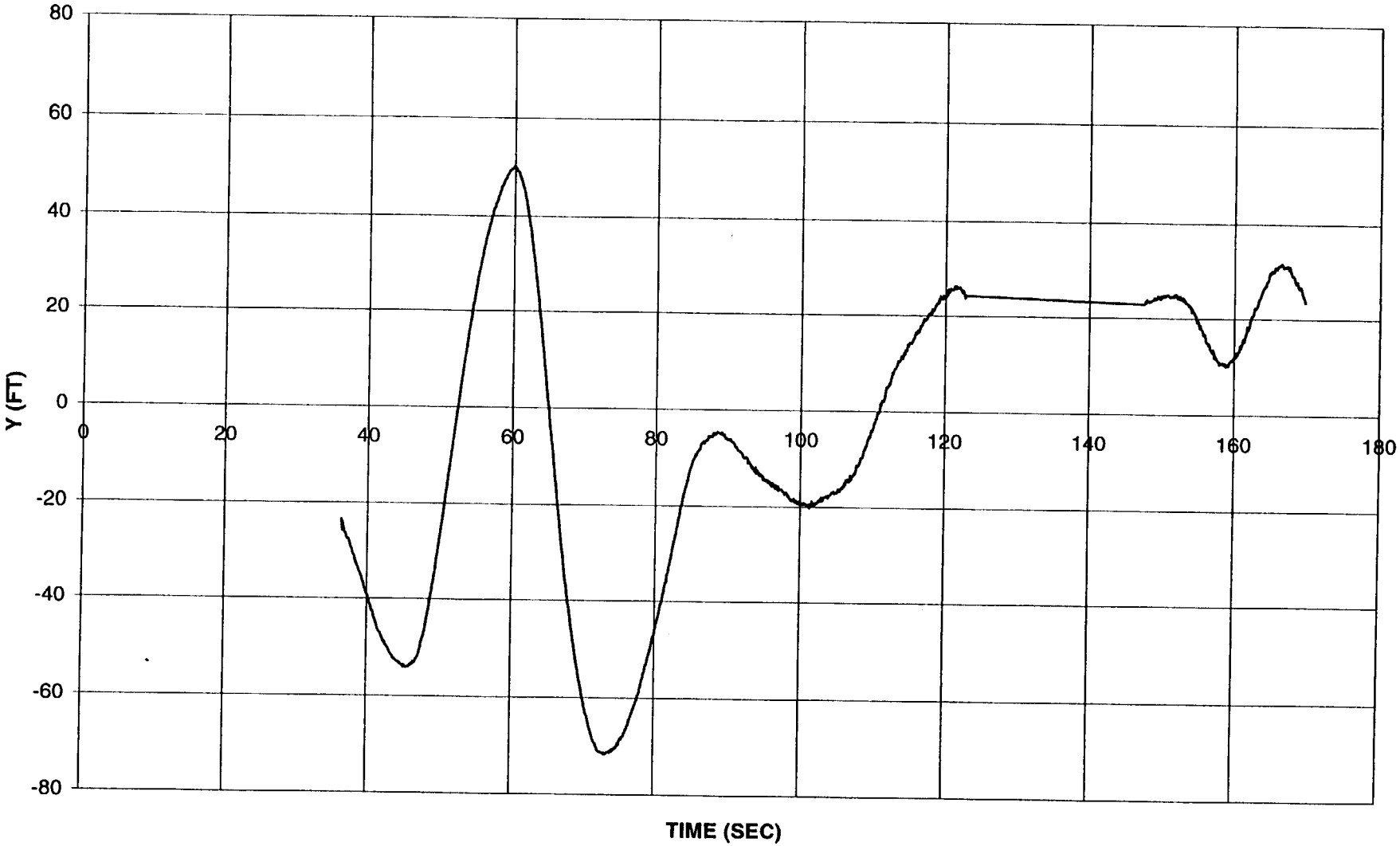

FIGURE 31 SIDEWARD DISTANCE DURING TRAJECTORY FOR TEST NUMBER 12565 (600 FT/MIN ROD)

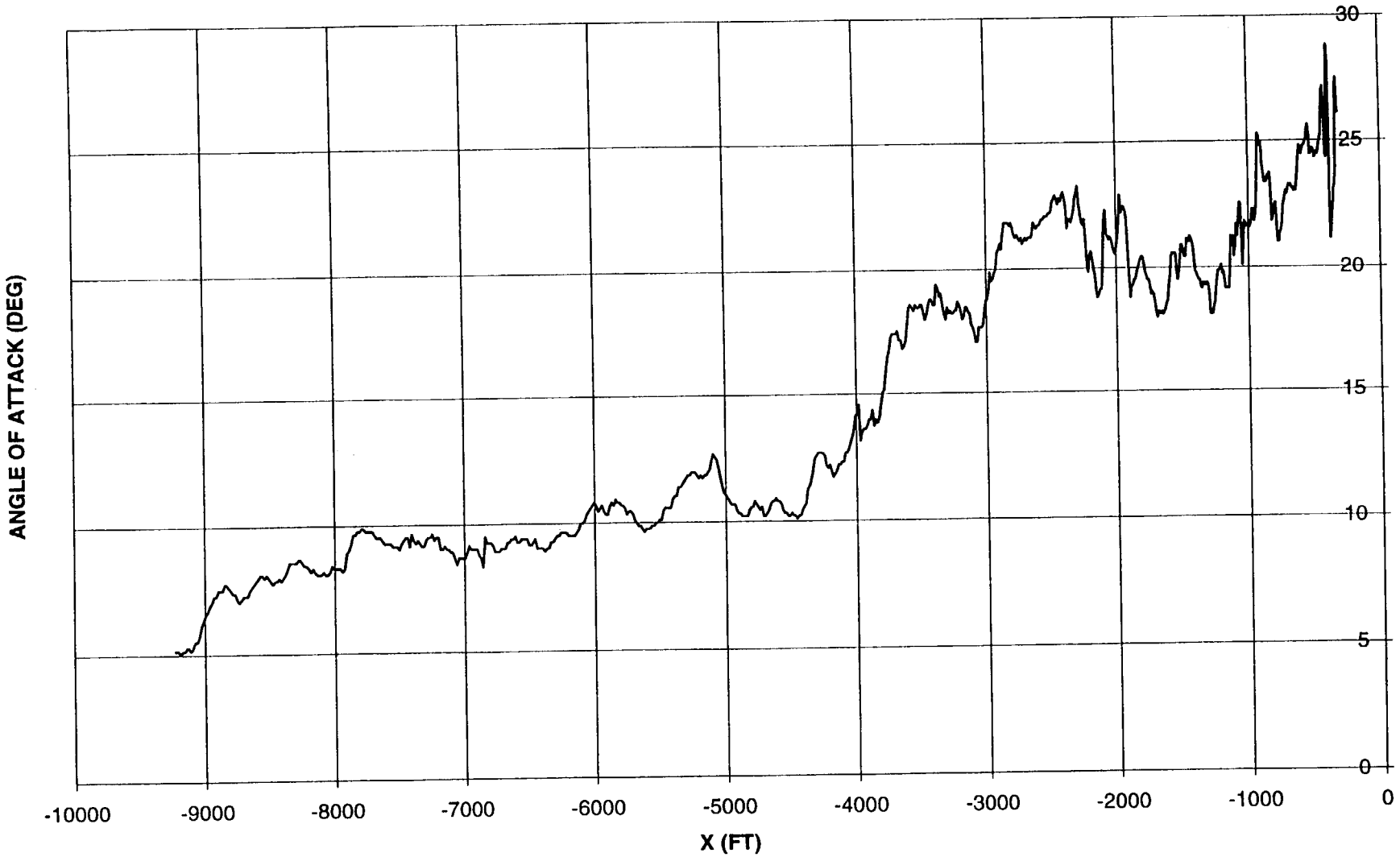

FIGURE 32 ANGLE OF ATTACK DURING TRAJECTORY FOR TEST NUMBER 12565 (600 FT/MIN ROD)

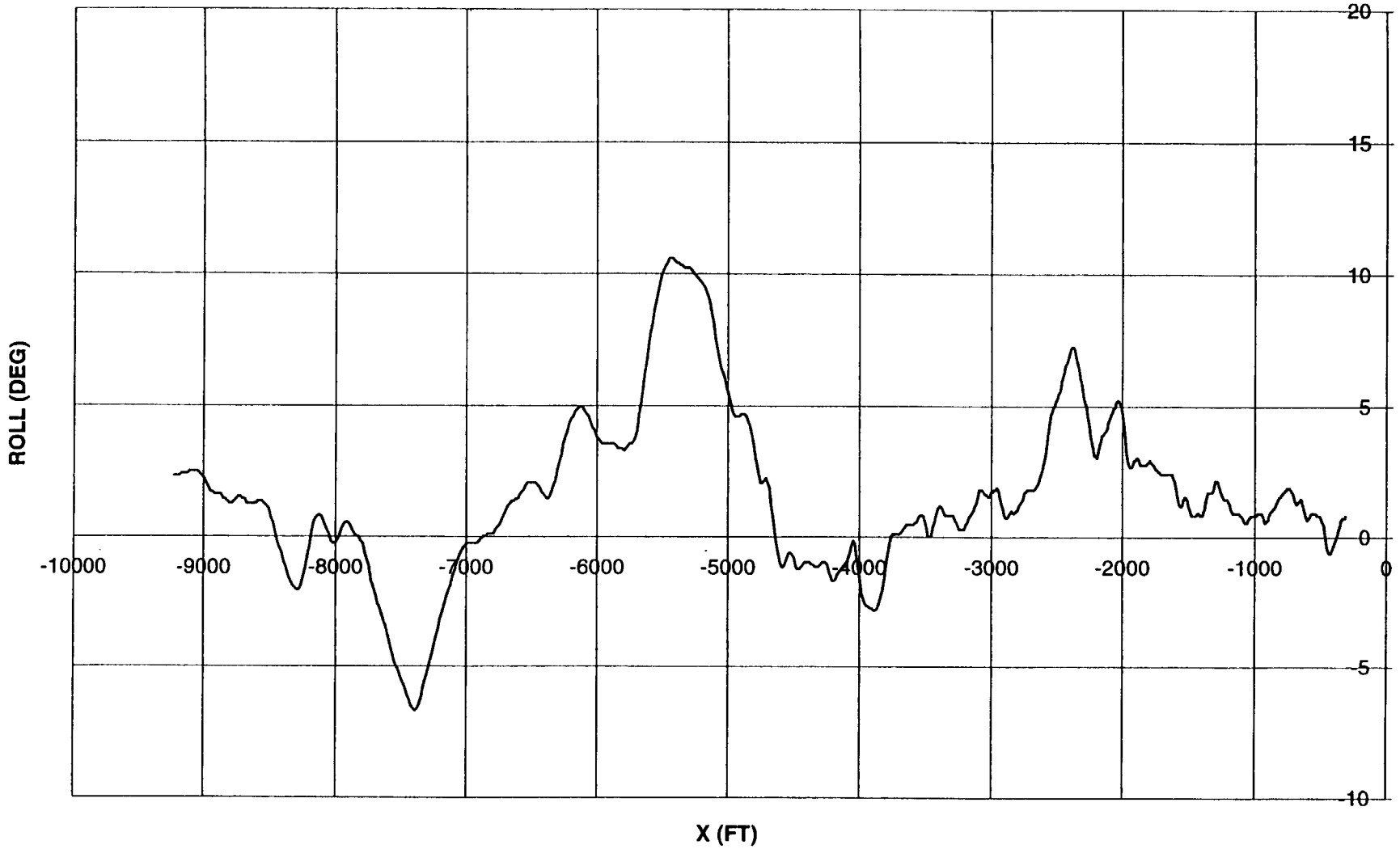

FIGURE 33 ROLL DURING TRAJECTORY (FLIGHT TEST DATA) FOR TEST NUMBER 12565 (600 FT/MIN ROD)

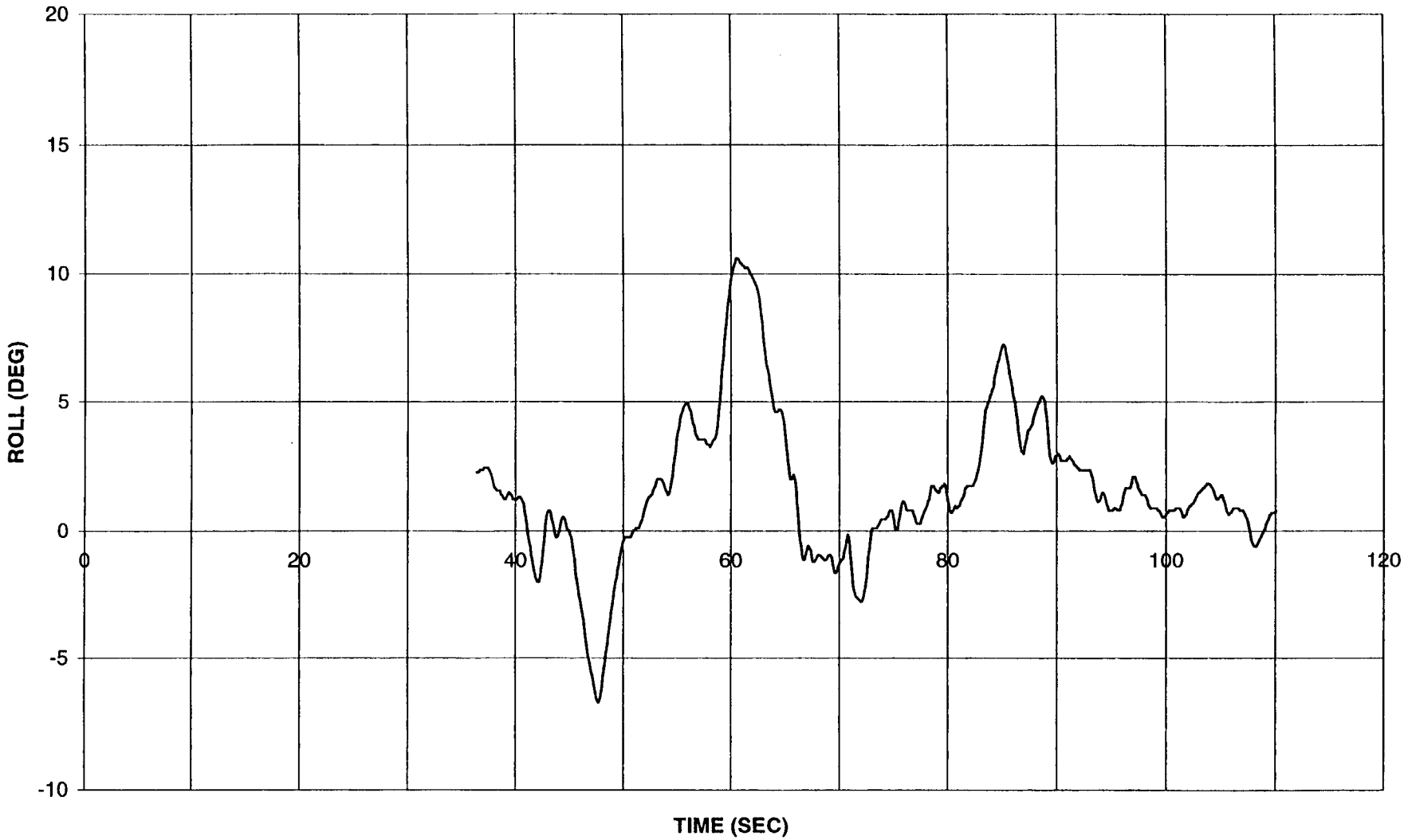

FIGURE 34 ROLL DURING TRAJECTORY (FLIGHT TEST DATA) FOR TEST NUMBER 12565 (600 FT/MIN ROD)

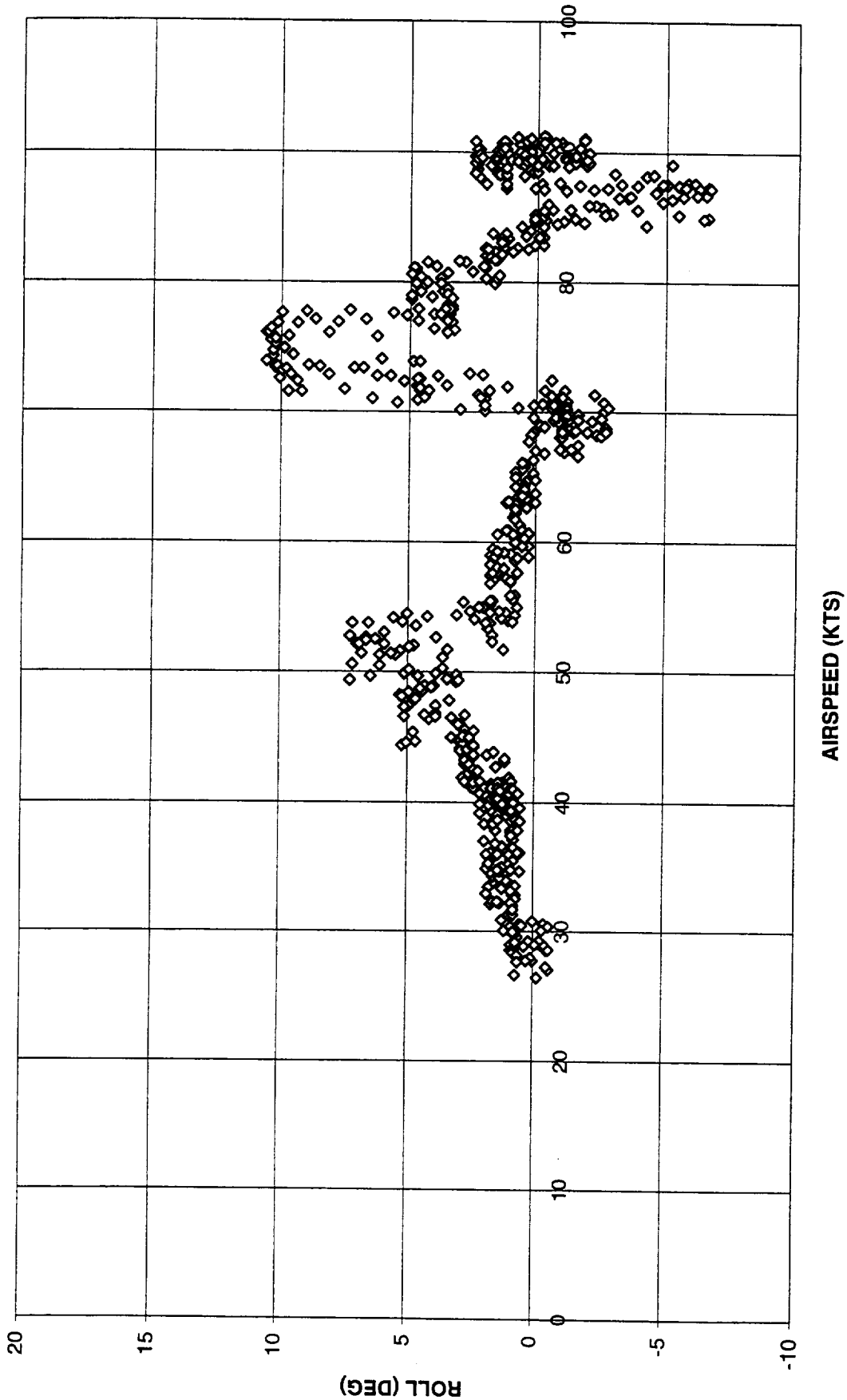

FIGURE 35 ROLL DURING TRAJECTORY (FLIGHT TEST DATA) FOR TEST NUMBER 12565 (600 FT/MIN ROD)

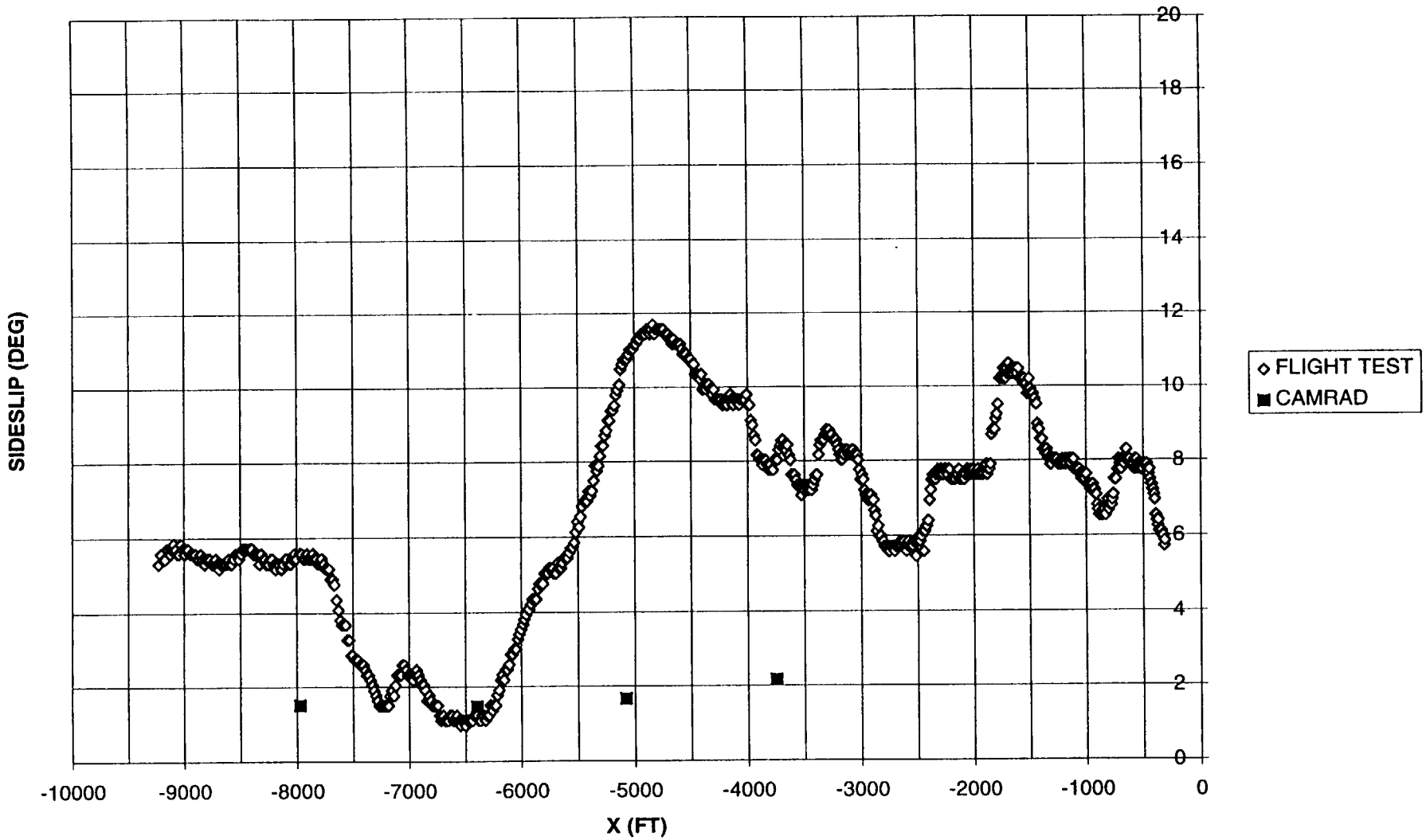

FIGURE 36 SIDESLIP DURING TRAJECTORY FOR TEST NUMBER 12565 (600 FT/MIN ROD)

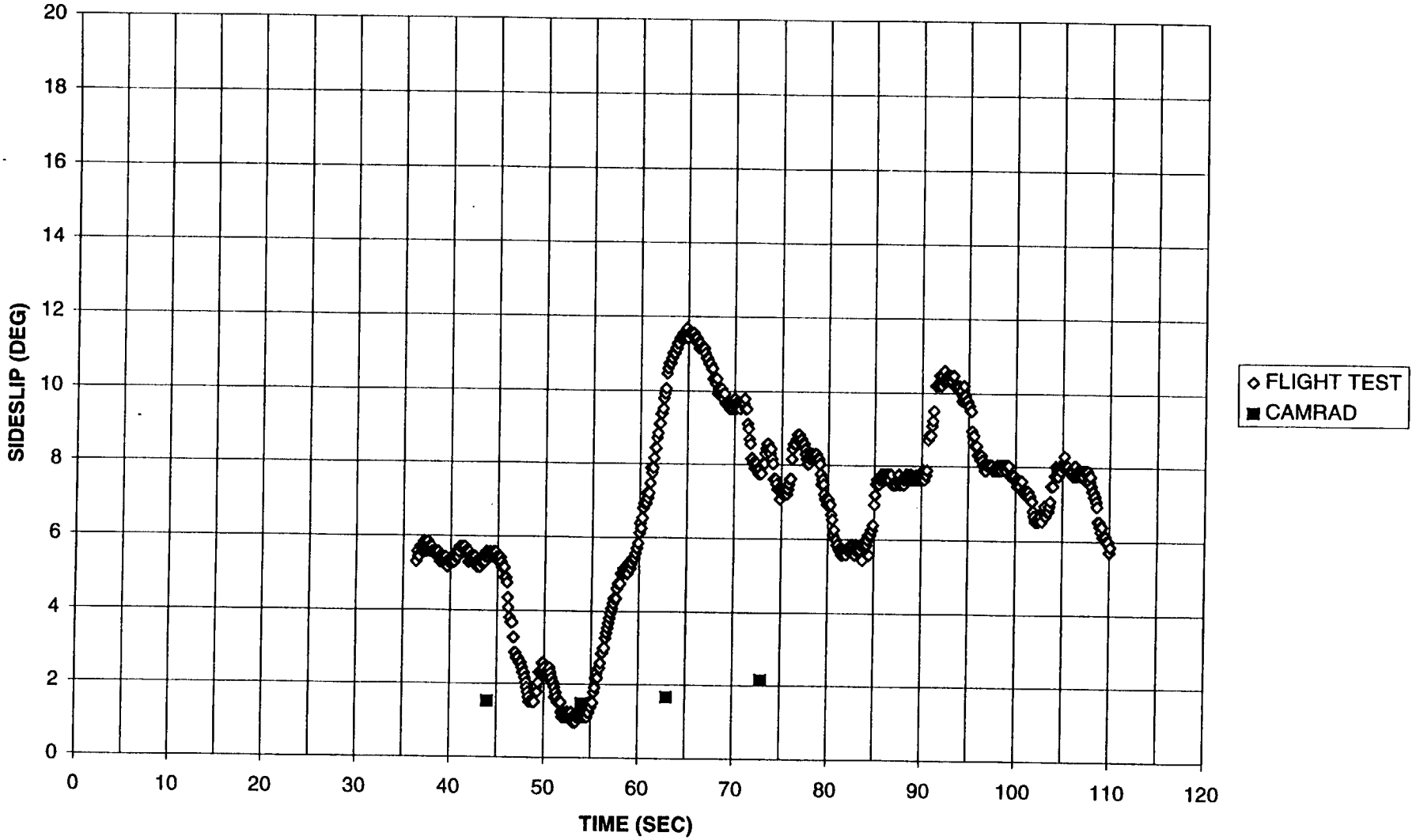

FIGURE 37 SIDESLIP TRAJECTORY FOR TEST NUMBER 12565 (600 FT/MIN ROD)

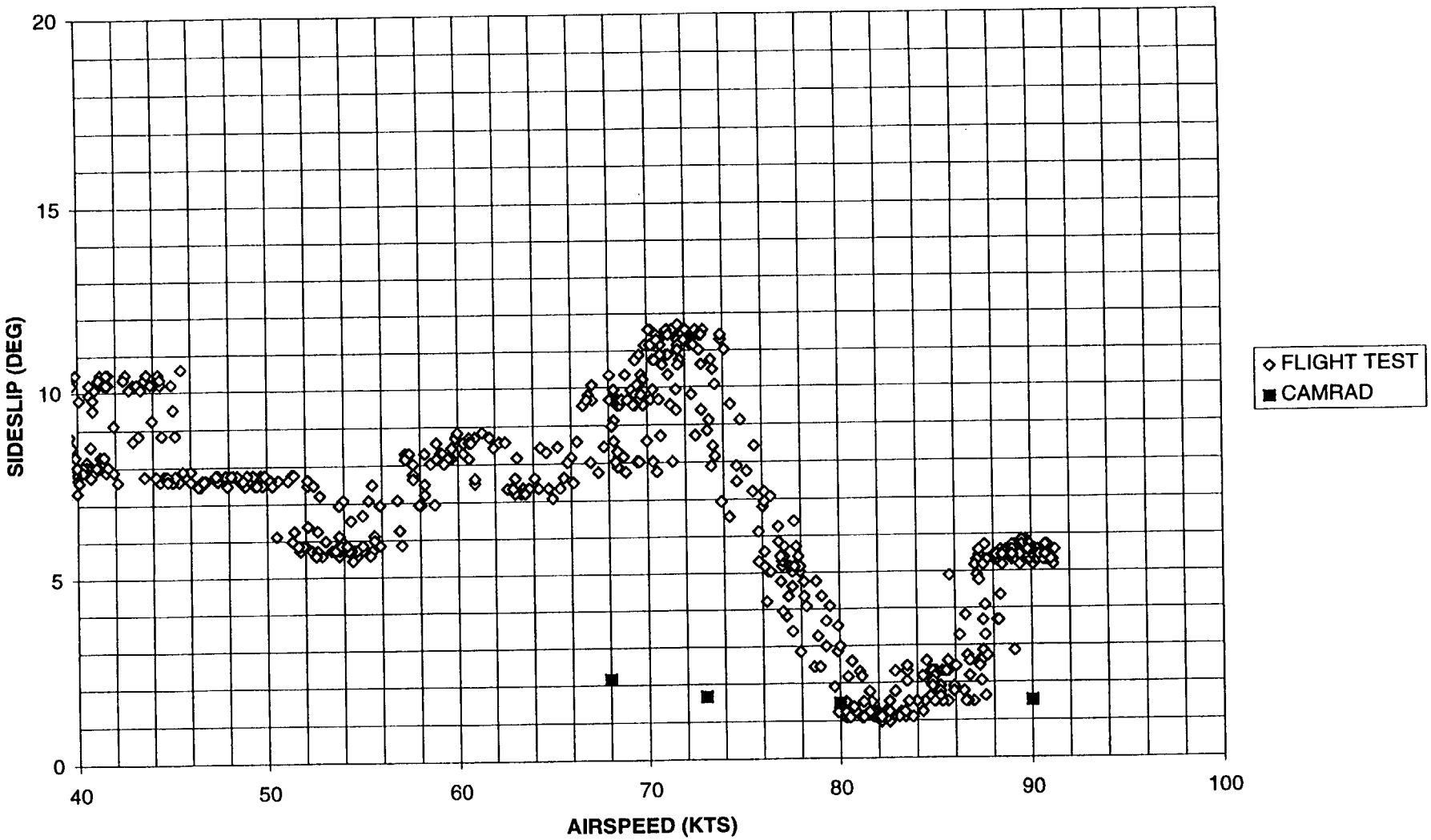

FIGURE 38 SIDESLIP DURING TRAJECTORY FOR TEST DURING 12565 (600 FT/MIN ROD)

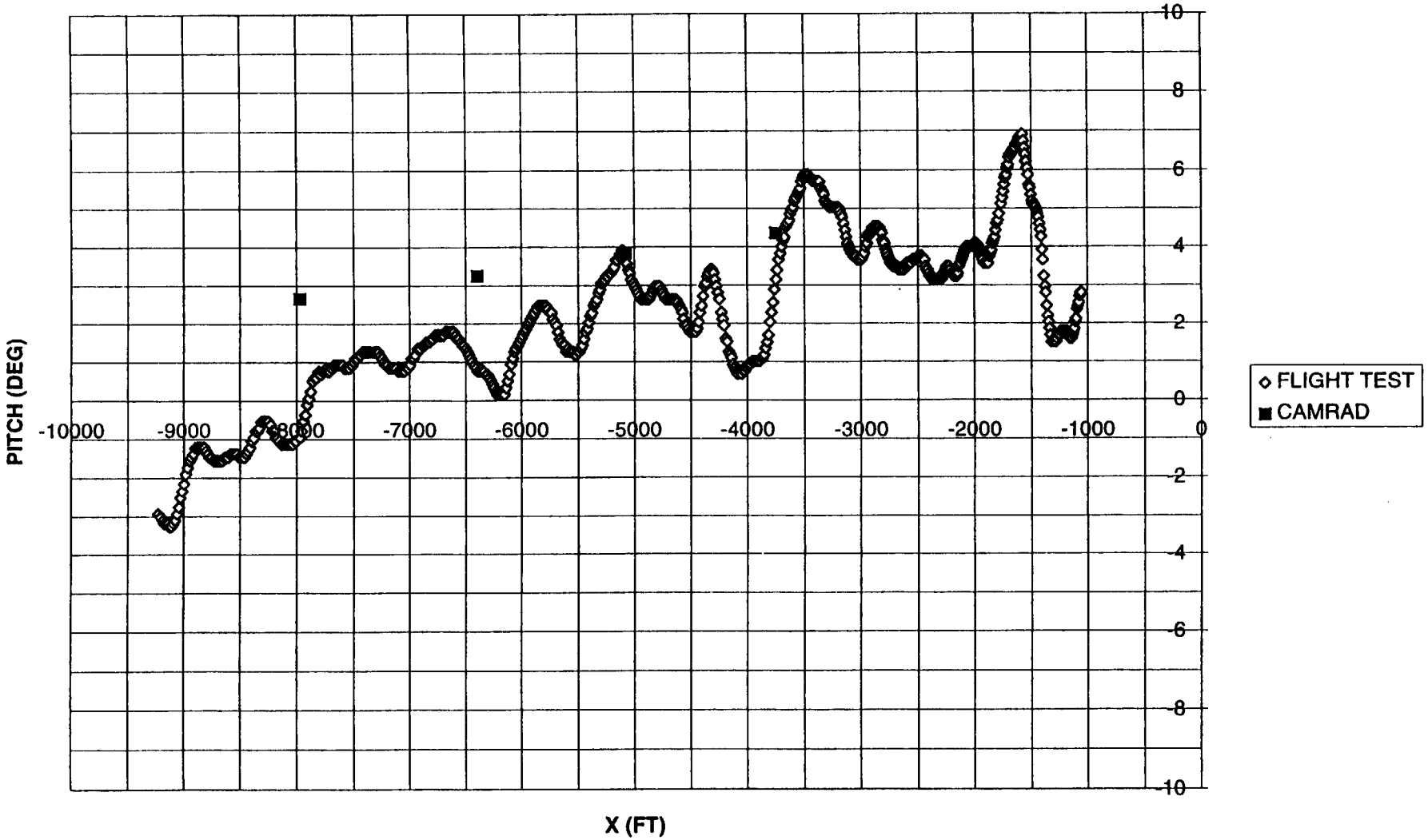

FIGURE 39 AIRCRAFT PITCH ANGLE DURING TRAJECTORY FOR TEST NUMBER 12565 (600 FT/MIN ROD)

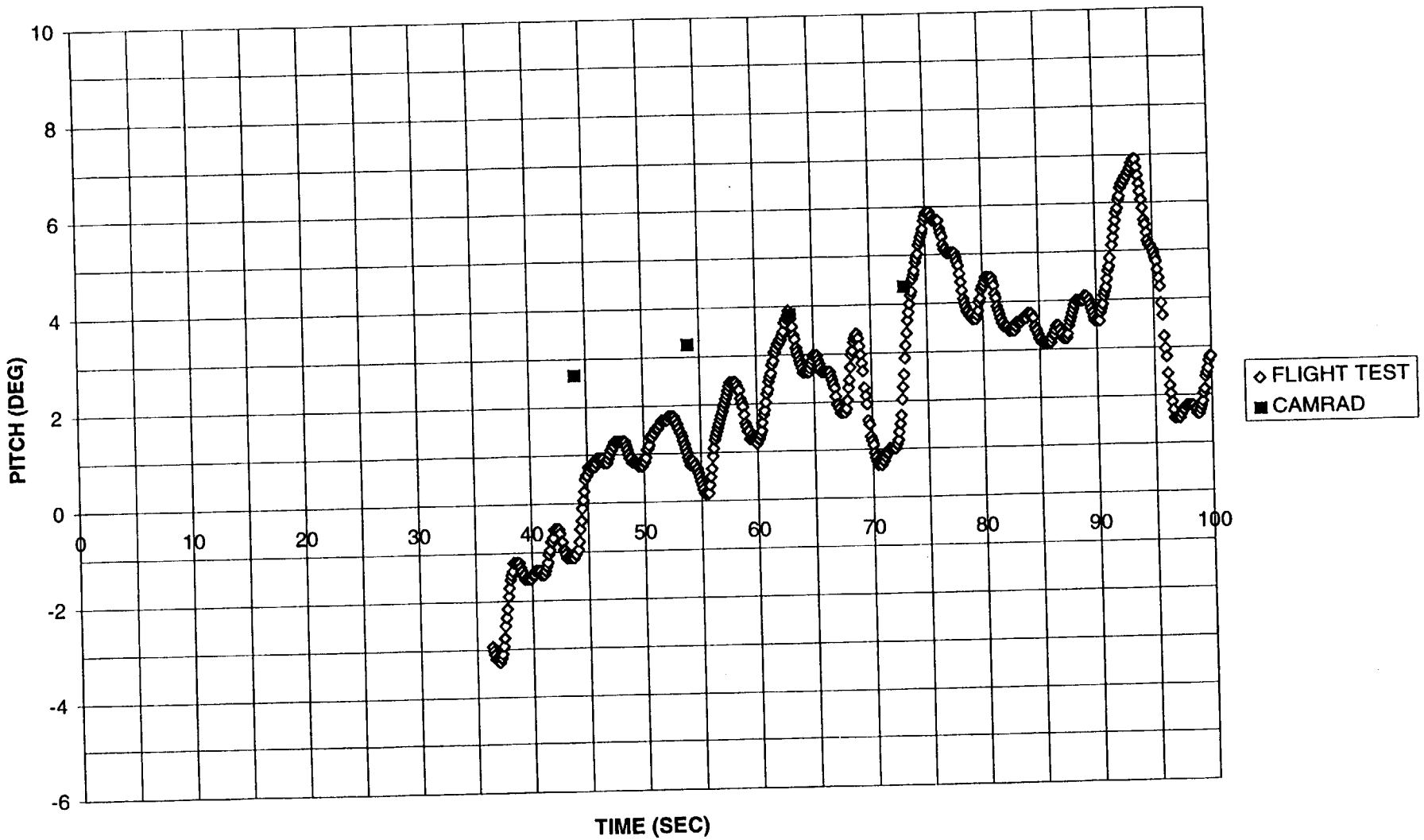

FIGURE 40 AIRCRAFT PITCH ANGLE (WITH TIME) DURING TRAJECTORY FOR TEST NUMBER 12565 (600 FT/MIN ROD)

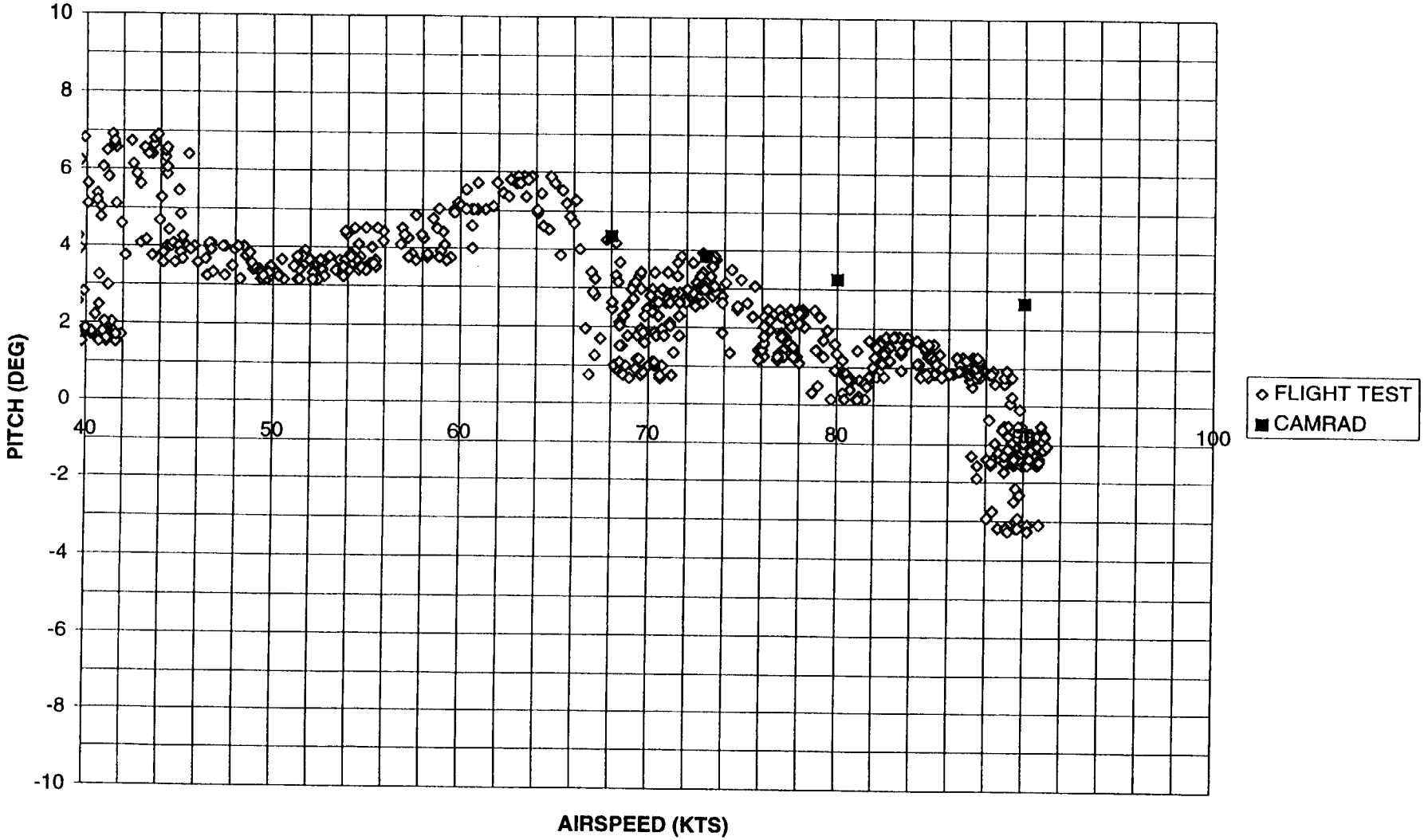

FIGURE 41 AIRCRAFT PITCH ANGLE (WITH AIRSPEED) DURING TRAJECTORY FOR TEST NUMBER 12565 (600 FT/MIN ROD)

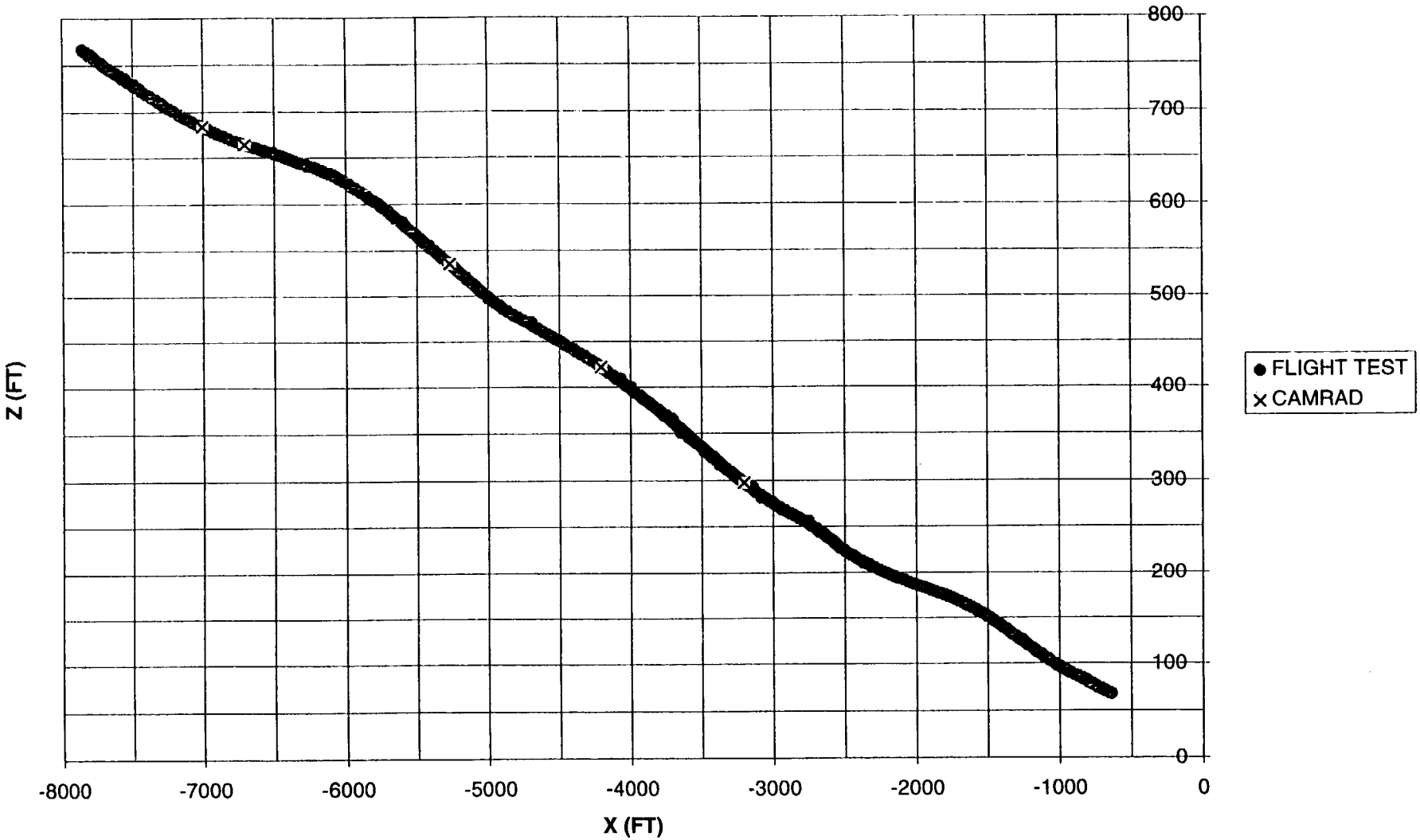

FIGURE 42 TRAJECTORY IN SPACE COORDINATES FOR TEST NUMBER 12567 (5.5 DEGREES APPROACH)

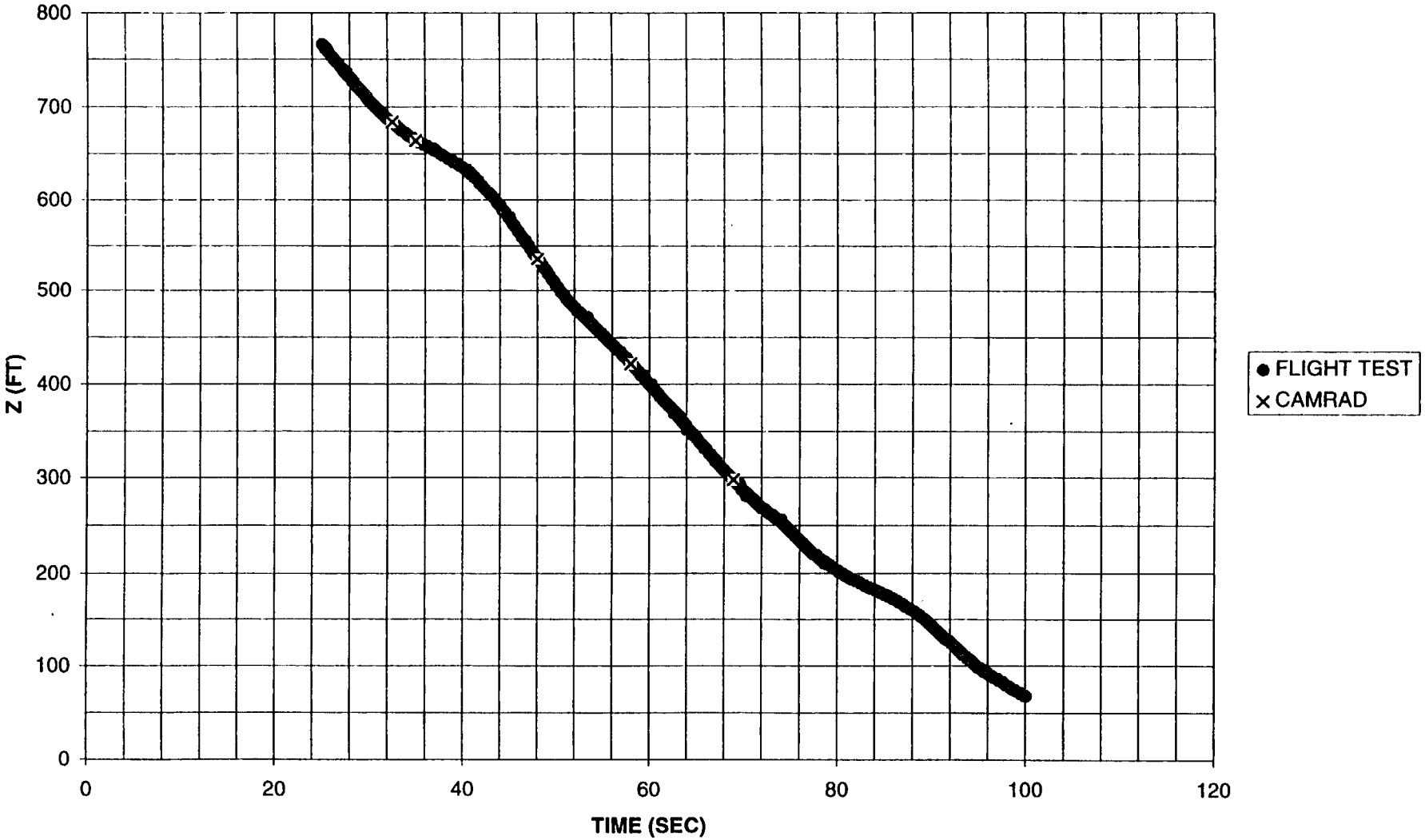

FIGURE 43 TRAJECTORY IN TIME FOR TEST NUMBER 12567 (5.5 DEGREES APPROACH)

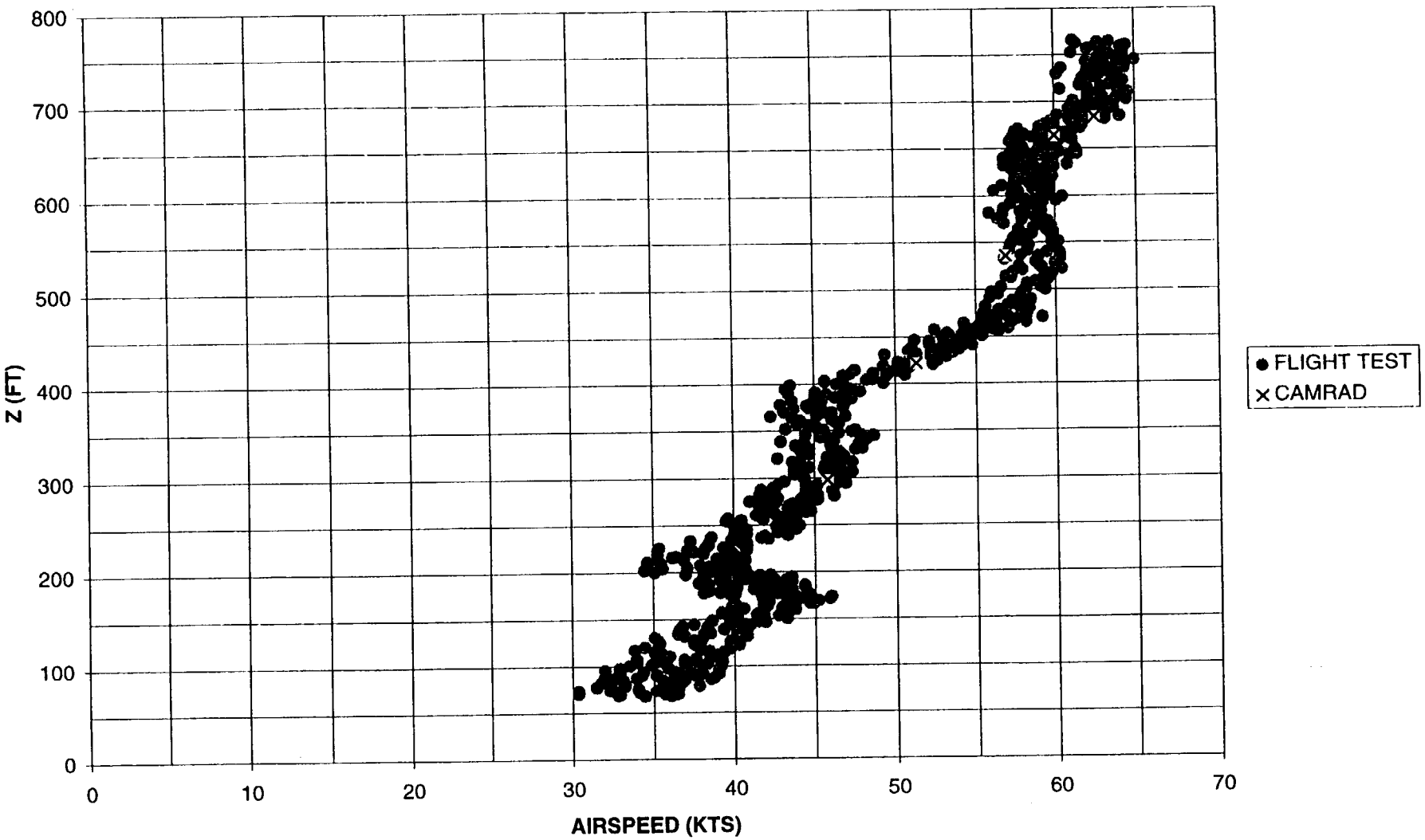

FIGURE 44 TRAJECTORY WITH AIRSPEED FOR TEST NUMBER 12567 (5.5 DEGREES APPROACH)

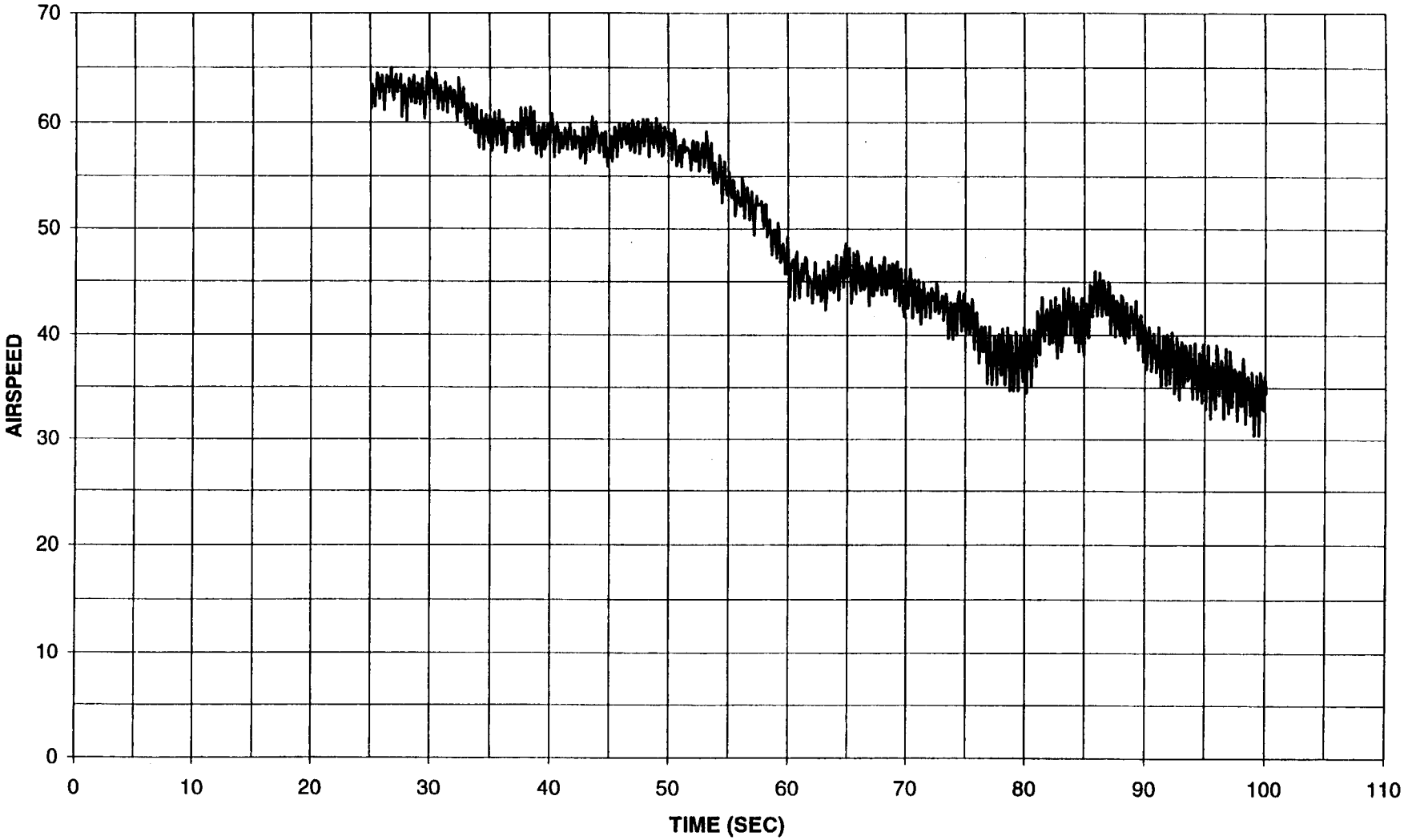

FIGURE 45 AIRSPEED DURING TRAJECTORY FOR TEST NUMBER 12567 (5.5 DEGREES APPROACH)

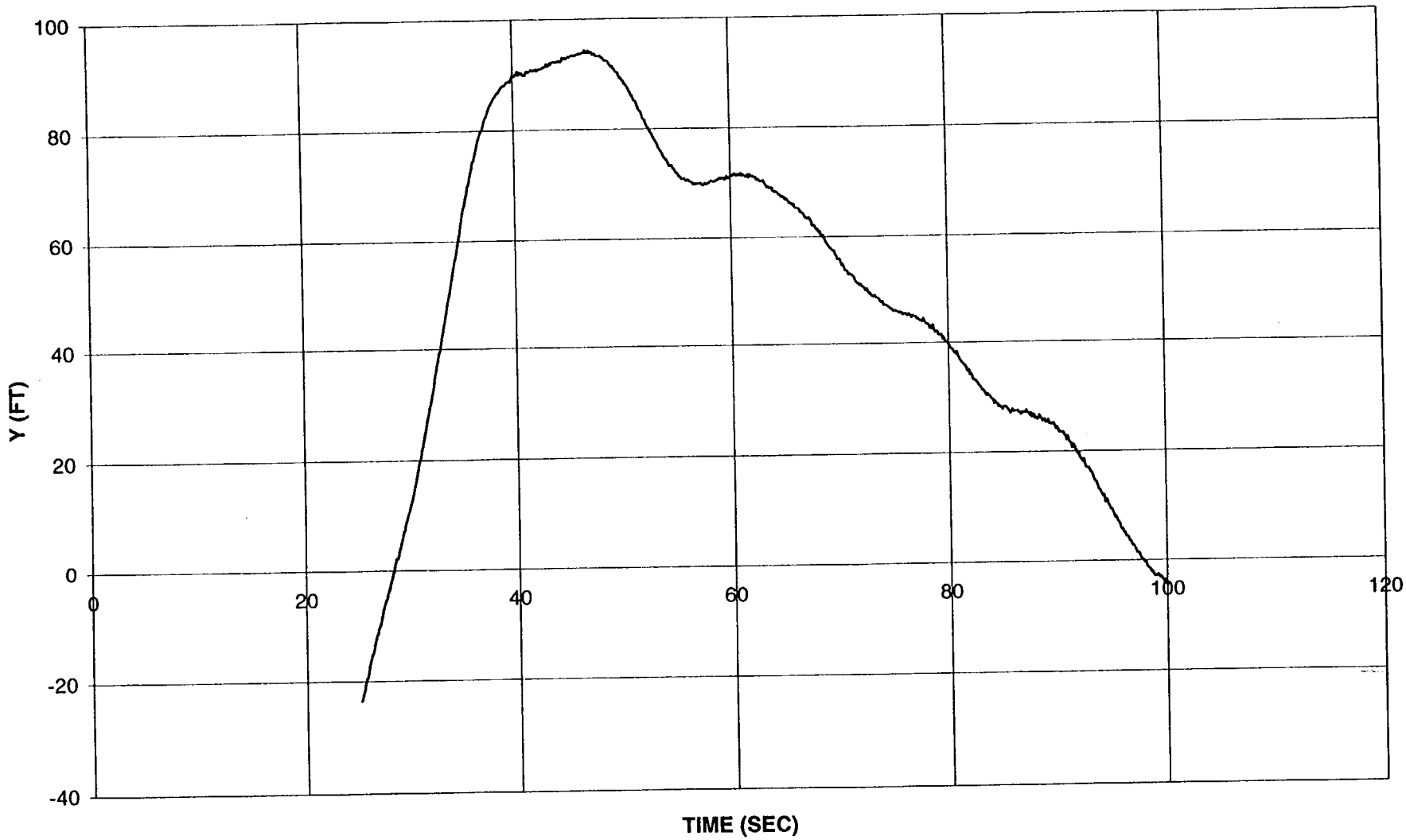

FIGURE 46 SIDEWARD DISTANCE DURING TRAJECTORY FOR TEST NUMBER 12567 (5.5 DEGREES APPROACH)

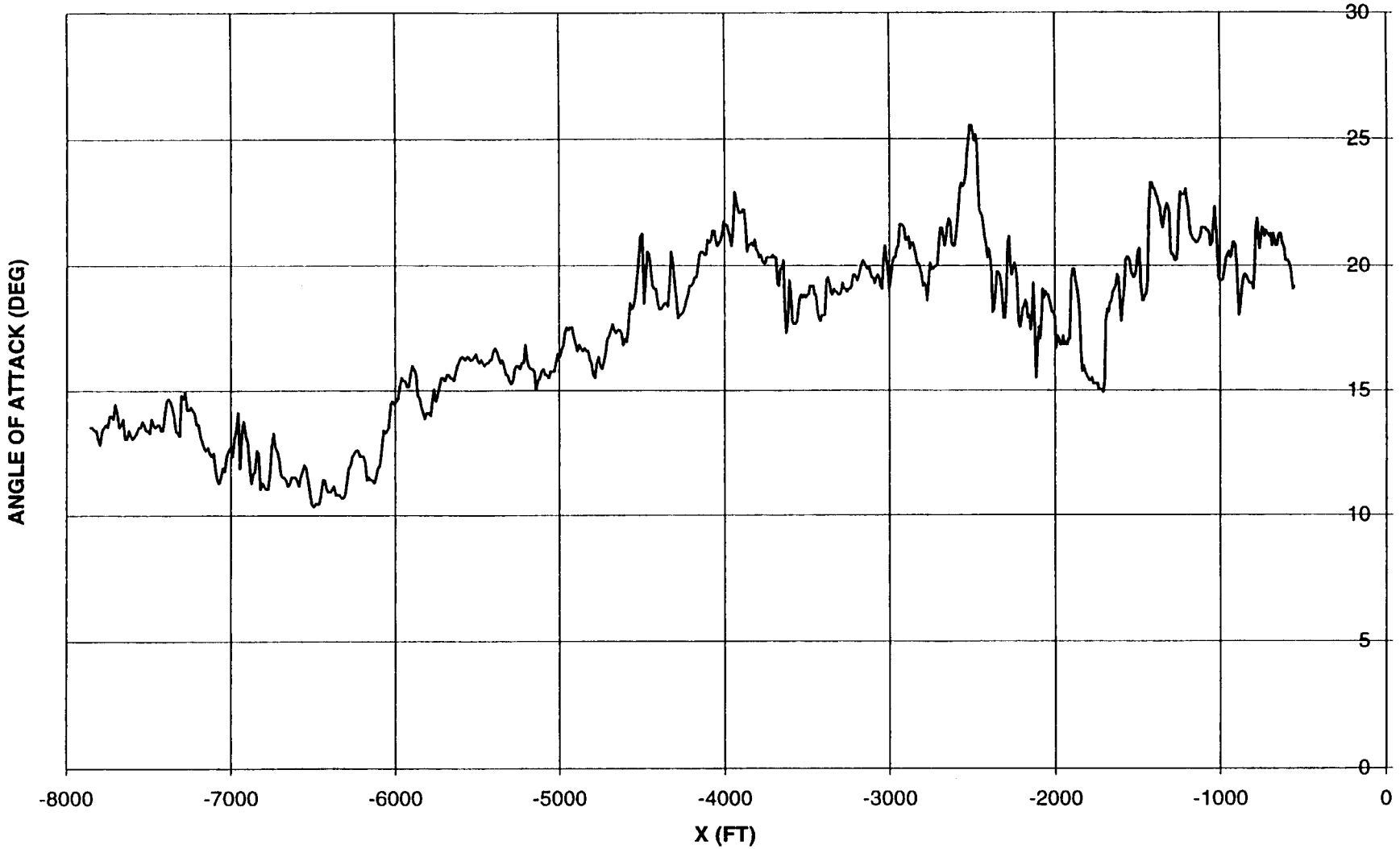

FIGURE 47 ANGLE OF ATTACK DURING TRAJECTORY FOR TEST NUMBER 12567 (5.5 DEGREES APPROACH)

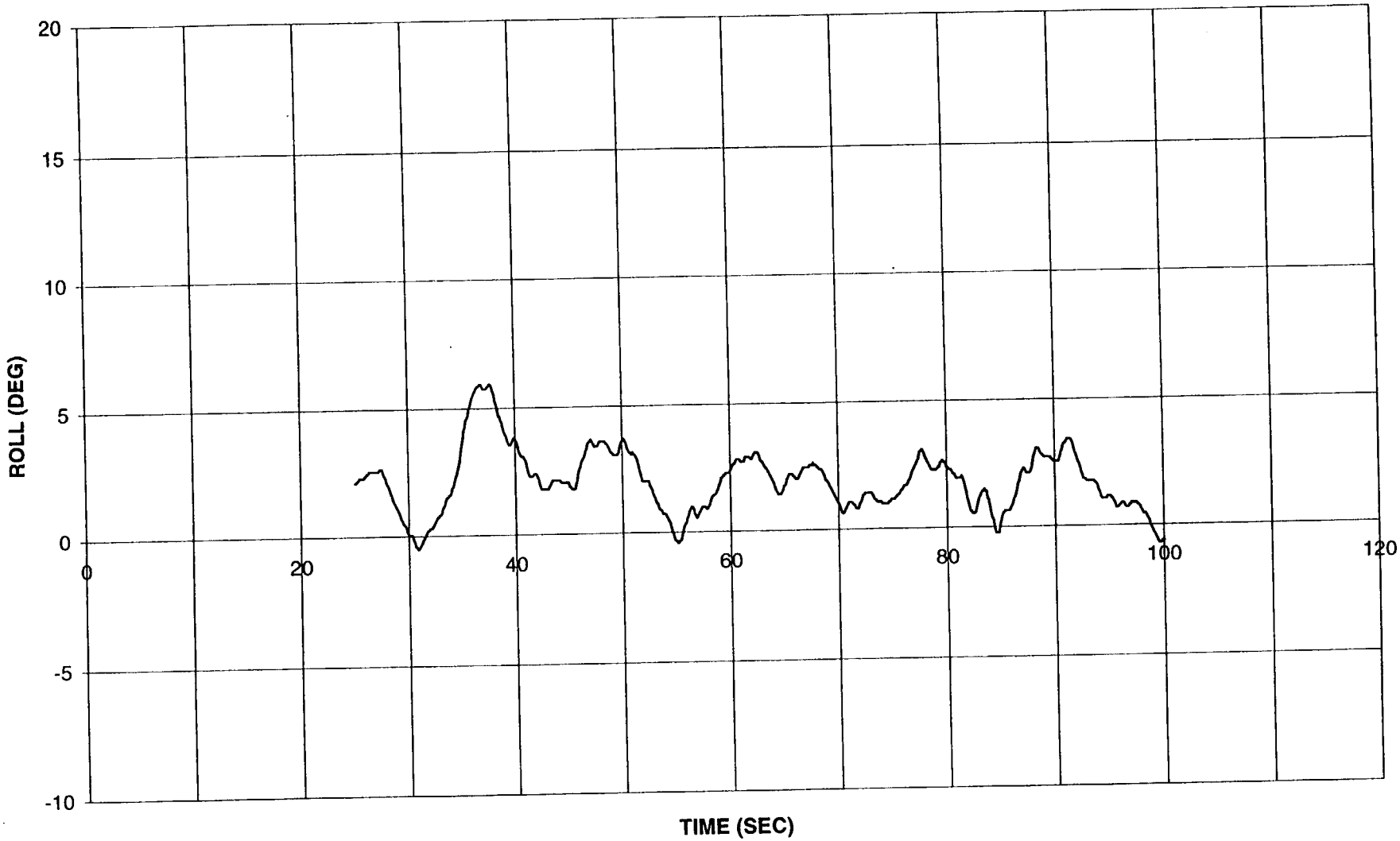

FIGURE 48 ROLL DURING TRAJECTORY (FLIGHT TEST DATA) FOR TEST NUMBER 12567 (5.5 DEGREES APPROACH)

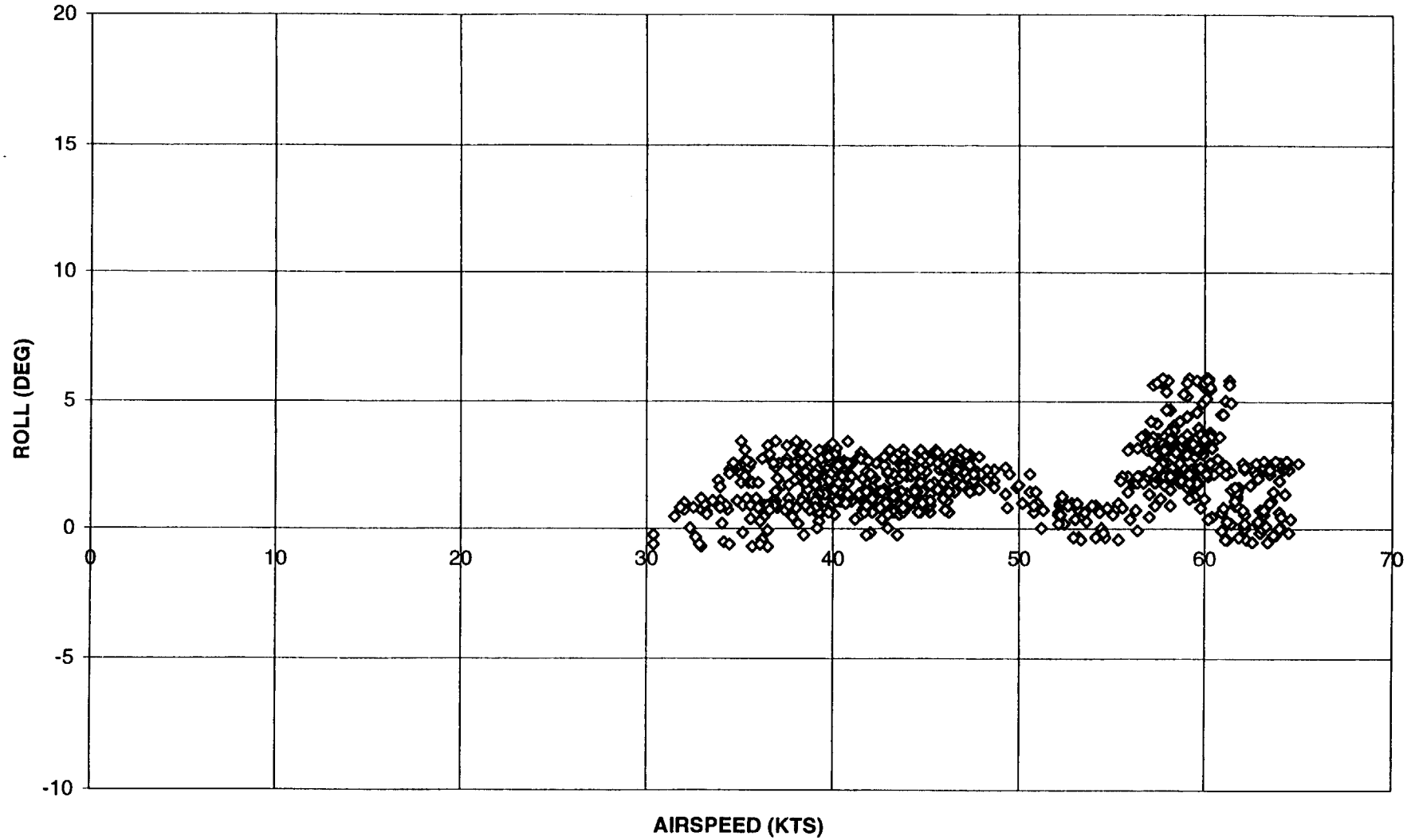

FIGURE 49 ROLL DURING TRAJECTORY (FLIGHT TEST DATA) FOR TEST NUMBER 12567 (5.5 DEGREES APPROACH)

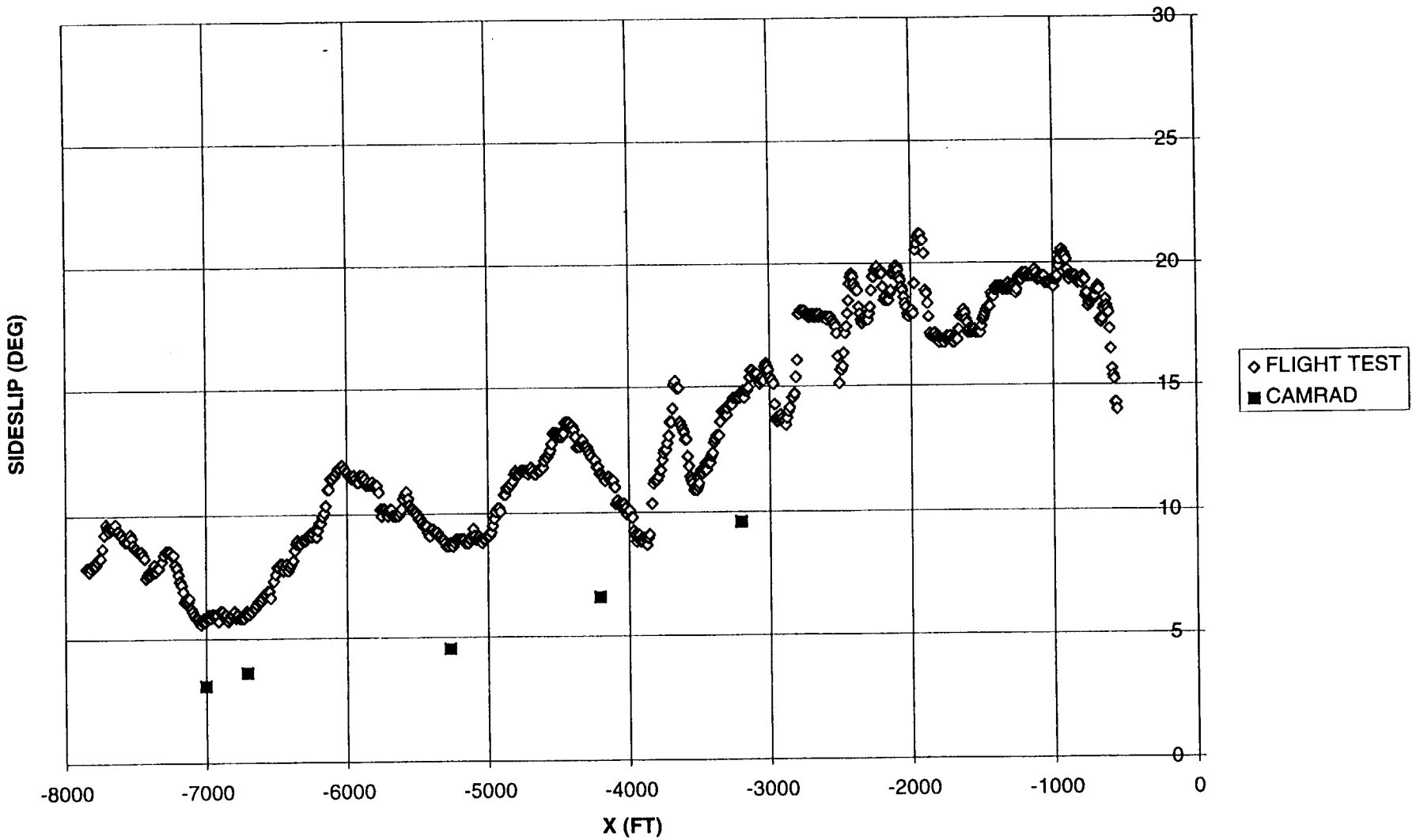

FIGURE 50 SIDESLIP DURING TRAJECTORY FOR TEST NUMBER 12567 (5.5 DEGREES APPROACH)

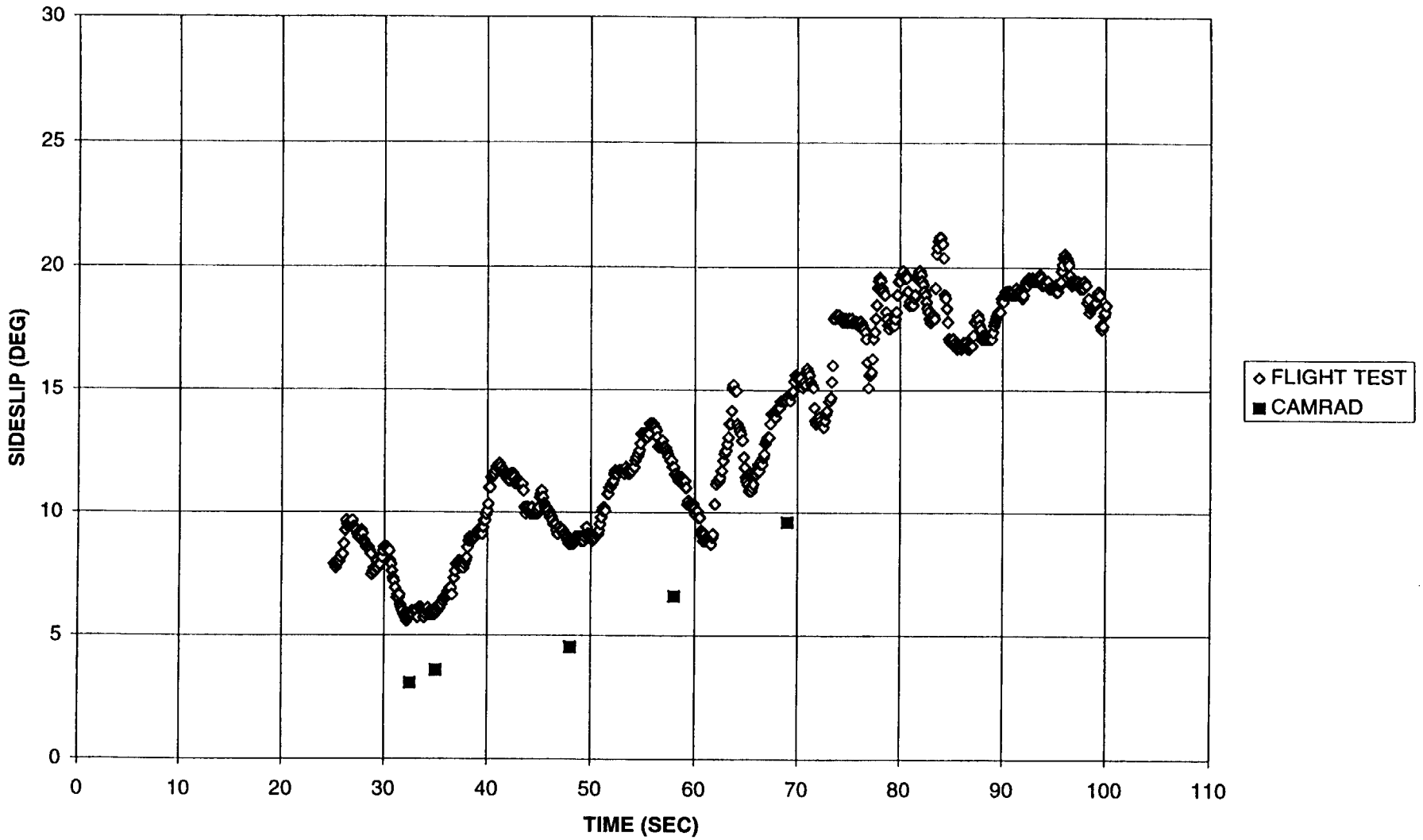

FIGURE 51 SIDESLIP DURING TRAJECTORY FOR TEST NUMBER 12567 (5.5 DEGREES APPROACH)

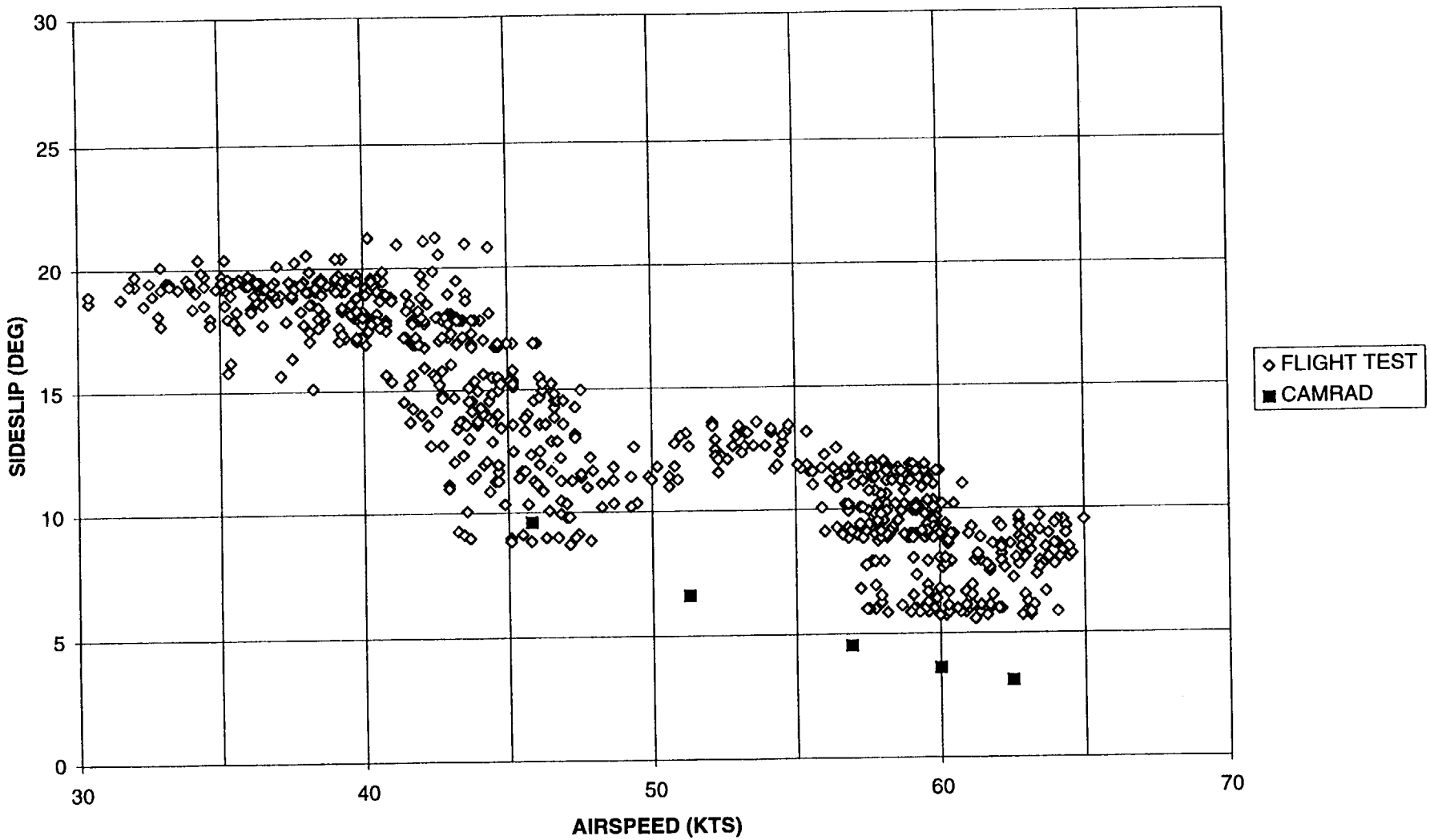

FIGURE 52 SIDESLIP DURING TRAJECTORY FOR TEST NUMBER 12567 (5.5 DEGREES APPROACH)

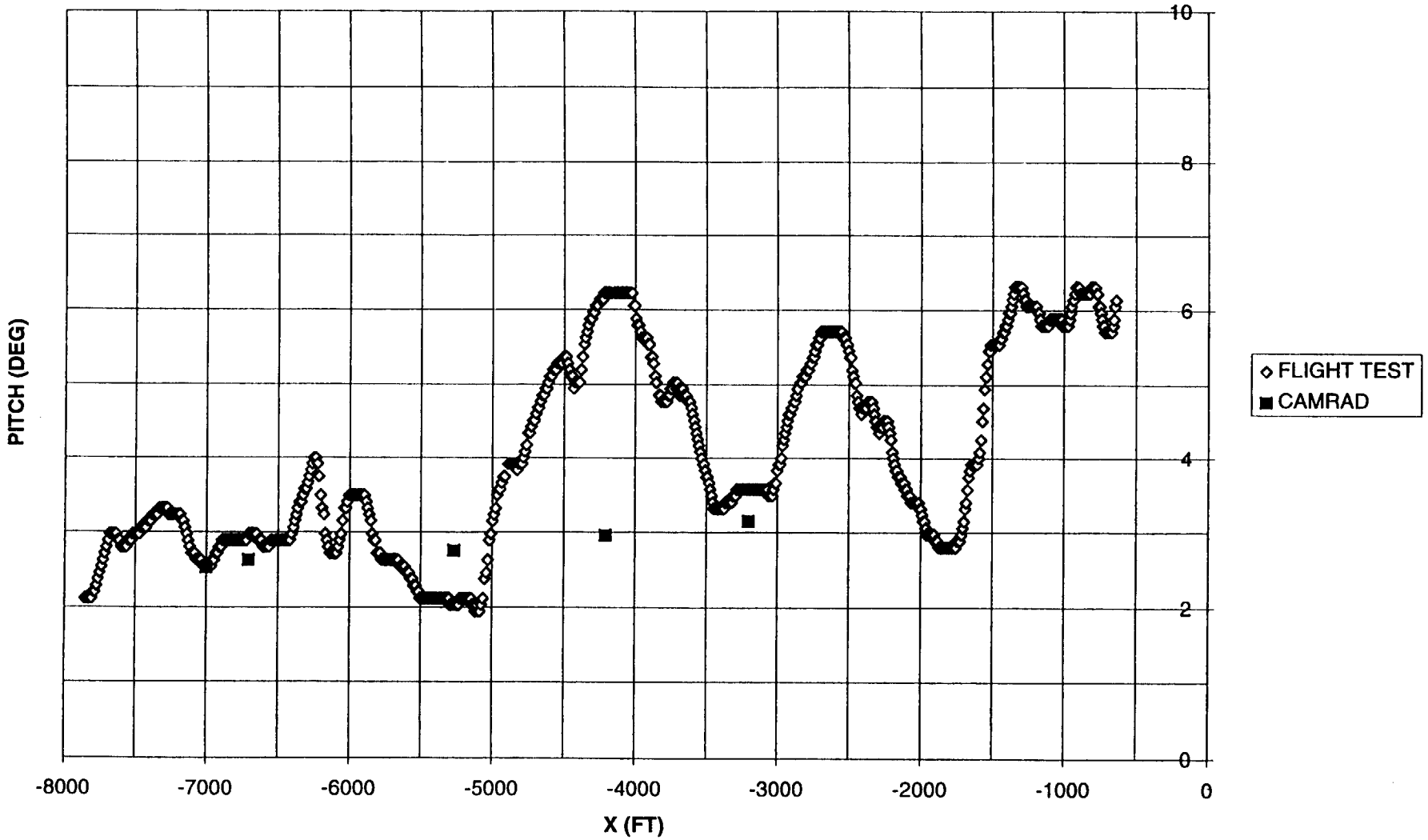

FIGURE 53 AIRCRAFT PITCH ANGLE DURING TRAJECTORY FOR TEST NUMBER 12567 (5.5 DEGREES APPROACH)

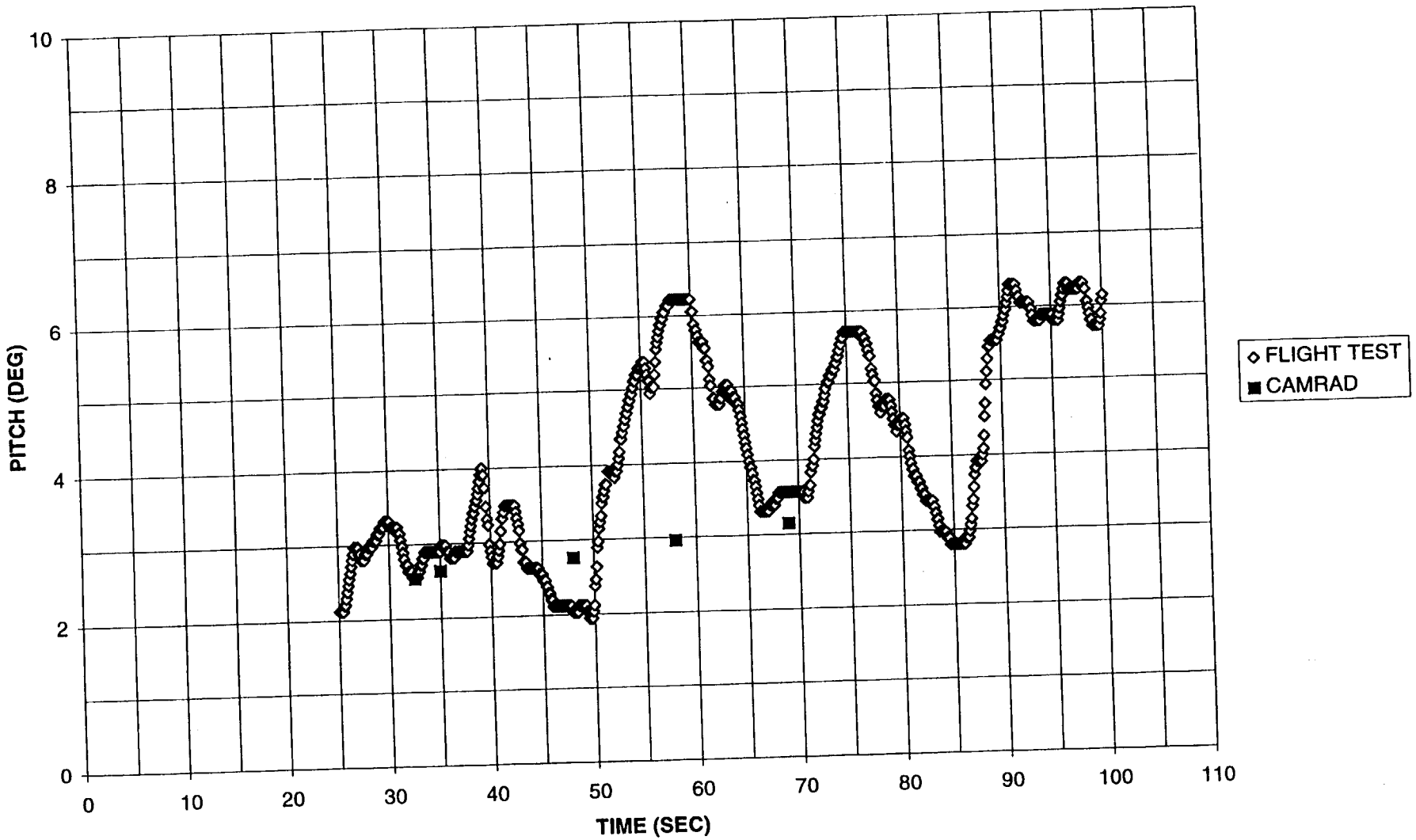

FIGURE 54 AIRCRAFT PITCH ANGLE (WITH TIME) DURING TRAJECTORY FOR TEST NUMBER 12567 (5.5 DEGREES APPROACH)

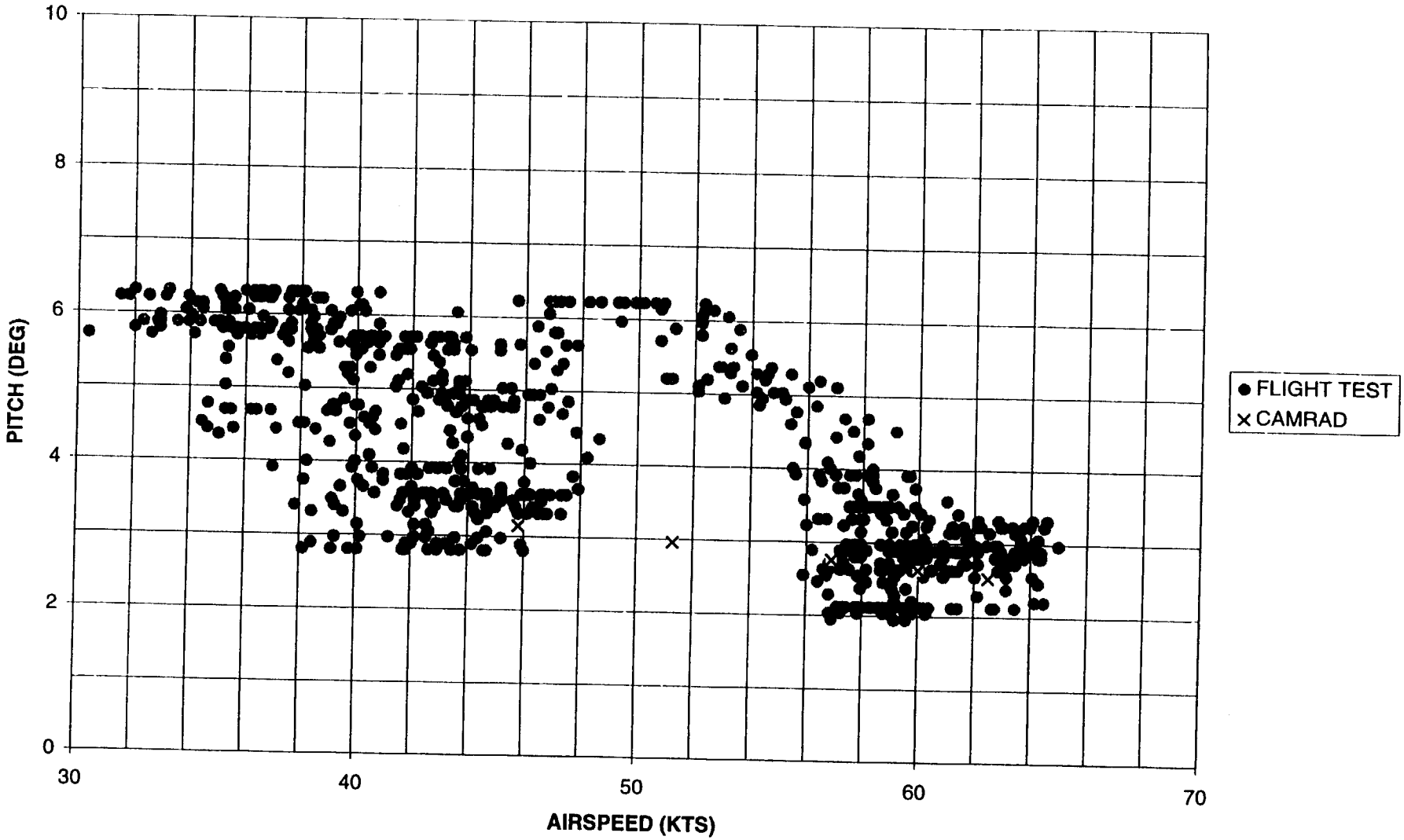

FIGURE 55 AIRCRAFT PITCH ANGLE (WITH AIRSPEED) DURING TRAJECTORY FOR TEST NUMBER 12567 (5.5 DEGREES APPROACH)

REPORT DOCUMENTATION PAGE

Form Approved
OMB No. 0704-0188

1. AGENCY USE ONLY (*Leave blank*)	2. REPORT DATE	3. REPORT TYPE AND DATES COVERED
	February 2000	Contractor Report

4. TITLE AND SUBTITLE
Rotorcraft Noise Abatement Flight Path Modeling

5. FUNDING NUMBERS
581-20-31-01
NAS1-20097
Task 13

6. AUTHOR(S)
H. Murty and C. Berezin

7. PERFORMING ORGANIZATION NAME(S) AND ADDRESS(ES)
Sikorsky Aircraft Corporation
6900 Main Street
Stratford, CT 06615-9129

8. PERFORMING ORGANIZATION REPORT NUMBER

9. SPONSORING/MONITORING AGENCY NAME(S) AND ADDRESS(ES)
National Aeronautics and Space Administration
Langley Research Center
Hampton, VA 23681-2199

10. SPONSORING/MONITORING AGENCY REPORT NUMBER
NASA/CR-2000-209353

11. SUPPLEMENTARY NOTES
Technical Monitor: David A. Conner

12a. DISTRIBUTION/AVAILABILITY STATEMENT
Unclassified-Unlimited
Subject Category 71 Distribution: Nonstandard
Availability: NASA CASI (301) 621-0390

12b. DISTRIBUTION CODE

13. ABSTRACT (*Maximum 200 words*)
This report addresses development of a rotor state/trim modeling capability for noise modeling of decelerating rotorcraft approaches. The resulting technique employs discretization of the descent trajectory as multiple steady state segments for input to CAMRAD.Mod1 to predict rotor states for acoustic analysis. Deceleration is included by modifying the CAMRAD.Mod1 free flight trim options to allow trim to the specified acceleration/deceleration components.

14. SUBJECT TERMS
Rotorcraft, Helicopter, Noise, Abatement, Acoustics, Modeling, Flight Path

15. NUMBER OF PAGES
77

16. PRICE CODE
A05

17. SECURITY CLASSIFICATION OF REPORT	18. SECURITY CLASSIFICATION OF THIS PAGE	19. SECURITY CLASSIFICATION OF ABSTRACT	20. LIMITATION OF ABSTRACT
Unclassified	Unclassified	Unclassified	UL

NSN 7540-01-280-5500

Standard Form 298 (Rev. 2-89)
Prescribed by ANSI Std. Z-39-18
298-102